Electrochemical coreduction of nitrite and CO$_2$ in an ionic liquid system

by

© Mona Bornak

A thesis submitted to the School of Graduate Studies in partial fulfillment of the requirement for the degree of

Master of Science

Department of Chemistry │ Faculty of Science

Memorial University of Newfoundland

St. John's, Newfoundland

September 2023

Abstract

Environmental concerns and demand for sustainability drive investigations of electrochemical reduction of CO_2, N_2, and nitrogen pollutants. The simultaneous reduction of CO_2 and nitrite to generate urea tackles multiple issues while producing valuable products. Moreover, incorporating ionic liquids (ILs) improves catalytic performance and selectivity.

This study investigates the performance of various catalysts, including cobalt and iron phthalocyanine, as well as Cu, Pd, Ir, MoS_2, TiO_2, and Rh nanoparticles, and graphene nanoplatelets in terms of urea production rates and yields. When a cobalt phthalocyanine catalyst was combined with a mixture of 1-butylpyridinium hexafluorophosphate ($BuPyPF_6$) and trihexyltetradecylphosphonium bis(trifluoromethylsulfonyl)imide ($P_{66614}NTf_2$), the hydrophobic nature of the catalyst layer increased, resulting in higher faradaic efficiency (25% at –0.064 V vs RHE). Combining a commercial carbon-supported Cu catalyst with CoPc proved effective in increasing urea production rates, although it led to a decrease in faradaic efficiency. However, the application of carbon black as the supporting layer proved advantageous when graphene and TiO_2 as the catalyst supports were used. TiO_2, in particular, showed promise as both the catalyst and supporting material, achieving an impressive 71% urea yield when combined with CoPc. Fe (III) tetrasulfophthalocyanine, in conjunction with the mixed IL binder, exhibited a high urea production rate but low yield.

Acknowledgments

I would like to extend my sincere gratitude to Prof. Jane Stockmann and Prof. Peter G. Pickup for their invaluable guidance, patience, and unwavering support during the course of my research. This work would not have been feasible without their support and guidance.

I am also deeply appreciative of Prof. Peter Pickup and Prof. Yuming Zhao, my committee members, for their constructive feedback and continuous support throughout my thesis journey.

Special acknowledgments go to the members of Prof. Stockmann and Prof. Peter Pickup's research group: Reza, Nazanin, Oforbuike, Hanna, Katelyn, Bradley, Leila, Bahareh, Jasmeen, and Ahmad. Their support and encouragement have been instrumental in the progress of my research.

I am grateful to Nicholas Ryan, Dr. Jian-Bin Lin, and Dr. Dylan Goudie for their generous sharing of time, experiences, and perspectives, which have played a vital role in making this research a reality.

My heartfelt appreciation also goes to Debbie Hickey for their kind assistance and support during my academic journey.

I would like to extend my appreciation to my parents, my sister Maryam, and my brother Hossein. Their emotional support was essential for the completion of this thesis.

Lastly, I want to express my deepest gratitude to my husband, Ramin, for standing by me with his continuous support throughout this transformative journey.

Table of contents

List of figures

List of tables

List of abbreviations

^{1}H-NMR	Proton nuclear magnetic resonance
BPA	Bisphenol A or 4,4′-(Propane-2,2-diyl)diphenol
BuPyPF$_6$	1-butyl-1-methylpyrrolidinium bis(trifluoromethylsulfonyl)imide
CB	Carbon black
CE	Counter electrode
CFP	Carbon fiber paper
CHO*	CHO intermediates
CO	Carbon monoxide
CO$_2$	Carbon dioxide
COOH*	COOH intermediates
CoPc	Cobalt phthalocyanine
CA	Chronoamperometry
CV	Cyclic voltammetry
DAM	Diacetyl monoxime
DFT	Density functional theory
FE	Faradaic efficiency
FePc	Iron (II) phthalocyanine
FeTsPc	Iron (III) phthalocyanine-4,4',4'',4'''-tetrasulfonic acid
GC	Glassy carbon
GCE	Glassy carbon electrode
HA	Humic acid

HPLC-MS	High-performance liquid chromatography-mass spectrometry
ILs	Ionic liquids
MoS_2	Molybdenum disulfide
MWCNTP	Multi-walled carbon nanotube powders
MWCNTPE	Multi-walled carbon nanotube paste electrodes
N_2	Nitrogen
$NaHCO_3$	Sodium bicarbonate
NH_3	Ammonia
$P_{66614}NTf_2$	1-butyl-1-methylpyrrolidinium bis(trifluoromethylsulfonyl)imide
PPy	Polypyrrole
RE	Reference electrode
RHE	Reversible hydrogen electrode
SCE	Saturated calomel electrode
SCILL	Solid catalyst with ionic liquid layer
STEM	Scanning transmission electron microscopy
TBBPA	Tetrabromobisphenol A or Tetrabromo 4,4′-(Propane-2,2-diyl)diphenol
THF	Tetrahydrofuran
WE	Working electrode
XAFS	X-ray absorption fine structure
XRD	X-ray diffraction

List of symbols

A	Amperes
C	Concentration
ca.	Approximately
e.g.	For example
eq.	Equation
E	Potential
E^0	Standard potential
F	Faraday constant
h	Hour
I	Current
mg	Milligram
min	Minute
mL	Milliliter
n	Number of electrons
Q	Charge
s	Second
t	Time
V	Volt(s)
V	Total electrolyte volume
vs	Versus

Chapter 1

Introduction

1.1 Urea and ammonia: Essential compounds in various industries

Urea ($CO(NH_2)_2$) and ammonia (NH_3) are critical chemical compounds utilized in a variety of sectors, such as the agricultural and pharmaceutical industries.[1] Urea is recognized as one of the most significant nitrogen-based fertilizers, primarily attributed to its high nitrogen content and low transportation cost, resulting in its usage exceeding other nitrogen-based fertilizers by 50%.[2] Furthermore, urea has versatile applications in other industries, such as manufacturing plastics, resins, urea-formaldehyde, and animal feed.[3] On the other hand, ammonia serves as an essential raw material for the production of various fertilizers, chemicals, fuels, and pharmaceutical products. Its importance is mainly due to its high nitrogen content, which makes it a primary source of nitrogen for fertilizers, and its versatile application in the fuels and production of chemicals and pharmaceuticals.[3] Demand for these two essential compounds has increased in tandem with the growth in population in recent years.[1–3]

1.2 Industrial synthesis of urea and ammonia

The Haber-Bosch process is the name given to the industrial method for synthesizing ammonia. It entails the reaction of nitrogen gas (N_2) with hydrogen gas (H_2) to yield ammonia.[4] The high bond energy of nitrogen gas requires that a large amount of energy be supplied in order to overcome the energy barrier for the reaction between nitrogen and hydrogen to occur.[5] This energy input is typically provided by high-pressure (i.e. 50 to 200 bar) and high-temperature (i.e. 650 to 750 K) conditions[6] in the presence of a metal catalyst.[4,5]

The industrial synthesis of urea is also a complex and energy-intensive process which involves several steps, including the production of ammonia, and then in the next step, urea is produced by the reaction between ammonia and carbon dioxide. As carbon dioxide is a stable molecule, it is difficult to react with ammonia at low temperatures and pressures.[7]

To overcome this challenge, the reaction is typically carried out at high pressure (about 150-200 atm) and high temperature (about 150-200 °C) to drive the reaction forward and ensure that the desired products are formed. During urea synthesis, ammonium carbamate is formed as an intermediate compound that is subjected to thermal decomposition, which results in the formation of urea.[7,8] As a result, developing a sustainable and environmentally friendly method for synthesizing ammonia and urea under mild conditions is highly valuable. It may serve as a replacement for the conventional synthesis process.

An alternative method is electrochemical simultaneous coreduction of CO_2 and NO_2^- under ambient temperature and pressure to produce urea and ammonia. Direct electrochemically controlled reactions are often more selective, energy-efficient, and environmentally friendly than the traditional methods. By utilizing renewable energy sources and non-toxic electrolytes, they substantially decrease greenhouse gas emissions and contribute to a net negative carbon economy.[9]

1.3 Electrochemical cells and flow cells

Urea and ammonia syntheses can occur in an electrochemical cell with a three-electrode system.[10] One of the most common electrochemical cells for this synthesis is the H-cell, which has two compartments separated by a proton exchange membrane, such as a Nafion membrane. The H-cell has three electrodes, including a working electrode (WE), a counter electrode (CE) and a reference electrode (RE). The electrocatalyst is loaded onto the WE, while the CE can be a Pt wire or carbon rod. Depending on the electrolyte pH, the RE can be Ag/AgCl, Hg/Hg_2SO_4, or Hg/HgO.[11]

However, the low solubility of CO_2 and N_2 in the electrolyte results in a low current density in the H-cell. As only gas molecules near the WE can diffuse and participate in the electrochemical reaction, flow cells have been used to solve this problem with three-phase reaction interfaces, including feeding gas, electrolyte, and electrocatalyst. The electrocatalyst is loaded onto the gas diffusion layer (GDL), allowing gas and liquid from different paths to face the solid catalyst and ensuring adequate contact between the gas species and the catalyst surface.[12] On the other hand, the hydrophobic layer will suppress the hydrogen evolution reaction by limiting the number of water molecules that move towards the electrode surface. Optimizing the distance between the RE,

2

GDL, and CE can reduce noise and resistance through the electrochemical cell. Therefore, flow cells can be effective for gas-solid interface catalyst reactions and improve urea yield and Faradaic efficiency.[10,13,14]

1.4 Calculation of faradaic efficiency and rate of formation for ammonia and urea

In chemical reactions, the overall yield is determined by the ratio of the actual amount of a product generated during the reaction to the maximum possible (theoretical) amount of that product. On the other hand, faradaic efficiency is assessed based on the ratio of the quantity of the desired compound to the potential yield derived from the total charge passed during an electrochemical reaction.[15,16] In other words, faradaic efficiency can be interpreted as the ratio of the yield of the reaction to the energy consumed (the charge being transferred) over the course of an electrochemical reaction so that the less energy consumed to produce a given amount (mole) of a desired compound, the higher the faradaic efficiency of that electrochemical reaction will be. The equation (1.1) is utilized to calculate the faradaic efficiency: [15,16]

$$Faradaic\ efficiency_{(i)}\ (\%)\ =\ \frac{[C_i] \times n_i \times F}{Q_{total}} \times\ 100 \qquad (1.1)$$

Where Q_{total} is total charge consumed during reaction, $[C_i]$ is the amount of product and n_i is the number of electrons transferred to form product i; F is Faraday constant (96485.3 C mol^{-1}) and i stands for the specific product.

Rate of formation of urea and ammonia[17]

In these theses, the equation (1.2) is employed for the calculation of the rates of urea and ammonia formation. In these theses, the electrode surface area-normalized rates of urea and ammonia formation have been applied.

$$Rate\ of\ reaction\ _{(i)}(Yield\ rate)\ =\ \frac{[C_i] \times V}{t \times A}\ (\text{mol s}^{-1}\text{ cm}^{-2}) \qquad (1.2)$$

Where t and V represent the total electrolysis time and electrolyte volume, respectively, while A denotes the electrode area and i stands for the specific product. [17]

1.5 Ionic liquids in electrochemical reactions

There has been significant research interest in using ionic liquids (ILs) as a reaction medium, binder, or catalyst surface modifier to enhance electrocatalytic activity in recent years.[19] ILs have shown promise in modifying the surfaces of carbon-based materials to increase their compatibility and stability, which in turn provides better binding sites for anchoring metal nanoparticles for electrocatalytic applications.[18,19] There are several advantages of using ILs in electrode modification:

Safety and ease of handling: IL-modified electrodes can be safely and easily handled because ILs, unlike typical organic solvents, have low vapor pressure and are nonflammable.[20]

Morphological studies can be done using scanning electron microscopy (SEM): Their low volatility makes it possible for them to spread evenly over the entire electrode surface when they are cast from a mixture with a volatile solvent. This property allows the morphology of the IL to be studied by SEM.[21]

Viscosity: The viscosity of ILs, although higher than typical polar organic solvents, is similar to that of some binder materials used in classic carbon paste electrodes (CPEs); this has helped to increase the use of IL-based CPEs.[22,23]

Stability: IL-modified electrodes have been observed to remain stable during voltammetric experiments, indicating that the dissolution rate of more hydrophilic ILs is slow. In addition, studies have suggested that the stability of IL deposits could be affected by their inclination to aggregate.[24,25]

1.6 Electrochemical coreduction of CO_2 and NO_2^- for urea and ammonia synthesis

In this chapter, an overview of the advancements made in the area of electrochemical synthesis of urea and ammonia through the coreduction of CO_2 and NO_2^- at ambient temperature and pressure will be provided. The following sections also discuss various advanced techniques for designing effective catalysts, mechanisms for the electrochemical reaction, the use of IL as electrocatalysts, and commonly used methods for determining the concentrations of urea and ammonia.

In 1995, Furuya et al. conducted an early investigation into the simultaneous reaction of CO_2 and NO_2^- at a gas diffusion electrode loaded with Cu.[26] Their findings revealed that in the presence of NO_2^-, ammonia was produced with a faradaic efficiency of 50% at −0.75 V vs. RHE. Upon introducing CO_2 to the system, urea production increased to 37% at the same potential, while the faradaic efficiency of ammonia decreased.[26] Subsequently, in 1996, the same group investigated Zn as a loaded catalyst, achieving 55% ammonia formation at −2.4 V vs. RHE. In 1998, in continuance to their last work, a variety of metal catalysts, including metals of groups 6 to 14 in addition to metal borides were tested by the same group.[27–30]

In 2001, Furuya et al.[31] introduced a new class of catalysts named metallophthalocyanines (M-Pc) as effective catalysts for the coreduction of CO_2 and nitrite. Among the various M-Pc catalysts tested, Co-Pc, Ni-Pc, and Pd-Pc exhibited the highest levels of urea formation. Notably, the highest level was achieved with Ni-Pc, demonstrating a faradaic efficiency of 40% for urea formation at −1.5 V vs. RHE.[31]

Zhang et al.[32] carried out a process to modify an electrode by incorporating surface oxygen vacancies on ZnO nanomaterials to improve the electrochemical reaction performance. The method involved preparing an oxygen vacancy ZnO electrode by subjecting a carbon fiber support to zinc-containing electrolytic deposition and then using air calcination to eliminate impurities.[32] Subsequently, the electrode surface underwent more than 2500 cyclic voltammetry (CV) scans to create oxygen defect sites. The presence of these oxygen defect sites was discovered to increase the efficiency of urea formation by strengthening the adsorption of active species on the electrode surface and by reducing the reaction barrier.[32] The efficiency of the urea reduction reaction was evaluated under CO_2 conditions using 0.2 M $NaHCO_3$ and 0.1 M $NaNO_2$ electrolyte, which resulted in a faradaic efficiency of 23.3% at −0.79 V vs. RHE.[32]

Zheng et al.[33] employed Cu-doped TiO_2 nanotubes enriched with oxygen vacancies (Cu-TiO_2) to enhance the efficiency of electrochemical CO_2 and NO_2^- reduction to urea. The incorporation of low-valence copper on the TiO_2 surface provided two benefits. Firstly, the copper dopant increased the number of oxygen vacancies, which created regions on the electrode surface with less oxygen and two Ti^{3+} ions, resulting in ideal sites for nitrite adsorption. Secondly, the low-valence copper dopant generated favorable active sites for CO_2 adsorption.[33] These Cu-TiO_2 electrode surface properties facilitated the adsorption of CO_2 and NO_2^-, generating more active

sites for the electrochemical coreduction of these species to produce urea. Comparing the linear sweep voltammetric (LSV) curves for the Cu-TiO$_2$ and undoped TiO$_2$ electrode using 0.2 M KHCO$_3$ and 0.02 M KNO$_2$ as electrolytes under CO$_2$ or Ar gas, it was found that Cu-TiO$_2$ had a higher current density and a smaller Tafel slope than undoped TiO$_2$.[33] This could be due to the fact that Cu-TiO$_2$ has many oxygen vacancies, which makes it easier for electrons to move between molecules and reactants to move through the catalyst. It was concluded that the Cu-TiO$_2$ catalyst had a higher catalytic activity level due to its higher number of active sites. This approach yielded urea with a faradaic efficiency of 43.1% at −0.4 V vs. RHE, which was significantly higher than that of undoped TiO$_2$.[33]

Shao et al.[34] synthesized a Te-doped nanocrystal electrode via a wet chemical process and found that modifying the surface electronic structure by incorporating other metals into the Pd surface enhances the adsorption of species. The X-ray photoelectron spectroscopy (XPS) results suggested electron transfer from Te to Pd, which facilitated the conversion of CO$_2$ to intermediate CO and NO$_2^-$ to intermediate NH$_2$, and it also paved the way for the reaction between CO and NH$_2$.[34] The electrochemical reaction was conducted in an H-cell with Te-doped nanocrystals loaded on carbon black in 0.1 M KHCO$_3$ and 0.01 M KNO$_2$ electrolytes under CO$_2$, which yielded urea with a faradaic efficiency of 12.2% at −1.1 V vs. RHE. A comparison of the faradaic efficiency of CO on Te-doped nanocrystals on carbon (Te-PdNCs/C) electrodes and PdNCs/C indicated that the former significantly suppressed hydrogen evolution.[34] Linear sweep voltammetry (LSV) analysis showed that PdNCs/C had a more significant peak current than Te-PdNCs/C, indicating that there was a limited nitrogen reduction reaction. This suggests that the surface of the electrode had been obstructed by the Te doping, which may have reduced the number of active sites available.[34] The influence of nitrite concentration on urea and ammonia was also investigated. It was discovered that the increment of the nitrite concentration has led to an increase in the faradaic efficiency of ammonia but a decrease in that of urea. To overcome mass transport limitations, the coreduction of CO$_2$ and nitrite was carried out in the flow cell with a gas diffusion-layered electrode, which produced urea with a faradaic efficiency of 10.2% at −1.2 V vs. RHE.[34]

In a recent study, ultra-thin, porous gold-copper nanofibers were employed by the Wang group as a catalyst.[35] By alloying copper with gold or other metals, the coordination and electronic structure of copper atoms can be modified, resulting in an increase in CO$_2$ adsorption, activation, and selectivity towards CO$_2$ reduction reactions. The electrode contains numerous defects, such as

twin boundaries, stacking faults, and atomic steps, that create numerous active sites for species adsorption. The experiment involved performing a linear sweep voltammetry (LSV) in a solution of 0.5 M KHCO$_3$, with both Ar and CO$_2$ gases. The results showed a greater current density under CO$_2$, indicating that CO$_2$ was reduced to CO, which was the primary product formed. The addition of 0.01 M KNO$_2$ to the electrolyte led to a higher current density, with ammonia as the primary product of nitrite reduction reaction. Finally, the coreduction of nitrite and CO$_2$ by introducing both CO$_2$ and nitrite to the system resulted in the highest current density and urea was observed as the main product, with a faradaic efficiency of 24.7% at −1.55 V vs. RHE.[35]

1.7 Electrodes modified with ILs in electrochemical reactions

Quezada et al.[36] has reported a reduction of CO$_2$ via an InSnO (indium tin oxide) electrode modified with cobalt 5,10,15,20 tetrakis(4-aminophenyl)porphyrin (Co-TAPP) by choosing 1-butyl-3-methylimidazolium tetrafluoroborate (BMImBF$_4$) as the reaction medium. This electrode was capable of generating a conductive polymer on its surface. The porphyrin layer was found to be penetrated by the IL which caused a more even dispersion of the conductive polymer on the electrode surface, making electron transfer easier, this improved the electrochemical reduction efficiency. Additionally, the investigators found that the electrode faradaic resistance was influenced by the motion of the large ions within the IL, as demonstrated through an analysis of electrochemical impedance spectroscopy (EIS).[36]

Masuda et al.[37] conducted a study on the electrochemical reduction of CO$_2$ using a novel electrode made of gold and modified with a phosphonium-type IL loaded with imidazole molecules in an aqueous solution. By strategically positioning the imidazole molecules into the vacant space between the IL molecules on the electrode surface, the researchers were able to facilitate their interaction with CO$_2$ molecules without forming direct bonds and promote their reduction reactions. According to their proposed mechanism, the addition of imidazole molecules to the electrode surface is followed by applying a negative potential, which causes the cationic head groups of the phosphonium-type IL to be attracted to the negatively charged electrode.[37] The ILs keep the imidazole molecules close enough to each other, causing the formation of hydrogen bonds between the imidazole molecules, and subsequently the release of protons which selectively

reduce CO_2. These outcomes demonstrate the vital role played by the formation of hydrogen bonds between imidazole moieties on the Au substrate in promoting the CO_2 reduction reaction.[37]

Li et al.[38] discussed the analysis of a titanium dioxide nanoparticle/IL composite electrode (TiO$_2$/CILE) using 1-butylpyridinium hexafluorophosphate for the detection of nitrite in a 5.0 mmol L^{-1} [Fe (CN)$_6$] $^{3-/4-}$ and 0.1 mol L^{-1} KCl solution.[38] In order to explore the electrocatalytic capabilities of the carbon ionic liquid electrode (CILE) and the titanium dioxide/carbon IL electrode (TiO$_2$/CILE) for nitrite oxidation, the CV technique was employed. The experiment was performed in a 0.1 M phosphate buffer solution (pH=6.0), with a scan rate of 50 mV s^{-1}. The obtained peak currents from the CV curves showed that the TiO$_2$/CILE electrode, in the absence of nitrite, did not exhibit any oxidation peak (curve a in Figure 1.1). The addition of IL to the electrode system resulted in an oxidation peak emergence, as indicated by the CV curve of the CILE electrode (curve b in Figure 1.1), where an increase in the peak current for the oxidation of nitrite was observed. Furthermore, adding TiO$_2$ to the electrode (curve c in Figure 1.1) resulted in the highest observed peak current. This fact can be ascribed to the high ionic conductivity of the ionic liquid, which plays a role in the heterogeneous electron transfer reaction between the electrode and nitrite, thereby promoting the rate of electron transfer.[38] The impact of the scan rate on the voltammetric signals revealed that the oxidation peak potential of nitrite shifted positively as the scan rate increased. A catalytic oxidation mechanism has also been proposed which involved the conversion of nitrite to nitrate via a reaction with water and the production of two protons and two electrons. The pH of the solution does not influence the peak potential of the nitrite oxidation, but it was observed that the peak current showed a pH dependency, so that the highest peak current has been occurred at pH = 6.[38]

As protons interact with nitrite, in acidic conditions (i.e. pH = 4 to 6), there's a greater chance for conversion of nitrite to HNO_2. Additionally, nitrite generates NO and NO_3^- due to following reaction (eq.1.3):

$$2H^+ + 3NO_2^- \rightarrow 2NO + NO_3^- + H_2O \qquad (1.3)$$
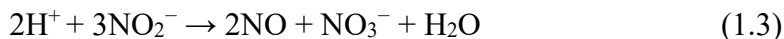
As a result, the peak current decreases.[38]

In basic conditions (i.e. pH = 6 to 8), on the other hand, there's a shortage of protons, making it challenging for nitrite to undergo oxidation which led to a decrement in the rate the electrochemical

reaction. Moreover, there might be an oxide layer forming on the electrode surface, contributing to the decrease in the peak current.[38]
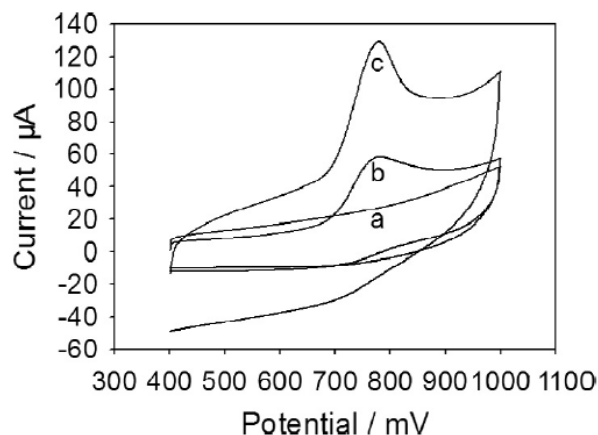
Figure 1.1 CV of 1 mM nitrite at (a) without nitrite at TiO₂/CILE, (b) CILE, and (c) TiO₂/CILE in 0.1 M phosphate buffer solutions. Adapted by permission from J. Electroanal. Chem. 2014, 719, 35–40. [38]

1.8 Methods for determining urea and ammonia concentrations

Various methods can be used to identify and quantify urea and ammonia produced from the coreduction of CO_2 and nitrite, including nuclear magnetic resonance (^{1}H-NMR) spectroscopy, high-performance liquid chromatography−mass spectrometry (HPLC-MS), the diacetyl monoxime method, and the salicylate method.

The diacetyl monoxime (DAM) method is a commonly used chemical technique for measuring urea concentration. This method involves the reaction of urea with DAM, thiosemicarbazide, and ferric chloride in an acidic medium, producing a chromogenic product. The color intensity produced is directly proportional to the urea concentration in the sample and can be measured using UV-Vis absorption spectroscopy at 520-530 nm.[39,40]

Despite the high sensitivity and specificity of the DAM method for urea measurement, it is susceptible to interference from different factors. One of the primary interfering factors is the presence of NO_2^- ions, which can undergo redox reactions with the color reagent, leading to false quantification of urea. The interference effect of NO_2^- ions varies with their concentration, with a relative error of ±7.5% observed at concentrations below 20 ppm, but higher concentrations significantly affect the accuracy of the DAM method. Moreover, other reducing agents, including

9

$S_2O_3{}^{2-}$, thiourea, and thiosulfate can interfere with the accuracy of the DAM method by reducing the ferric ion in the reagent system and producing a chromogenic product similar to that of urea. Hence, the DAM method may not be suitable for determining urea concentration accurately in samples containing these interfering species.[39-41]

The most widely used technique for measuring the amounts of ammonia and urea is known as the salicylate method, also referred to as the indophenol blue method.[41,43] The method for ammonia analysis involves the reaction of sodium salicylate with sodium hypochlorite with sodium nitroprusside as a catalyst to form a colored complex that can be measured at 655 nm with a UV-vis spectrophotometer.[42] The salicylate method is utilized to analyze urea via the breakdown of urea to NH_3 and CO_2 by urease. The resulting urea can be determined through the quantification of NH_3 with and without the presence of urease. The accuracy of this method can be compromised by several factors, including the concentration of $NO_2{}^-$ and $NH_4{}^+$ and the presence of certain ions such as Co^{2+}, Fe^{2+}, and Mn^{2+}, which can produce unreliable results.[41-43]

Using ^{1}H-NMR spectroscopy, the product electrolyte is mixed with DMSO-d_6. Various factors, such as temperature, pH value, and solvent can have an impact on the signal intensity of hydrogen. HPLC testing offers several advantages, such as high resolution, good repeatability, and less impurity interference. The integral area of the corresponding peak tested by ^{1}H-NMR or HPLC shows a linear relationship with the urea concentration.[44]

1.9 The mechanism for urea synthesis with coreduction of CO_2 and nitrite

There are two possible mechanisms for the production of urea. The first mechanism involves the creation of the CO* intermediate through electrocatalytic reduction of CO_2, while the NH_2* precursor forms during the $NO_2{}^-$ reduction reaction. NH_2* binds to CO* through a tandem reaction pathway, resulting in the formation of NH_2CONH_2 (urea) (eq. 1.7).

The second mechanism involves the reduction of $NO_2{}^-$ on the electrode surface. Then, the NH_2* intermediate is formed through several proton-coupled electron transfer processes and CO_2 reduction, forming the COOH* intermediate through a single proton-coupled electron transfer process. Finally, urea is produced via the coupling of NH_2* and COOH* intermediates (eq. 1.10).[18,32,33]

$$CO_2(g) + 2H^+(aq) + 2e^- \rightarrow CO^*(\text{intermediate}) + H_2O \qquad (1.4)$$

$$NO_2^-(aq) + 6H^+(aq) + 5e^- \rightarrow NH_2^*(\text{intermediate}) + 2H_2O \qquad (1.5)$$

$$CO^*(\text{intermediate}) + 2NH_2^*(\text{intermediate}) \rightarrow NH_2CONH_2(aq) \qquad (1.6)$$

The overall reaction is:

$$CO_2(g) + NO_2^-(aq) + 14H^+(aq) + 12e^- \rightarrow NH_2CONH_2(aq) + 5H_2O \quad (1.7)$$
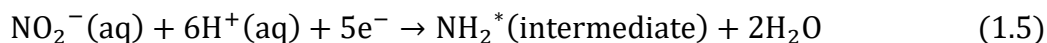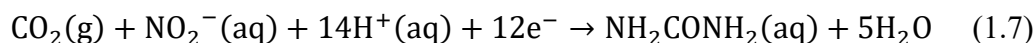
Another mechanism would be:

$$NO_2^- + 6H^+ + 5e^- \rightarrow NH_2^* + 2H_2O \qquad (1.8)$$

$$CO_2(g) + H^+(aq) + e^- \rightarrow COOH^* \qquad (1.9)$$

$$CO_2(g) + 2NH_2^* + H^+(aq) + e^- \rightarrow NH_2CONH_2(aq) + H_2O + CO \qquad (1.10)$$

1.10 Scope of the thesis

In this MSc thesis, three systematic projects are introduced. These works mainly focus on the electrochemical conversion of two globally concerning materials - CO_2 and nitrite - into increasingly demanding chemicals: urea and ammonia. To achieve this, modification of the electrode surface using different kinds of catalysts and co-catalysts, aided by diverse hydrophobic and hydrophilic ILs as binders, is applied. The yielded urea and ammonia are characterized utilizing different analytical methods, including DAM and salicylate methods, respectively.

The objective of Chapter 2 is to investigate the effects of incorporating hydrophobic and hydrophilic ionic liquids, specifically $P_{66614}NTf_2$ and $BuPyPF_6$, as well as their mixtures, on the coreduction of CO_2 and nitrite using a carbon-supported cobalt phthalocyanine catalyst (CoPc/C) as well as one with Cu as the co-catalyst (CoPc/Cu/C). This investigation aims to control the hydrophobicity of the CoPc microenvironment, with the goal of influencing activity and product selectivity in the electrochemical reduction process.

In Chapter 3, the simultaneous coreduction of CO_2 and nitrite is investigated via the application of FePc and FeTsPc supported on carbon black as catalysts in conjunction with ILs as the binder. In addition, Chapter 4 focuses on the utilization of MoS_2 supported on carbon black-modified

electrode surface as the catalyst with different binders including ILs and Nafion for coreduction of CO_2 and nitrite.

Finally, Faradaic efficiency and the rate of formation for urea and ammonia in all diverse electrochemical systems are summarized in the last chapter.

1.11 References

(1)   Wang, J.; Feng, T.; Chen, J.; Ramalingam, V.; Li, Z.; Kabtamu, D. M.; He, J.-H.; Fang, X. Electrocatalytic Nitrate/Nitrite Reduction to Ammonia Synthesis Using Metal Nanocatalysts and Bio-Inspired Metalloenzymes. *Nano Energy* **2021**, 86, 106088. https://doi.org/10.1016/j.nanoen.2021.106088.

(2)   Xia, M.; Mao, C.; Gu, A.; Tountas, A. A.; Qiu, C.; Wood, T. E.; Li, Y. F.; Ulmer, U.; Xu, Y.; Viasus, C. J.; Ye, J.; Qian, C.; Ozin, G. Solar Urea: Towards a Sustainable Fertilizer Industry. *Angew. Chem*. **2022**, 134 (1). https://doi.org/10.1002/ange.202110158.

(3)   Zamfirescu, C.; Dincer, I. Ammonia as a Green Fuel and Hydrogen Source for Vehicular Applications. *Fuel Process. Technol*. **2009**, 90 (5), 729–737. https://doi.org/10.1016/j.fuproc.2009.02.004.

(4)   Rafiqul, I.; Weber, C.; Lehmann, B.; Voss, A. Energy Efficiency Improvements in Ammonia Production—Perspectives and Uncertainties. *Energy* **2005**, 30 (13), 2487–2504. https://doi.org/10.1016/j.energy.2004.12.004.

(5)   Ren, W.; Mei, Z.; Zheng, S.; Li, S.; Zhu, Y.; Zheng, J.; Lin, Y.; Chen, H.; Gu, M.; Pan, F. Wavelength-Dependent Solar N_2 Fixation into Ammonia and Nitrate in Pure Water. *Research* **2020**, 2020, 2020/3750314. https://doi.org/10.34133/2020/3750314.

(6)   Vojvodic, A.; Medford, A. J.; Studt, F.; Abild-Pedersen, F.; Khan, T. S.; Bligaard, T.; Nørskov, J. K. Exploring the Limits: A Low-Pressure, Low-Temperature Haber–Bosch Process. *Chem. Phys. Lett*. **2014**, 598, 108–112. https://doi.org/10.1016/j.cplett.2014.03.003.

(7)   Yuan, M.; Chen, J.; Xu, Y.; Liu, R.; Zhao, T.; Zhang, J.; Ren, Z.; Liu, Z.; Streb, C.; He, H.; Yang, C.; Zhang, S.; Zhang, G. Highly Selective Electroreduction of N_2 and CO_2 to Urea over Artificial Frustrated Lewis Pairs. *Energy Environ. Sci.* **2021**, 14 (12), 6605–6615. https://doi.org/10.1039/D1EE02485J.

(8)   Barzagli, F.; Mani, F.; Peruzzini, M. From Greenhouse Gas to Feedstock: Formation of Ammonium Carbamate from CO_2 and NH_3 in Organic Solvents and Its Catalytic Conversion into Urea under Mild Conditions. *Green Chem*. **2011**, 13 (5), 1267. https://doi.org/10.1039/c0gc00674b.

(9)   Tang, C.; Zheng, Y.; Jaroniec, M.; Qiao, S. Electrocatalytic Refinery for Sustainable Production of Fuels and Chemicals. *Angew. Chem. Int. Ed*. **2021**, 60 (36), 19572–19590. https://doi.org/10.1002/anie.202101522.

(10)   Chen, C.; Zhu, X.; Wen, X.; Zhou, Y.; Zhou, L.; Li, H.; Tao, L.; Li, Q.; Du, S.; Liu, T.; Yan, D.; Xie, C.; Zou, Y.; Wang, Y.; Chen, R.; Huo, J.; Li, Y.; Cheng, J.; Su, H.; Zhao, X.; Cheng, W.; Liu, Q.; Lin, H.; Luo, J.; Chen, J.; Dong, M.; Cheng, K.; Li, C.; Wang, S. Coupling N_2 and CO_2 in H_2O to Synthesize Urea under Ambient Conditions. *Nat. Chem.* **2020**, 12 (8), 717–724. https://doi.org/10.1038/s41557-020-0481-9.

(11)   Alinejad, S.; Quinson, J.; Wiberg, G. K. H.; Schlegel, N.; Zhang, D.; Li, Y.; Reichenberger, S.; Barcikowski, S.; Arenz, M. Electrochemical Reduction of CO_2 on Au Electrocatalysts in a Zero-Gap, Half-Cell Gas Diffusion Electrode Setup: A Systematic Performance Evaluation and Comparison   to   an   H-cell   Setup**.   *ChemElectroChem*   **2022**,   9   (12). https://doi.org/10.1002/celc.202200341.

(12)   Huang, Y.; Yang, R.; Wang, C.; Meng, N.; Shi, Y.; Yu, Y.; Zhang, B. Direct Electrosynthesis of Urea from Carbon Dioxide and Nitric Oxide. *ACS Energy Lett*. **2022**, 7 (1), 284–291. https://doi.org/10.1021/acsenergylett.1c02471.

(13)   Wang, J.; Yao, Z.; Hao, L.; Sun, Z. Electrocatalytic Coupling of CO_2 and N_2 for Urea Synthesis.   *Curr.   Opin.   Green   Sustain.   Chem*.   **2022**,   37,   100648. https://doi.org/10.1016/j.cogsc.2022.100648.

(14)   Weekes, D. M.; Salvatore, D. A.; Reyes, A.; Huang, A.; Berlinguette, C. P. Electrolytic CO_2 Reduction   in   a   Flow   Cell.   *Acc.   Chem.   Res*.   **2018**,   51   (4),   910–918. https://doi.org/10.1021/acs.accounts.8b00010.

(15)   Fuller, T. F.; Harb, J. N. *Electrochemical Engineering*; Wiley: Hoboken, NJ, **2018**.

(16)   Kempler, P. A.; Nielander, A. C. Reliable Reporting of Faradaic Efficiencies for Electrocatalysis Research. *Nat. Commun.* **2023**, 14 (1), 1158. https://doi.org/10.1038/s41467-023-36880-8.

(17)   Wang, M.; Liu, S.; Qian, T.; Liu, J.; Zhou, J.; Ji, H.; Xiong, J.; Zhong, J.; Yan, C. Over 56.55% Faradaic Efficiency of Ambient Ammonia Synthesis Enabled by Positively Shifting the

Reaction Potential. *Nat. Commun.* **2019**, 10 (1), 341. https://doi.org/10.1038/s41467-018-08120-x.

(18)   Cui, Y.; He, B.; Liu, X.; Sun, J. Ionic Liquids-Promoted Electrocatalytic Reduction of Carbon Dioxide. *Ind. Eng. Chem. Res*. **2020**, 59 (46), 20235–20252. https://doi.org/10.1021/acs.iecr.0c04037.

(19)   Opallo, M.; Lesniewski, A. A Review on Electrodes Modified with Ionic Liquids. *J. Electroanal. Chem*. **2011**, 656 (1–2), 2–16. https://doi.org/10.1016/j.jelechem.2011.01.008.

(20)   Wadhawan, J. D.; Schröder, U.; Neudeck, A.; Wilkins, S. J.; Compton, R. G.; Marken, F.; Consorti, C. S.; de Souza, R. F.; Dupont, J. Ionic Liquid Modified Electrodes. Unusual Partitioning and Diffusion Effects of $Fe(CN)_6^{4-/3-}$ in Droplet and Thin Layer Deposits of 1-Methyl-3-(2,6-(S)-Dimethylocten-2-Yl)-Imidazolium Tetrafluoroborate. *J. Electroanal. Chem*. **2000**, 493 (1–2), 75–83. https://doi.org/10.1016/S0022-0728(00)00308-9.

(21)   Zhao, F.; Wu, X.; Wang, M.; Liu, Y.; Gao, L.; Dong, S. Electrochemical and Bioelectrochemistry Properties of Room-Temperature Ionic Liquids and Carbon Composite Materials. *Anal. Chem*. **2004**, 76 (17), 4960–4967. https://doi.org/10.1021/ac0494026.

(22)   Buzzeo, M. C.; Evans, R. G.; Compton, R. G. Non-Haloaluminate Room-Temperature Ionic Liquids in Electrochemistry—A Review. *ChemPhysChem* **2004**, 5 (8), 1106–1120. https://doi.org/10.1002/cphc.200301017.

(23)   Švancara, I.; Walcarius, A.; Kalcher, K.; Vytřas, K. Carbon Paste Electrodes in the New Millennium. *Open Chem*. **2009**, 7 (4), 598–656. https://doi.org/10.2478/s11532-009-0097-9.

(24)   Samec, Z.; Langmaier, J.; Kakiuchi, T. Charge-Transfer Processes at the Interface between Hydrophobic Ionic Liquid and Water. *Pure Appl. Chem*. **2009**, 81 (8), 1473–1488. https://doi.org/10.1351/PAC-CON-08-08-36.

(25)   Blesic, M.; Marques, M. H.; Plechkova, N. V.; Seddon, K. R.; Rebelo, L. P. N.; Lopes, A. Self-Aggregation of Ionic Liquids: Micelle Formation in Aqueous Solution. *Green Chem*. **2007**, 9 (5), 481. https://doi.org/10.1039/b615406a.

(26)   Shibata, M.; Yoshida, K.; Furuya, N. Electrochemical Synthesis of Urea on Reduction of Carbon Dioxide with Nitrate and Nitrite Ions Using Cu-Loaded Gas-Diffusion Electrode. *J. Electroanal. Chem*. **1995**, 387 (1–2), 143–145. https://doi.org/10.1016/0022-0728(95)03992-P.

(27)   Shibata, M.; Yoshida, K.; Furuya, N. Electrochemical Synthesis of Urea at Gas-Diffusion Electrodes I. Simultaneous Reduction of Carbon Dioxide and Nitrite Ions at Zn Catalysts. *Denki Kagaku Oyobi Kogyo Butsuri Kagaku* **1996**, 64 (10), 1068–1073. https://doi.org/10.5796/kogyobutsurikagaku.64.1068.

(28)   Shibata, M.; Yoshida, K.; Furuya, N. Electrochemical Synthesis of Urea at Gas-Diffusion Electrodes. *J. Electroanal. Chem*. **1998**, 442 (1–2), 67–72. https://doi.org/10.1016/S0022-0728(97)00504-4.

(29)   Shibata, M.; Yoshida, K.; Furuya, N. Electrochemical Synthesis of Urea at Gas-Diffusion Electrodes: IV. Simultaneous Reduction of Carbon Dioxide and Nitrate Ions with Various Metal Catalysts. *J. Electrochem. Soc*. **1998**, 145 (7), 2348–2353. https://doi.org/10.1149/1.1838641.

(30)   Shibata, M.; Yoshida, K.; Furuya, N. Electrochemical Synthesis of Urea at Gas-Diffusion Electrodes V. Simultaneous Reduction of Carbon Dioxide and Nitrite Ions with Various Boride Catalysts. *Denki Kagaku Oyobi Kogyo Butsuri Kagaku* **1998**, 66 (6), 584–589. https://doi.org/10.5796/kogyobutsurikagaku.66.584.

(31)   Shibata, M.; Furuya, N. Electrochemical Synthesis of Urea at Gas-Diffusion Electrodes. *J. Electroanal. Chem*. **2001**, 507 (1–2), 177–184. https://doi.org/10.1016/S0022-0728(01)00363-1.

(32)   Meng, N.; Huang, Y.; Liu, Y.; Yu, Y.; Zhang, B. Electrosynthesis of Urea from Nitrite and CO_2 over Oxygen Vacancy-Rich ZnO Porous Nanosheets. *Cell Rep. Phys. Sci*. **2021**, 2 (3), 100378. https://doi.org/10.1016/j.xcrp.2021.100378.

(33)   Cao, N.; Quan, Y.; Guan, A.; Yang, C.; Ji, Y.; Zhang, L.; Zheng, G. Oxygen Vacancies Enhanced Cooperative Electrocatalytic Reduction of Carbon Dioxide and Nitrite Ions to Urea. *J. Colloid Interface Sci*. **2020**, 577, 109–114. https://doi.org/10.1016/j.jcis.2020.05.014.

(34)   Feng, Y.; Yang, H.; Zhang, Y.; Huang, X.; Li, L.; Cheng, T.; Shao, Q. Te-Doped Pd Nanocrystal for Electrochemical Urea Production by Efficiently Coupling Carbon Dioxide Reduction with Nitrite Reduction. *Nano Lett*. **2020**, 20 (11), 8282–8289. https://doi.org/10.1021/acs.nanolett.0c03400.

(35)   Liu, S.; Yin, S.; Wang, Z.; Xu, Y.; Li, X.; Wang, L.; Wang, H. AuCu Nanofibers for Electrosynthesis of Urea from Carbon Dioxide and Nitrite. *Cell Rep. Phys. Sci.* **2022**, 3 (5), 100869. https://doi.org/10.1016/j.xcrp.2022.100869.

(36)   Quezada, D.; Honores, J.; García, M.; Armijo, F.; Isaacs, M. Electrocatalytic Reduction of Carbon Dioxide on a Cobalt Tetrakis(4-Aminophenyl)Porphyrin Modified Electrode in BMImBF₄. *New J. Chem.* **2014**, 38 (8), 3606–3612. https://doi.org/10.1039/C4NJ00519H.

(37)   Iijima, G.; Kitagawa, T.; Katayama, A.; Inomata, T.; Yamaguchi, H.; Suzuki, K.; Hirata, K.; Hijikata, Y.; Ito, M.; Masuda, H. CO_2 Reduction Promoted by Imidazole Supported on a Phosphonium-Type Ionic-Liquid-Modified Au Electrode at a Low Overpotential. *ACS Catal.* **2018**, 8 (3), 1990–2000. https://doi.org/10.1021/acscatal.7b03274.

(38)   Li, Y.; Wang, H.; Liu, X.; Guo, L.; Ji, X.; Wang, L.; Tian, D.; Yang, X. Nonenzymatic Nitrite Sensor Based on a Titanium Dioxide Nanoparticles/Ionic Liquid Composite Electrode. *J. Electroanal. Chem.* **2014**, 719, 35–40. https://doi.org/10.1016/j.jelechem.2014.02.006.

(39) Chen, L.; Ma, J.; Huang, Y.; Dai, M.; Li, X. Optimization of a Colorimetric Method to Determine Trace Urea in Seawater: Trace Urea Analysis in Seawater. *Limnol. Oceanogr. Methods* **2015**, 13 (6), 303–311. https://doi.org/10.1002/lom3.10026.

(40) Langenfeld, N. J.; Payne, L. E.; Bugbee, B. Colorimetric Determination of Urea Using Diacetyl Monoxime with Strong Acids. *PLoS ONE* **2021**, 16 (11). https://doi.org/10.1371/journal.pone.0259760.

(41)   Huang, Y.; Wang, Y.; Liu, Y.; Ma, A.; Gui, J.; Zhang, C.; Yu, Y.; Zhang, B. Unveiling the Quantification Minefield in Electrocatalytic Urea Synthesis. *Chem. Eng. J.* **2023**, 453, 139836. https://doi.org/10.1016/j.cej.2022.139836.

(42)   Giner-Sanz, J. J.; Leverick, G. M.; Pérez-Herranz, V.; Shao-Horn, Y. Salicylate Method for Ammonia Quantification in Nitrogen Electroreduction Experiments: The Correction of Iron III Interference. *J. Electrochem. Soc.* **2020**, 167 (13), 134519. https://doi.org/10.1149/1945-7111/abbdd6.

(43)   Zhao, W.; Qin, J.; Teng, W.; Mu, J.; Chen, C.; Ke, J.; Huang, J. C.; Liu, B.; Wang, S. Catalytic Photo-Redox of Simulated Air into Ammonia over Bimetallic MOFs Nanosheets with

Oxygen Vacancies. *Appl. Catal. B Environ*. **2022**, 305, 121046. https://doi.org/10.1016/j.apcatb.2021.121046.

(44)   Wei, X.; Wen, X.; Liu, Y.; Chen, C.; Xie, C.; Wang, D.; Qiu, M.; He, N.; Zhou, P.; Chen, W.; Cheng, J.; Lin, H.; Jia, J.; Fu, X.-Z.; Wang, S. Oxygen Vacancy-Mediated Selective C–N Coupling toward Electrocatalytic Urea Synthesis. *J. Am. Chem. Soc*. **2022**, 144 (26), 11530–11535. https://doi.org/10.1021/jacs.2c03452.

Chapter 2

Electrochemical synthesis of urea from carbon dioxide and nitrite at cobalt phthalocyanine-ion liquid electrodes

2.1 Statement of co-authorship

This chapter, excluding subsections 2.5.4 to 2.5.7, has been submitted under the above title to the J. Electrochem. Soc. It is presented here in a modified format that includes all contributions for completeness and context. This was a collaborative research study between the following co-authors:

Mona Bornak,[a] Jasmeen Akther,[a] Chaojie Song,[b] Khalid Fatih,[b] T. Jane Stockmann,*[a] and Peter G. Pickup*[a]

[a] Department of Chemistry, Memorial University of Newfoundland, St. John's, NL, A1B 3X7, Canada.

[b] Energy, Mining and Environment, National Research Council Canada, 4250 Wesbrook Mall, Vancouver, BC, V6T 1W5, Canada

* Corresponding authors

E-mail: tstockmann@mun.ca

E-mail: ppickup@mun.ca

2.2 Author contributions

M. B.: Experimental work, formal analysis, investigation, validation, writing—original draft, review & editing. J. A.: Contribution to the experimental work, some parts of formal analysis, investigation, and validation, writing—review & editing. C. S.: Project administration, investigation, review & editing, funding acquisition. K. F.: Project administration, investigation, review & editing, funding acquisition. T. J. S.: Conceptualization, methodology, writing—original draft, writing—review & editing, validation, supervision, project administration, funding acquisition. P. G. P.: Conceptualization, methodology, writing—original draft, writing—review &

19

editing, validation, supervision, project administration, funding acquisition. All authors have read and agreed to the submitted version of the manuscript.

2.3 Introduction

Environmental concerns and the need for more sustainable production of fuels, commodity chemicals, and fertilizers has prompted massive growth in research on the electrochemical reduction of CO_2, N_2, and nitrogen pollutants.[1] Coreduction of CO_2 with nitrite to produce urea is a particularly attractive process because it can remove two serious pollutants from the environment while producing a high value product.[2-4]

Shibata et al.[5] demonstrated in 1995 that urea could be generated by coreduction of CO_2 and NO_2^- under ambient conditions at Cu loaded gas diffusion electrodes. Subsequently, they showed that a variety of other metals were effective for this process,[6] and that metallophthalocyanines could also produce substantial yields of urea.[7] $FeTiO_3$ nanoparticles,[8] Cu doped TiO_2,[9] Te doped Pd,[10] AuCu nanofibers, and ZnO nanosheets [11] have also been shown to produce urea from coreduction of CO_2 and NO_2^-. A faradaic efficiency (yield) of 43% has been reported at a rate of 21 $\mu mol\ h^{-1}$ for Cu doped TiO_2 at -0.4 V vs RHE.[9]

Selectivity for the formation of urea from CO_2 and NO_2^- is determined by both the catalyst and the matrix used to support and immobilise it within the catalyst layer. Shibata et al.[7,12] employed gas diffusion electrodes with a hydrophobic carbon black layer on the gas side and a hydrophilic carbon black layer in contact with an aqueous 0.2 M $KHCO_3$ + 0.02 M KNO_2 electrolyte. In contrast, Cao et al.[9] and Feng et al.[10] simply drop cast their Cu doped TiO_2 and Te doped Pd catalysts onto carbon paper and glassy carbon, respectively, with Nafion as a binder. Liu et al.[13] also used Nafion to bind AuCu nanofibers to carbon paper, while Siva et al.[8] applied a paste of $FeTiO_3$ mixed with polyvinylidene fluoride and N-methyl-2-pyrrolidone to a stainless-steel plate.

Incorporation of ionic liquids (IL) into catalyst layers offers greatly increased scope for manipulation of the microenvironment within which electrocatalytic reactions occur, including the local hydrophobicity/hydrophilicity in the vicinity of the catalyst. When employed over a solid, often nanoparticle/nanoporous catalyst it is sometimes referred to as a 'solid catalyst with ionic liquid layer' (SCILL).[14,15] An IL layer can also be used to select for certain reaction pathways/products as well as lower the overall thermodynamic energy barrier or improve the

reaction kinetics. Indeed, Zhang et al.[16] employed a layer of 1-butyl-3-methylimidazolium bis(trifluoromethylsulfonyl)imide (BMImNTf$_2$) IL over a Cu-foam nanocatalyst to select and investigate different CO_2 reduction reaction pathways. The authors discovered that CO_2 reduction pathways involving a carbene intermediate could be suppressed using the IL layer, i.e., mechanisms generating ethanol or n-propanol.[16] Meanwhile, Suryanto et al.[17] demonstrated the catalytic properties of trihexyltetradecylphosphonium bis(trifluoromethylsulfonyl)imide (P$_{66614}$NTf$_2$) IL, in which the phosphonium cation catalyzes NH_3 electrogeneration from N_2 through a ylide intermediate. Earlier work from MacFarlane's group utilized a similar IL; however, they swapped the NTf_2^- anion for tris(pentafluoroethyl)trifluorophosphate (eFAP), i.e., P$_{66614}$eFAP. MacFarlane and coworkers [18] were able to achieve as high as 60% faradaic efficiencies, which they credit to the combination of the hydrophobic IL, which has a high N_2 solubility, and the nanoporous Fe electrocatalyst.

Other reports have used SCILL in combination with molecular or metal nanoparticle catalysts for NO_2^- reduction, which is a more thermodynamically favourable starting point than direct N_2 reduction when operating in aqueous environments. Su et al. [19] employed a 1-butyl-3-methylimidazolium ferricyanide IL with a poly(3-(aminopropyl)trimethoxysilane) layer for NO_2^- reduction in a sensor, while Li et al.[20] used a mixture of TiO_2, 1-butylpyridinium hexafluorophosphate (BuPyPF$_6$), and graphite powder as a carbon paste electrode for NO_2^- oxidation and electrochemical analysis.

Here we have investigated the SCILL effects of P$_{66614}$NTf$_2$, a hydrophobic IL, and BuPyPF$_6$, a hydrophilic one, on coreduction of CO_2 and NO_2^- at a carbon supported cobalt phthalocyanine catalyst (CoPc/C). Addition of these IL and their mixtures to the catalyst layer allows the hydrophobicity of the CoPc microenvironment to be controlled, which influences activity and product selectivity.

2.4 Experimental

2.4.1 Catalyst preparation

Carbon black (CB) (100 mg; Vulcan XC-72; Cabot) was dispersed in tetrahydrofuran (5 mL; THF; 99.9%; Sigma Aldrich) by sonication for 1 h. Cobalt (II) phthalocyanine (10 mg; 97%; Sigma Aldrich) in THF (1 mL) was then added and the mixture was sonicated for 2 h. The solvent was

allowed to evaporate at room temperature in a fume hood overnight, and then the catalyst was dried in an oven at 80 °C for 1 h. A CoPc/Cu/C, CoPc/Pd/C, CoPc/Rh/C, CoPc/Ir/C, CoPc/TiO$_2$, and CoPc/G catalyst were prepared using the same method, with the only difference being the substitution of carbon black with commercial carbon-supported Cu, Pd, Rh, and Ir catalysts, titanium dioxide nanoparticles, and graphene nanoplatelets (Cu/C; 40% Cu on Vulcan carbon; Fuel Cell Store), (Pd/C; 40% Pd on Vulcan carbon; Fuel Cell Store), (Rh/C; 20% Rh on Vulcan carbon; Fuel Cell Store), (Ir/C; 20% Ir on Vulcan carbon; Fuel Cell Store), (Titanium(IV) oxide, Aeroxide(R) P25, ThermoScientific™; rutile; 35 to 65 m²/g), and (Graphene nanoplatelets grade 4 > 500 m²/g Sigma Aldrich), respectively.

X-ray diffraction (Figure A1 in Appendix A) of the CoPc/C catalyst showed very small peaks for crystalline CoPc, indicating good dispersion of the CoPc molecules over the carbon surface. This was supported by transmission electron microscopy (Figure A2 in Appendix A), which shows no evidence of CoPc particles.

2.4.2 Electrode preparation

CoPc/C, Cu/C, CoPc/Cu/C, Pd/C, CoPc/Pd/C, CoPc/Rh/C CoPc/Ir, CoPc/TiO$_2$ and CoPc/G (10 mg) and the IL (10 mg; P$_{66614}$NTf$_2$ (≥95.0%, Sigma Aldrich), and/or BuPyPF$_6$ (98.0+%, Fisher Scientific)) were dispersed in 0.3 mL of THF and 2-propanol (1:1 volume ratio) by sonication for 1 h to form a uniform catalyst ink. The ink was drop coated onto glassy carbon (GC; 0.071 cm^2; CH Instruments) or carbon fiber paper (CFP; 1 cm^2; TGP-H-090 Toray industries-total thickness of 280 µm) electrodes to give a catalyst loading of 1.5 mg cm^{-2} and IL loading of 1.5 mg cm^{-2} (or 0.75 mg cm^{-2} for Figures 2.1 and 2.2). Electrodes prepared on CFP with a mixture of the two IL were heated in an oven for 30 min at 75 °C to improve stability. SEM images (Figure A3) show that uniform catalyst layers were formed on the CFP electrodes when the mixed IL was employed.

Nafion containing electrodes were generated similarly using an ink prepared by dispersing 10 mg of CoPc/C in a mixture of H$_2$O (150 µL), 2-propanol (75 µL; 99.5% ACS grade; Caledon), and of a 5% Nafion^{TM} solution (75 µL; 5.14 mass% in a mixture of lower aliphatic alcohols and 51.9% water; Dupont) followed by sonication for 3 h. The CoPc/C and Nafion loadings were 1.5 mg cm^{-2} and 0.5 mg cm^{-2}, respectively.

Electrode with supporting layer (SL) were improved by applying a carbon black support layer (SL) with a density of 1 mg/cm^2 to the CFP before deposition of the catalyst ink. To create the SL,

10 mg of carbon black was dispersed in 100 μL of 2-propanol and sonicated for 30 min, resulting in a well-dispersed SL solution. The SL was then applied to clean and dry CFP substrates using a pipette, ensuring a uniform distribution for maximum effectiveness.

2.4.3 Electrochemistry.

Electrochemical measurements were made at ambient temperature in a glass cell with a Pt counter electrode and a saturated calomel reference electrode (SCE; 0.241 V vs SHE). Potentials are reported relative to RHE (reversible hydrogen electrode), at -0.486 V vs SHE under N_2 (pH = 8.30) or -0.395 V vs SHE under CO_2 (pH = 6.75). CV is conducted with a scan rate of 10 mV s^{-1}. The working and counter electrode compartments were separated by a porous glass frit. All measurements were made in aqueous 0.1 M $NaHCO_3$ at an ambient temperature of ca. 20 °C. All the applied working electrodes are carbon fiber paper (CFP) ones unless otherwise stated.

2.4.4 Product analysis

Urea and ammonia in the electrolysis solutions were measured by UV-Vis spectrophotometry by the salicylate [21] and diacetyl monoxime (DAM) methods,[22, 23] respectively, as described in the following sections. For urea analysis, it was necessary to deionize samples prior to analysis to prevent interference from NO_2^-.[24]

Analysis of urea and ammonia: Urea concentrations in electrolysis solutions were determined by using the DAM spectrophotometric method. To prepare the standard solutions of urea, a daily mixture of 0.1 M $NaHCO_3$ and 5 mM $NaNO_2$ was used. Freshly prepared DAM solution (50.0 g L^{-1}) and thiosemicarbazide (TSC) solution (2.0 g L^{-1}) in DI water were employed. Additionally, a $Fe_2(SO_4)_3$ solution (600 mg L^{-1}) was prepared by dissolving $Fe_2(SO_4)_3$ in a 5% H_2SO_4 solution (v/v) to prevent hydrolytic decomposition. This solution was stored in an amber glass bottle at 4°C.

Before analyzing the urea samples, both the standard solutions and the samples were deionized using a 0.8 x 4 cm polypropylene column (Poly-Prep® Chromatography Columns; Bio-Rad) filled with 1.00 g (1.7 mL bed volume) of biotechnology grade mixed bed ion exchange resin (AG® 501-X8; Bio-Rad). After deionization, 2 mL aliquots of the standards and samples from electrolysis were placed in 20 mL glass vials. Subsequently, freshly prepared solutions of DAM (0.225 mL), TSC (0.0375 mL), $Fe_2(SO_4)_3$ (0.0375 mL), and 50% H_2SO_4 (2 mL) were added sequentially. The resulting mixture was diluted to a final volume of 5 mL and heated for 30 minutes

in a water bath at 90°C, followed by cooling to room temperature. Using an Agilent Cary 100 spectrophotometer, the absorbance of the resulting red compound was measured at 520 nm against a reagent blank at room temperature [24]. To avoid interference from nitrite, samples were deionized with mixed bed ion exchange resin AG 501-X8 Mixed Bed Resin, analytical grade; Bio-Rad) prior to analysis. Freshly prepared solutions of 2,3-butanedione monoxime (99%; Sigma-Aldrich; 0.225 mL at 50.0 g l^{-1}), thiosemicarbazide (98%, puriss. p.a; Sigma-Aldrich; 0.0375 mL at 2.0 g L^{-1}), $Fe_2(SO_4)_3$ (97%; Sigma-Aldrich; 0.0375 mL at 600 mg L^{-1} in 5% H_2SO_4) and 50% H_2SO_4 (98%, ACS grade; Fisher Scientific; 2 mL) were added sequentially to 2 mL aliquots of the deionized sample. The resulting mixture was diluted to 5 mL, heated for 30 min in a water bath at 90 °C and cooled to ambient temperature. The absorbance was measured at 520 nm using a double beam Agilent Cary 100 UV–vis Spectrophotometer.

Ammonia concentrations were determined by the salicylate spectrophotometric method. [25] Salicylic acid (0.1 g; ⩾99.0% ACS grade; Sigma-Aldrich) and trisodium citrate dehydrate (0.1 g; reagent grade; Sigma-Aldrich) in 2 mL of 1 M NaOH (97% ACS grade; BDH), sodium hypochlorite solution (0.07 mL in 0.93 mL DI water; reagent grade, available chorine 4.00%–4.99%; Sigma-Aldrich), and sodium nitroferricyanide (2 mg; ⩾99% ACS grade; Sigma-Aldrich), in 0.2 mL of DI water, were added sequentially to each sample. Following dilution to 10 mL with DI water, and 2 h in the dark at ambient temperature, the absorbance of each solution was measured 655 nm.

2.5 Results and discussion

2.5.1 Electrodes modified with ILs and CoPc/C catalysts

Initially, glassy carbon (GC) electrodes were used to characterize the effects of the IL on the electrochemistry of the CoPc complex and electrochemical reduction of CO_2 and NO_2^-, in comparison with Nafion as a binder. Figure 2.1 shows voltammograms in 0.1 M $NaHCO_3$ under N_2.

Individually, the $P_{66614}NTf_2$ and $BuPyPF_6$ IL gave poor quality voltammograms relative to Nafion, with no clear redox wave for the Co (II/I) couple, which appears at a formal potential ($E^{0\prime}$) of 0.08 V with the Nafion binder. In contrast, a 1:3 mixture (by mass) of $BuPyPF_6$ and $P_{66614}NTf_2$

was found to produce a reversible wave at $E^{0\prime} = 0.59$ V. The positive shift of the Co(II/I) formal potential relative to the Nafion containing electrode demonstrates that the IL mixture substantially changes the environment of the CoPc complex, with the more positive potential characteristic of a more hydrophobic (less aqueous environment). [26] Suppression of the current at potentials below ca. -0.3 V by the ionic liquids is also consistent with a more hydrophobic environment and indicates that the catalyst is coated with a layer of IL (i.e., that it is a SCILL). This is supported by the TEM image shown in Figure A4 of Appendix A.
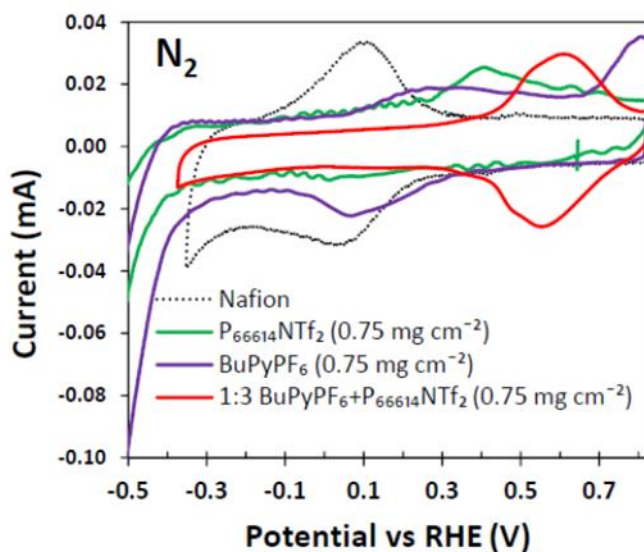
Figure 2.1 *Cyclic voltammograms for GC electrodes modified with Nafion, BuPyPF$_6$ and/or P$_{66614}$NTf$_2$ as a binder and CoPc/C as catalyst in 0.1 M NaHCO$_3$ under N$_2$.*

Cyclic voltammograms for electrodes prepared with a 1:3 mixture of BuPyPF$_6$ and P$_{66614}$NTf$_2$ (mixed IL) in 0.1 M NaHCO$_3$, with and without 5 mM NaNO$_2$ under N$_2$ and CO$_2$, are shown in Figure 2.2. Changing the purge gas from N$_2$ to CO$_2$ in the absence of NO$_2^-$ caused a -0.09 V shift of the Co(II/I) peaks due to the effect of the decrease in pH from formation of H$_2$CO$_3$ in the electrolyte solution (i.e., there was not a significant change vs. SCE). There was only a small increase in the cathodic current at potentials below ca. -0.3 V, indicating that there was not significant reduction of CO$_2$ at potentials above -0.4 V.
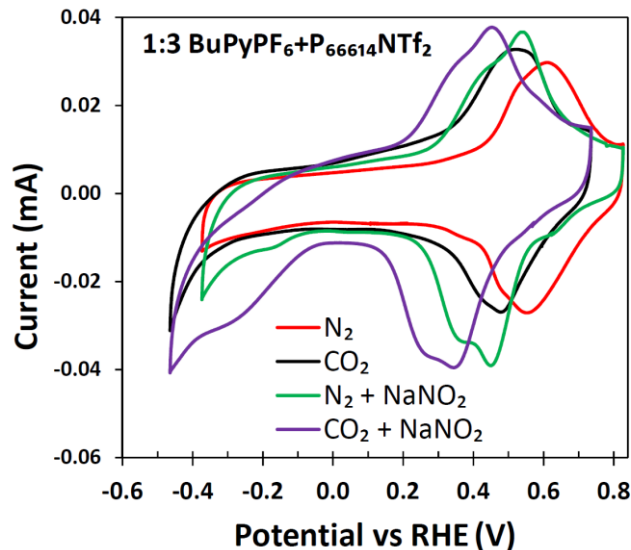
Figure 2.2 Cyclic voltammograms for GC electrodes modified with the mixed IL (BuPyPF$_6$+P$_{66614}$NTf$_2$) as a binder and CoPc/C as catalyst in 0.1 M NaHCO$_3$ with and without 5 mM NaNO$_2$ under N$_2$ and CO$_2$.

When NO_2^- was added to the electrolyte, the Co (II/I) redox waves changed substantially under both N$_2$ and CO$_2$, with a significant shift to lower potentials and splitting into a peak and a shoulder. This suggests that there was coordination of NO_2^- to an axial site of the CoPc.[27] Under N$_2$, there was a new reduction wave starting at ca. −0.1 V that can be attributed primarily to reduction of NO_2^- to NH$_3$.[7]

When both NO_2^- and CO$_2$ were present there was a large increase in current at potentials below –0.05 V, with a shoulder at −0.3 V that was more than double the current at this potential for either NO_2^- or CO$_2$ alone. This suggests that there was coreduction of NO_2^- and CO$_2$ in addition to their individual reduction processes. A previous report has demonstrated that urea is produced under these conditions, in addition to CO and NH$_3$.[7]

In order to determine product yields, 1 cm^2 carbon fibre paper (CFP) electrodes were used for electrolysis of NO_2^- and CO$_2$ in 0.1 M Na$_2$CO$_3$. A new electrode was used for each 2 h electrolysis experiment, and a cyclic voltammogram was recorded in the electrolysis solution before each electrolysis. Figure 2.3A shows these initial voltammograms for electrodes prepared with Nafion, BuPyPF$_6$, and a 1:3 mixture of BuPyPF$_6$ and P$_{66614}$NTf$_2$. The electrode prepared with the BuPyPF$_6$ and P$_{66614}$NTf$_2$ mixture was heated at 75 °C for 30 min before use to improve stability, and this resulted in significant changes in the voltammogram relative to the GC electrode shown in Figure

26

2.2. Notably, the onset of coreduction of NO_2^- and CO_2 shifted to lower potentials, implying that melting of the IL mixture increased its coverage of the catalyst surface.

The voltammograms in Figure 2.3A demonstrate a very strong dependence of the catalyst activity on its environment, and that $BuPyPF_6$ and $P_{66614}NTf_2$ are very effective for manipulation of the microenvironment and activity, demonstrating SCILL character. Whereas $BuPyPF_6$ alone increased activity for the coreduction of NO_2^- and CO_2 and shifted the reduction wave to less negative potentials (lower overpotentials), the mixed IL greatly suppressed activity and increased the overpotential. Presumably, the opposite effects of the hydrophobic and hydrophilic IL influence the activity of the catalyst differently for each reaction pathway (i.e., for formation of urea, ammonia, CO, H_2, etc.) and this offers a larger scope for manipulating reaction selectivity.
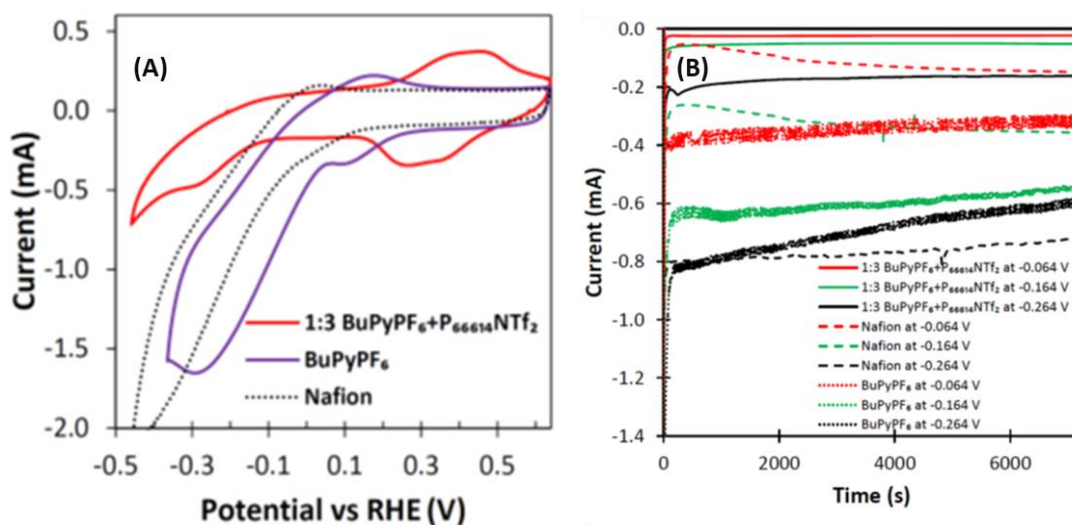
Figure 2.3 (A) CVs for CFP electrodes modified with Nafion, $BuPyPF_6$ and/or the mixed IL as a binder and CoPc/C as catalyst in 5 mM $NaNO_2$ under CO_2 in 0.1 M $NaHCO_3$ (B) current vs time plot at potentials indicated inset for the electrolysis of the same solution and the aforementioned electrodes.

Selectivity for the formation of urea and ammonia ($NH_3 + NH_4^+$) was determined by analysis of samples prepared by constant potential electrolysis (2 h) of 5 mM $NaNO_2$ under CO_2. Figure 2.3B shows current vs time curves at three different potentials, and Figures 2.4A and 2.4B show faradaic efficiencies and rates for formation of urea and ammonia, respectively. Average currents and concentrations of urea and ammonia are shown in Table A1 in Appendix A.

The effects of the IL on the electrolysis current are broadly consistent with those seen in CV with $BuPyPF_6$ (dotted lines in Figure 2.3B) providing higher currents than Nafion (dashed lines) at all three potentials, and the mixed IL providing much lower currents (solid lines). However,

rates of urea formation (Figure 2.4A) show a much different effect of the mixed IL. The rate at −0.064 V was much higher than for Nafion, and rates were similar for the three electrodes at −0.164 V. This shows that the mixed IL greatly increases selectivity for formation of urea, particularly at higher potentials (lower overpotential). This is quantified by the faradaic efficiencies in Figure 2.3B. Whereas the Nafion and $BuPyPF_6$ electrodes produced urea with very low efficiency (1.1% to 3.8%) at all three potentials, the mixed IL produced urea with efficiencies of 25.3% at −0.064 V and 13.8% at −0.164 V. The highest efficiency was obtained at the lowest overpotential, resulting in a considerable enhancement of overall energy efficiency.
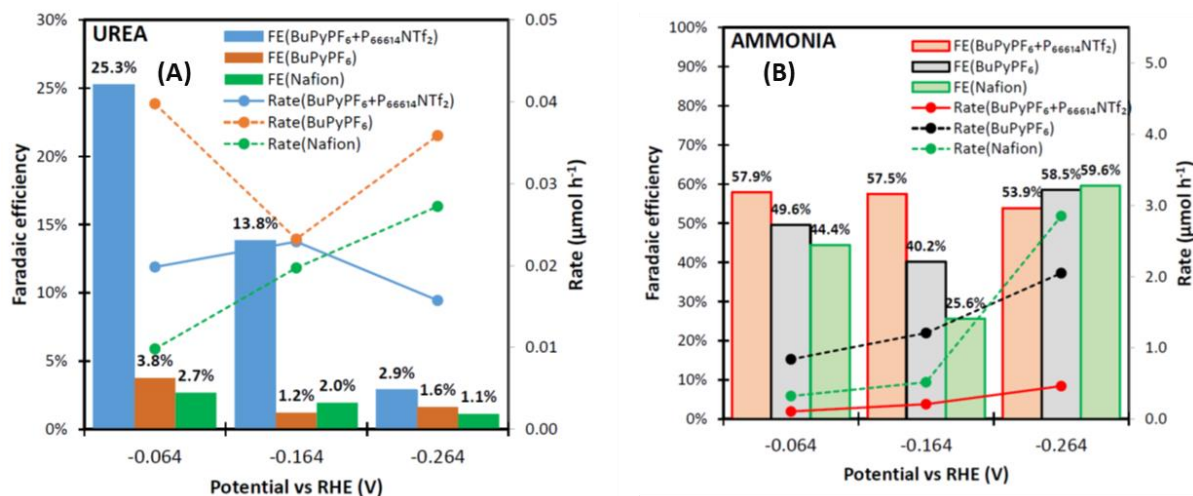
Figure 2.4 Faradaic efficiencies (FE) and rates for formation of (A) urea and (B) ammonia from electrolysis of 5 mM $NaNO_2$ under CO_2 in 0.1 M $NaHCO_3$ at CFP electrodes with CoPc/C as a catalyst with different IL or Nafion ink formulations as shown inset.

In contrast to urea, rates of ammonia production did follow the trends seen in the electrolysis currents, resulting in similar faradaic efficiencies for the three electrode types (Figure 2.4B). On average the mixed IL gave slightly higher efficiencies than $BuPyPF_6$, while the lowest efficiency was obtained with Nafion at the intermediate potential (−0.164 V). It is notable that the mixed IL electrode gave a very high combined faradaic efficiency of 83% for formation of urea plus ammonia.

2.5.2 CFP electrodes modified with ILs and Cu/C and CoPc/Cu/C catalysts

Although the mixed IL greatly increases the efficiency for urea production from coreduction of NO_2^- and CO_2 at CoPc/C electrodes, rates of urea and ammonia production are too low for practical applications. Shibata and Furuya[7] have shown that the efficiency of urea formation at metal (M) phthalocyanine electrodes depends on the rates of formation of intermediates from both

NO_2^- and CO_2 reduction. Their proposed mechanism for coupling of adsorbed PcM–CO and PcM–NH_2 intermediates has been applied in a number of more recent studies,[3, 9, 13, 28, 29] and serves as a starting point for the design of more active and selective catalysts and electrode structures.

CoPc can reduce CO_2 to a PcCo–CO intermediate bound in one of the axial positions, or NO_2^- to PcCo–NH_2. However, formation of both simultaneously and their coupling requires two CoPc molecules in a suitable (co-facial) arrangement and is therefore very slow. Higher rates could be possible by reaction of the PcCo-NH_2 and/or PcCo-CO intermediates with -NH_2 and/or -CO intermediates on a second catalyst (co-catalyst). [28, 29] Here Cu metal nanoparticles on a carbon black support were employed as a co-catalyst, since Cu and Cu alloys have been shown to be effective for production of urea from NO_2^- and CO_2.[5, 13]

Cu/C and CoPc/Cu/C catalyst on CFP electrodes with the mixed IL binder (1:3 mixture of $BuPyPF_6$ and $P_{66614}NTf_2$) were prepared in the same way as CFP electrodes modified with mixed IL ($BuPyPF_6$ + $P_{66614}NTf_2$) as a binder and CoPc/C as catalysts by using a commercial Cu/C catalyst in place of carbon black. Figure 2.5A shows cyclic voltammograms for 5 mM $NaNO_2$ under CO_2. Currents at the Cu/C catalyst were much higher than at the CoPc/C catalyst, and somewhat higher than those at the $BuPyPF_6$ and Nafion electrodes in Figure. 2.3A. Adsorption of CoPc onto the Cu/C catalyst (CoPc/Cu/C) decreased the current significantly, but it remained much higher than for CoPc/C($BuPyPF_6$+$P_{66614}NTf_2$).
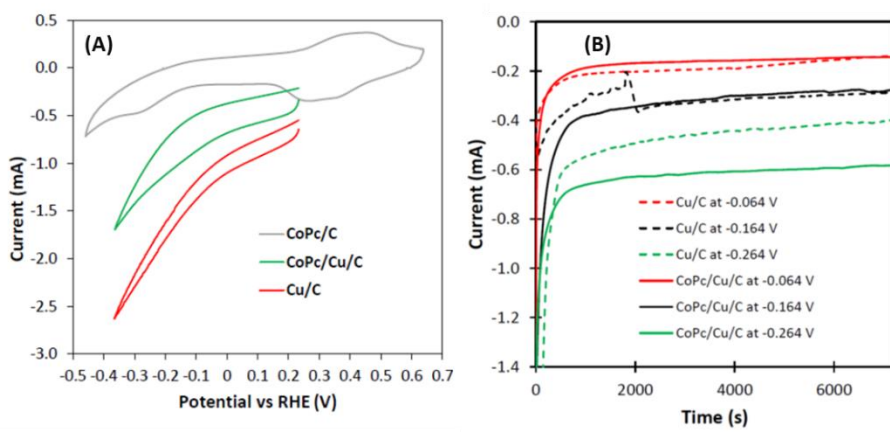
Figure 2.5 (A)Cyclic voltammograms performed at the electrodes modified with mixed IL as a binder and CoPc/C, Cu/C and CoPc/Cu/C as catalysts in 5 mM NaNO2 and 0.1 M NaHCO3 under CO2. (B) Current vs time plot for electrolysis of the same solution and electrodes.

Figure 2.5B shows current vs time plots for electrolysis of 5 mM $NaNO_2$ under CO_2 at Cu/C ($BuPyPF_6$ + $P_{66614}NTf_2$) and CFP electrodes modified with mixed IL ($BuPyPF_6$ + $P_{66614}NTf_2$) as a binder and CoPc/Cu/C as catalysts. In contrast with the voltammetric data, currents were similar for the Cu/C and CoPc/Cu/C catalyst at the two highest potentials, and highest for the CoPc/Cu/C catalyst at −0.264 V. This indicates that the voltammograms were dominated by short term activity, which was also indicated by decreasing currents on successive cycles (not shown). Nevertheless, both sets of electrodes provided much higher currents than electrodes with CoPc/C as a catalyst (Figure 2.3B). In particular, the average current of −0.173 mA at –0.064 V for the electrode with CoPc/Cu/C catalyst was nearly 7 times higher than for the electrode with CoPc/C in Figure 2.4 (−0.025 mA). Average currents and concentrations of urea and ammonia are shown in Table A2 of Appendix A.

The higher currents at the CoPc/Cu/C catalyst provided much higher rates for production of urea (Figure 2.6A) and ammonia (Figure 2.6B), and the faradaic efficiency for ammonia was also increased (Figure. 2.6B). The Cu/C catalysts also provided higher rates and efficiencies for ammonia production than for CoPc/C catalyst. However, faradaic efficiencies for urea formation at CoPc/Cu/C catalyst were substantially lower than for CoPc/C catalyst, and very low ($\leq$ 3.7%) for Cu/C catalyst. Nonetheless, the goal of increasing the rate of urea production has been achieved by combining CoPc catalyst with a Cu co-catalyst, and a 335% increase in rate at −0.064 V was obtained at the expense of only a 36% decrease in faradaic efficiency.
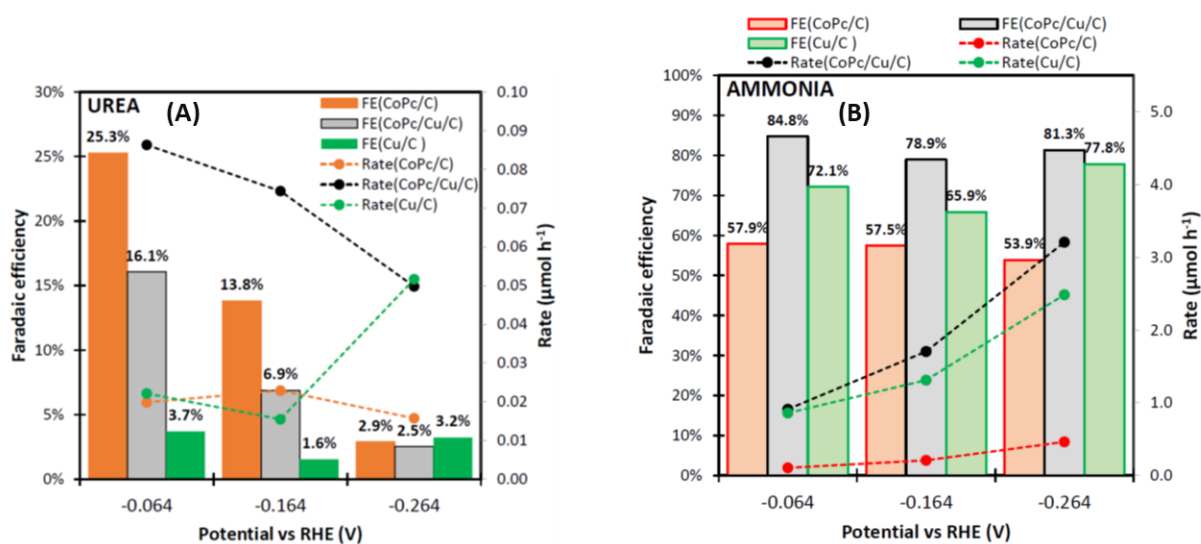
Figure 2.6 Faradaic efficiencies and rates for formation of (A) urea and (ammonia) from electrolysis of 5 mM $NaNO_2$ under CO_2 in 0.1 M $NaHCO_3$ at CFP electrodes modified with mixed IL as a binder and CoPc/C, Cu/C and CoPc/Cu/C as catalysts.

2.5.3 Proposed mechanism of coreduction of CO_2 and NO_2^- on the CoPc/C and CoPc/Cu/C catalysts

Coreduction of CO_2 and NO_2^- involves many different reactions that produce numerous products.[1, 4, 30] In most cases the primary products (CO, NH_3, H_2, etc.) arise from the reduction of CO_2 and NO_2^- (and H_2O) separately,[9, 10] without coupling to form urea and other C-N containing products. There are a multitude of factors involved in determining the rates of the reaction pathways, and therefore the activity and selectivity of a particular catalyst,[27] and the influence of the catalyst environment.[30]

The selectivity of a specific catalyst for production of urea depends on the reaction pathways and mechanisms, which vary between catalysts, and the populations and locations of key intermediates.[28] For CoPc catalyst (and other metal phthalocyanines), Shibata and Furuya[7] proposed a Langmuir−Hinshelwood-type mechanism in which metal bound –NH_2 and –CO intermediates couple to produce urea (eq. 2.1).

$$2\ PcCo\text{-}NH_2 + PcCo\text{-}CO \rightarrow (NH_2)_2CO + 3\ CoPc \qquad (2.1)$$
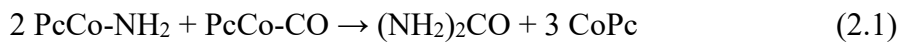
Although this is not possible with isolated phthalocyanine molecules,[28] it could occur at pairs of phthalocyanine molecules in approximately co-facial orientations. Alternatively, urea can be formed through an Eley−Rideal mechanism in which Co-NH_x species couple with free CO_2,[28] or by reaction with –CO bound to the catalyst support.[31]

The rates of each of these proposed mechanisms will be strongly influenced by the environment of the CoPc molecules, and its influence on their electronic structure, arrangement (e.g., aggregation vs adsorption on the carbon support), mobility (e.g., via solubilization), and the mobility and local concentrations/activities of reactants and products.[30, 32] The cyclic voltammograms in Figure 1 and chronoamperometry (CA) in Figure 2.4 show that the IL employed in this work cause major changes in the environment of the CoPc catalyst and will have a significant influence on all of these properties and processes. Most notably, the shift in $E^{0\prime}$ for the Co (II/I) couple (Figure 2.1) show a strong electronic effect, while suppression of the current obtained during electrolysis shows decreased mobility and activity of reactants.

In terms of changing the faradaic efficiency for urea production, the higher solubility of CoPc in ionic liquids than water[33] may be the key factor. It would increase the concentration of mobile CoPc molecules and result in a higher rate for Langmuir−Hinshelwood-type (eq. 2.1) and other mechanisms via dynamic formation of coupling sites. In addition, the effect of the IL on CO_2 solubility may promote urea formation.[30] Other ways in which the IL could increase urea production, relative to ammonia, are by decreasing the concentration of NO_2^- within the catalyst layer and decreasing H^+ and H_2O activity, which would decrease the rate of ammonia formation. The role of IL hydrophobicity towards decreasing access of water and the reactants is illustrated in Figures 1 and 3, where currents were decreased greatly when the mixed IL was used. This decreased the rate of ammonia formation greatly, relative to using the $BuPyPF_6$ IL alone, but had a much smaller effect on the rate of urea formation.

The effects of Cu on the rate of urea formation can be attributed in part to its ability to catalyze the coreduction of NO_2^- and CO_2 to urea.[9, 13, 28] However, the results in Figure 2.6A show that this was only significant at −0.264 V. At lower potentials, there was a substantial synergistic effect. This suggests that the $–NH_x$ and –CO reactive intermediates that produce urea were formed at Cu and Co sites, respectively. Coupling to form urea (eq. 2.2), could then occur at CoPc molecules adsorbed on, or close to, the Cu surface.

$$2\ Cu\text{-}NH_x + PcCo\text{-}CO + (4\text{-}2x)\ H^+ \rightarrow (NH_2)_2CO + 2\ Cu + CoPc \qquad (2.2)$$
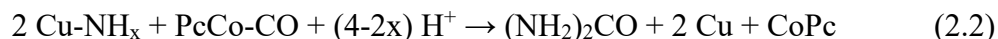
The much higher rates of ammonia formation at Cu/C relative to CoPc/C in Figure 2.6B indicate that the alternate reaction, between $PcCo\text{-}NH_2$ and Cu-CO is much less likely. In addition, it has been shown that the favoured mechanism for urea formation at Cu is via coupling of CO_2 with $Cu\text{-}NH_x$ species.[27] The strong synergistic effect seen here suggests that reaction 2.2 is more favorable.

2.5.4 Other carbon supported metal nanoparticles as co-catalysts

Additional commercially available activated carbon supported nanoparticles were investigated as co-catalysts, including Pd/C, Rh/C, and Ir/C. Palladium metal nanoparticles supported on carbon (Pd/C) were chosen due to their favourable characteristics, including a high surface area and remarkable catalytic efficiency.[34] The preparation of CoPc/Pd/C, CoPc/Rh/C, and CoPc/Ir/C electrodes on CFP followed the same procedure as the CoPc/C electrode. A mixed IL binder comprising a 1:3 mixture of $BuPyPF_6$ and $P_{66614}NTf_2$ was employed, substituting carbon black with Pd/C, Rh/C, and Ir/C as the supporting materials. The utilization of various co-catalysts was

investigated in the electrochemical reduction of 5 mM $NaNO_2$ under CO_2 conditions in 0.1 M $NaHCO_3$. The following sections explore the preliminary results of these investigations.

2.5.4.1 Pd/C as co-catalyst

Figure 2.7A presents cyclic voltammograms recorded for 5 mM $NaNO_2$ under CO_2 at CFP electrodes modified with the mixed IL ($BuPyPF_6$ + $P_{66614}NTf_2$) combined with Pd/C, CoPc/Pd/C and CoPc/C catalysts. Notably, the CoPc/Pd/C catalyst exhibited significantly higher currents compared to the Pd/C and CoPc/C catalyst. This substantial increase in current can be attributed to the enhanced adsorption of CoPc on the Pd/C catalyst, highlighting the synergistic effect of the combined materials.
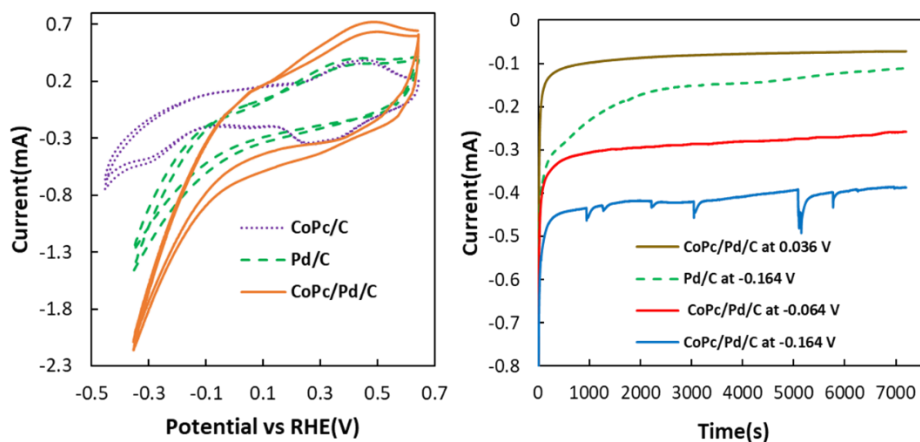
Figure 2.7 (A) CVs obtained using electrodes modified with mixed IL as a binder and catalysts (CoPc/C, Pd/C, and CoPc/Pd/C) in a solution containing 5 mM $NaNO_2$ and 0.1 M $NaHCO_3$ under CO_2. (B) i-t response for the same solution and electrodes with Pd/C and CoPc/Pd/C as catalysts with indicated potentials as shown in the inset.

Furthermore, Figure 2.7B illustrates the current versus time plots during the electrolysis of 5 mM $NaNO_2$ under CO_2 at the aforementioned electrodes. The CoPc/Pd/C catalyst (solid, blue trace) demonstrated higher currents than Pd/C catalyst (dashed, green curve) at the two highest potentials, as confirmed by CV. Moreover, the currents obtained with the CoPc/Pd/C catalyst were significantly greater than those observed with the CoPc/C catalyst (Figure 2.4). However, at the lowest potential, the current was lower than that of the Pd/C catalyst.

33

Table 2.1 presents the average currents and urea concentrations obtained from the electrolysis of 5 mM $NaNO_2$ under CO_2 in 0.1 M $NaHCO_3$ at CFP electrodes modified with mixed IL (BuPyPF$_6$ + P$_{66614}$NTf$_2$) as a binder and Pd/C and CoPc/Pd/C as catalysts over a 2-hour period. Notably, at an applied potential of 0.036 V vs. RHE, the CoPc/Pd/C catalyst exhibited the lowest average current. Nevertheless, it demonstrated the highest concentration of urea, the greatest faradaic efficiency, and the highest rate of urea formation (Figure 2.10). Conversely, the Pd/C catalyst displayed a higher average current but showed lower urea concentration and rate of urea formation at this potential. As the potential becomes more negative for the CoPc/Pd/C catalyst, the urea concentration decreases, with both faradaic efficiency and rate exhibiting a similar trend. Notably, the rate of urea formation for this catalyst surpasses that of CoPc/C catalyst at all potentials (Figure 2.10). These findings suggest that the addition of CoPc as a catalyst, combined with the Pd/C co-catalyst, significantly enhances the rate of urea production. This can be attributed to the adsorption of CoPc catalyst onto the surface of Pd/C nanoparticles, resulting in synergistic effects and an increased surface area of available active sites for the -NH$_x$ (to be adsorbed on Pd) and -CO (to be adsorbed on CoPc), which results in the heightened adsorption of nitrite and CO_2 species on the catalyst's surface.

Table 2.1 *Average currents and concentrations of urea for electrolysis of 5 mM NaNO$_2$ under CO$_2$ in 0.1 M NaHCO$_3$ at CFP electrodes modified with mixed IL (BuPyPF$_6$ + P$_{66614}$NTf$_2$) as a binder and Pd/C and CoPc/Pd/C as catalysts over 2 hours.*

Potential vs. RHE (V)	CoPc/Pd/C		Pd/C	
	Average current (mA)	Urea concentration (μM)	Average current (mA)	Urea concentration (μM)
0.036	−0.087	6.0	N/A	N/A
−0.064	−0.290	4.5	N/A	N/A
−0.164	−0.420	3.8	−0.192	2.6

2.5.4.2 Rh/C and Ir/C as co-catalysts

In addition to Pd/C nanoparticles, the utilization of Rh/C and Ir/C nanoparticles were explored as alternative commercial co-catalysts. Figure 2.8 presents cyclic voltammograms recorded for

CFP electrodes modified with an IL mixture ($BuPyPF_6 + P_{66614}NTf_2$) as a binder and CoPc/Rh/C, CoPc/Ir/C, and CoPc/C as catalysts in a 5 mM $NaNO_2$ under CO_2 in 0.1 M $NaHCO_3$. The CV results reveal a noticeable increase in current when Rh/C or Ir/C nanoparticles are employed as a co-catalyst compared to the CoPc/C catalyst. Additionally, the CoPc/Rh/C catalyst exhibits significantly higher current than the CoPc/Ir/C catalyst.
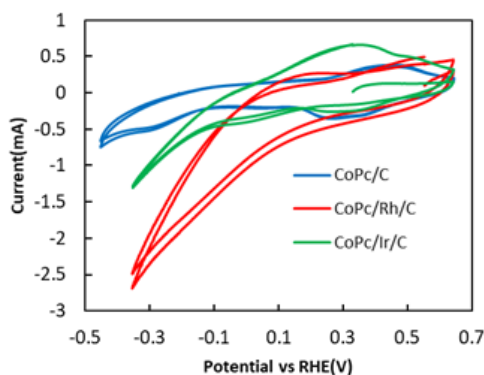
Figure 2.8 *CVs at electrodes modified with an IL mixture as a binder and CoPc/Rh/C, CoPc/Ir/C, and CoPc/C as catalysts in 5 mM $NaNO_2$ and 0.1 M $NaHCO_3$ under CO_2.*

Figure 2.9 depicts the current versus time plot obtained during the electrolysis of 5 mM $NaNO_2$ under CO_2 at CFP electrodes modified with the IL mixture ($BuPyPF_6 + P_{66614}NTf_2$) as a binder/co-catalyst. Interestingly, both CoPc/Rh/C and CoPc/Ir/C catalysts (solid lines) exhibited higher currents across all applied potentials compared to the CoPc/C catalyst (dash lines).
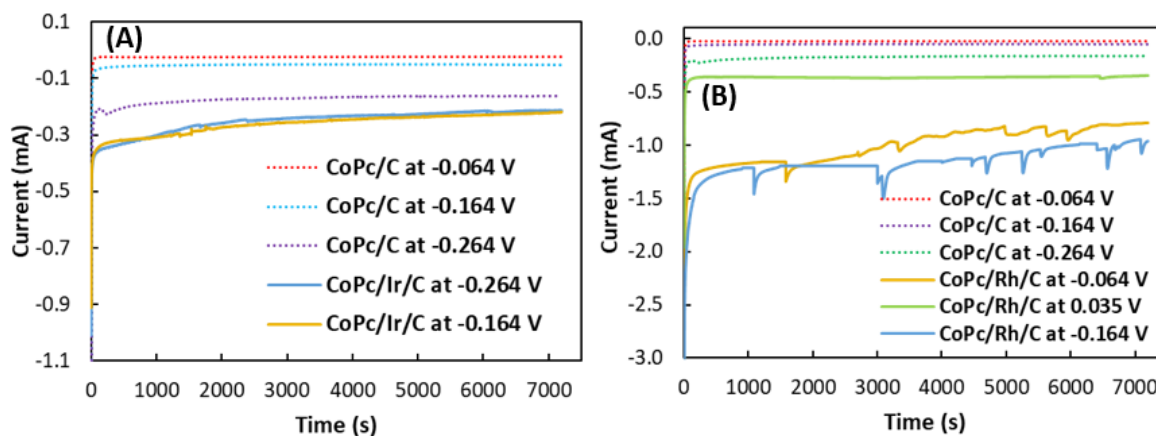
Figure 2.9 *CA responses recorded at potentials indicated inset for electrolysis of 5 mM $NaNO_2$ under CO_2 in 0.1 M $NaHCO_3$ at CFP electrodes modified with mixed IL as a binder and (A) CoPc/Ir/C and CoPc/C as catalysts, (B) CoPc/Rh/C and CoPc/C as catalysts.*

35

The chronoamperometry results revealed a significant enhancement in average current when utilizing CoPc/Rh/C as the catalyst, particularly as the applied potential became more negative. At the high over potential of –0.264 V, the average current reached was –1.16 A. Simultaneously, the concentration of urea displayed an incremental rise with increasingly negative potentials, reaching 6.0 µM at –0.0264 V (Table 2.2). However, the faradaic efficiency of urea formation remained notably low across all potentials, with the highest value observed at –0.064 V, reaching only 1.25%. Furthermore, the rate of urea formation exhibited an ascending trend, culminating at 0.04 µmol h^{-1} as shown in the aforementioned potential (Figure 2.10A).

In contrast, ammonia formation demonstrated distinct characteristics. The highest concentration of ammonia, amounting to 988 µM, was observed at –0.064 V, corresponding to the potential that yielded the highest rate of ammonia production at 6.0 µmol h^{-1} . Importantly, this potential also exhibited the highest faradaic efficiency, reaching an impressive 94.7% (Figure 2.10B).

The product analysis on the 5 mM NaNO$_2$ and 0.1 M NaHCO$_3$ solution after a 2-hour electrolysis utilizing on the CoPc/Ir/C catalyst demonstrates a minimal presence of urea, to the extent that its contribution can be considered negligible, at two specific potentials (–0.164 and –0.264 V) ((Table 2.2). Nevertheless, the highest recorded faradaic efficiency for ammonia formation was observed at –0.264 V, reaching a value of 12.5%. Additionally, the rate for ammonia formation is also observed to be very low (Figure 2.10B).

Table 2.2 Specifications of urea and ammonia formation using CoPc/Rh/C and CoPc/Ir/C catalysts. All other experimental parameters were the same as described in Table 2.1.

Potential vs. RHE (V)	CoPc/Rh/C			CoPc/Ir/C		
	Average current (mA)	Urea concentration (µM)	Ammonia concentration (µM)	Average current (mA)	Urea concentration (µM)	Ammonia concentration (µM)
0.036	−0.36	2.4	267	N/A	N/A	N/A
−0.064	−1.00	4.4	988	−0.260	No urea found	22.7
−0.164	−1.16	6.0	750	−0.250	No urea found	32.5

In summary, the utilization of CoPc as a catalyst, combined with different co-catalysts such as Pd/C, Rh/C, and Ir/C nanoparticles, demonstrated significant enhancements in current, and rates of urea formation, and ammonia formation under CO_2 conditions.
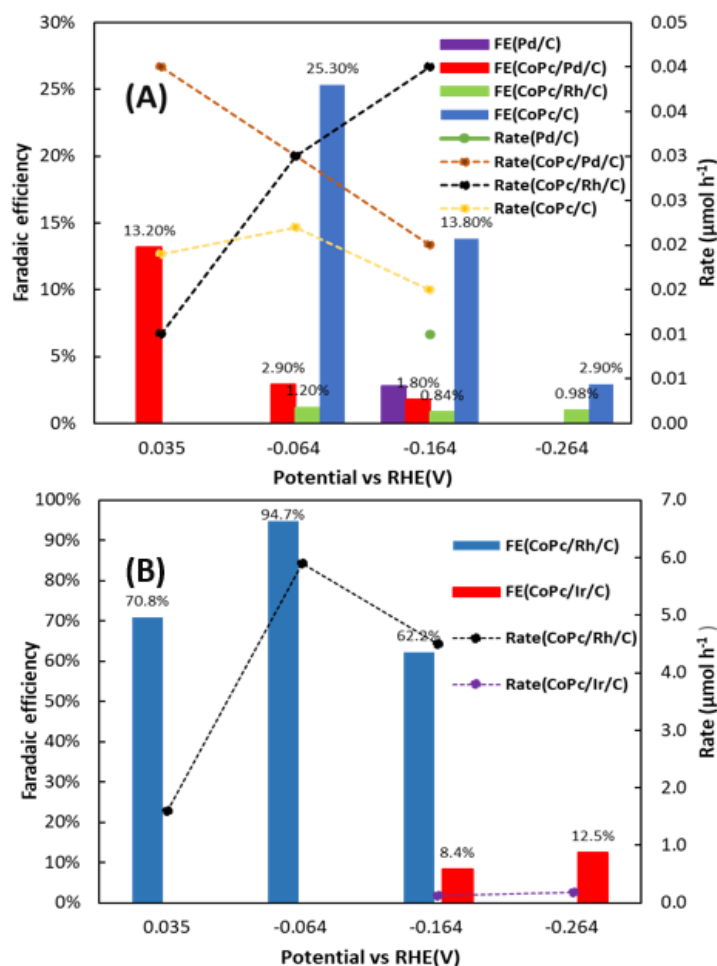
Figure 2.10 FE and formation rates of (A) urea and (B) ammonia during electrolysis utilizing diverse catalysts: CoPc/C, Pd/C, CoPc/Pd/C, CoPc/Ir/C and CoPc/Rh/C.

2.5.5 Application of carbon black as the supporting layer on the CFP electrodes

To enhance the rate of urea formation, titanium dioxide nanoparticles (TiO_2) and graphene nanoplatelets (G) were incorporated as supports that can also act as co-catalysts. However, a challenge arose during the application of the catalyst onto the surface of CFP. The porous structure of CFP posed a problem as the catalyst ink penetrated through the surface, compromising the stability of the electrode. To address this issue and improve electrode stability, a thin layer of carbon black was strategically applied as a supporting material on the CFP prior to the deposition of the catalyst ink. This layer, known as the 'Supporting Layer' (SL), acts as a physical barrier, effectively preventing the undesired penetration of the catalyst ink and enhancing the adhesion of the catalyst components.

2.5.5.1 SL on CFP electrodes with the CoPc/C catalyst

To investigate the influence of a supporting layer (SL) on the electrochemical behavior of the electrode, CFP electrodes modified with mixed IL ($BuPyPF_6$ + $P_{66614}NTf_2$) as a binder and CoPc/C as catalyst with a carbon black SL coating density of 1 mg cm^{-2}, were prepared. The purpose was to assess how the presence of the supporting layer impacts the electrode's performance and characteristics. .

Interestingly, the introduction of SL to the electrode led to a noticeable increase in current at potentials below approximately -0.049 V. Furthermore, it resulted in a reduction in the intensity of the Co (II)/Co(I) redox peaks, which supports the notion of reduced availability of the electroactive catalyst on the electrode surface (green line in Figure 2.11a).

On the other hand, the voltammogram shape and current magnitude for the electrode containing SL were nearly identical to those of the electrode without SL but with half the amount of mixed IL (0.75 mg cm^{-2}) (black dashed line). This observation implies that this phenomenon may be attributed to the absorption of some of the IL into the SL.

Furthermore, the chronoamperometric results demonstrated that the addition of the supporting layer led to an increase in the magnitude of the average current compared to the electrode without supporting layer (Table 2.4 and Table A.1). Moreover, it was observed that by increasing the negativity of the applied potentials, urea production also increased. Notably, greater amounts of urea were produced at potentials of −0.164 V and −0.264 V (4.4 µM and 7.7 µM, respectively (Table 2.3), compared to the system without the supporting layer under identical conditions. However, despite achieving higher average currents, the faradaic yield of urea remained relatively low, with the highest value of 9.3% recorded at −0.064 V (Figure 2.14). Additionally, the rate of urea formation significantly increased, particularly at −0.264 V, where it escalated from 0.01 µmol h^{-1} to 0.05 µmol h^{-1} compared with the electrode without a SL (Figure 2.14).
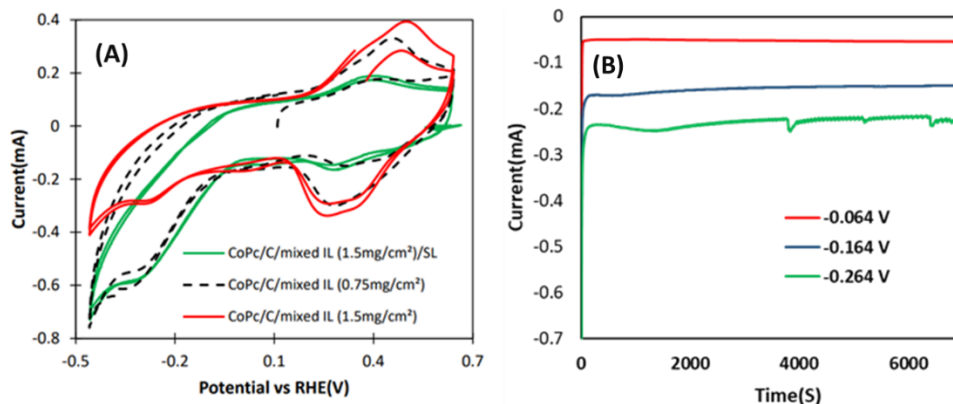
Figure 2.11(A) Comparison of CVs of electrodes customized with different amounts of mixed IL and CoPc/C with and without a SL in 5 mM NaNO$_2$ and 0.1 M NaHCO$_3$ under CO$_2$. (B) Chronoamperometry plots for electrolysis of the same solution with the CoPc/C/mixed IL(1.5mg/cm^2)/SL electrode.

Table 2.3 Average currents and urea concentrations of urea utilizing CoPc/C as catalyst with a SL. All experimental parameters are described in Table 2.1.

Potential vs. RHE (V)	Average current (mA)	Urea concentration (μM)
−0.064	−0.053	2.6
−0.164	−0.158	4.4
−0.264	−0.231	7.7

2.5.5.2 SL on CFP electrodes with CoPc/TiO$_2$ catalyst

The CFP electrodes were modified with a mixed IL (BuPyPF$_6$ + P$_{66614}$NTf$_2$) as a binder and CoPc/TiO$_2$ as a catalyst using the same procedure as with the CFP electrodes modified with mixed IL (BuPyPF$_6$ + P$_{66614}$NTf$_2$) as a binder and CoPc/C as a catalyst. However, instead of using carbon black, TiO$_2$ nanoparticles were employed as the supporting material. Prior to the catalyst ink deposition, a thin layer of carbon black was applied to the CFP as a supporting layer. Cyclic voltammograms were obtained for 5 mM NaNO$_2$ under CO$_2$ in 0.1 M NaHCO$_3$, and the results are depicted in Figure 2.12A. Notably, the currents observed at the CoPc/TiO$_2$ catalyst (Table 2.4) were significantly higher than those at the CoPc/C catalyst (Table A.1 of Appendix A) below a

potential of approximately −0.16 V. Furthermore, a decrease in intensity was observed in the Co (II)/Co(I) redox peaks (Figure 2.12).
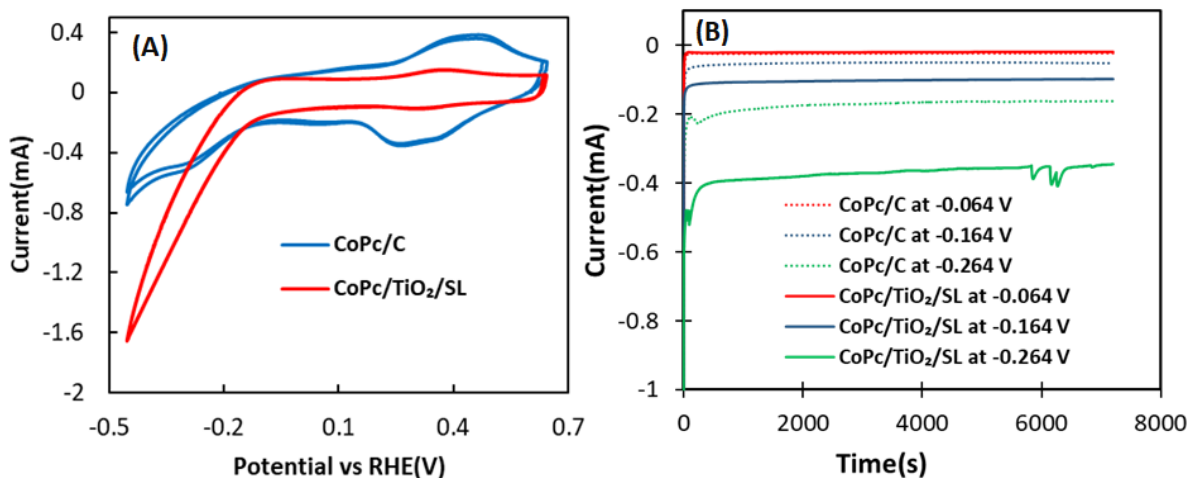
Figure 2.12 *(A) Cyclic voltammograms recorded using electrodes with mixed IL (as binder) as well as a SL, containing CoPc/TiO₂ and CoPc/C as catalysts, in 5 mM NaNO₂ and 0.1 M NaHCO₃ under CO₂. (B) CA for the electrolysis of the same solution and electrodes at potentials indicated inset.*

Figure 2.12B illustrates current vs. time plots during the electrolysis of 5 mM $NaNO_2$ under CO_2 at the $CoPc/TiO_2$ and CoPc/C catalyst. Consistent with the voltammetric data, the current at −0.264 V and –0.164 V for the CoP/TiO_2 catalyst (solid lines) were significantly higher than that of the CoPc/C catalyst (dotted lines). However, the currents were nearly identical at the lowest potentials for both CoPc/C and $CoPc/TiO_2$ catalysts. Average currents and concentrations of urea are shown in Table 2.4

Table 2. 4 *Specifications of urea formation using a CoPc/TiO₂ catalyst with a SL. Electrolysis details are described in Table 2.1.*

Potential vs. RHE (V)	Average current (mA)	Urea concentration (μM)
−0.064	−0.021	7.1
−0.164	−0.103	3.8
−0.264	−0.375	3.7

The $CoPc/TiO_2$ catalyst demonstrated a remarkably high faradaic efficiency (71%) (Figure 2.14) and a sufficiently high urea concentration. However, it exhibited a notably lower average current at the lowest potential, which is very similar to the average current for the CoPc/C catalyst

41

(Table A.1 of Appendix A). Nonetheless, the rate of urea formation at that potential was significantly increased compared to the CoPc catalyst with the SL (Table 2.3). On the other hand, at the highest potential, the electrode provided a much higher average current but lower urea concentration, faradaic efficiency, and rate (Figure 2.14).

In conclusion, TiO_2 nanoparticles, with their high surface area[35] and charge transfer properties,[36] enhance the accessibility of reactants to the active sites of the CoPc catalyst, thereby increasing the rate of urea formation at a lower potential. Consequently, this electrode system can be considered a useful system for achieving high-yield urea formation at the lowest overpotential with a low current.

2.5.5.3 SL on CFP electrodes with CoPc/G catalyst and Nafion as a binder

CFP electrodes modified with Nafion as a binder, a CoPc supported on graphene nanoplatelets (CoPc/G) as catalyst, and a carbon black SL were prepared using a similar procedure as the CoPc/C/SL electrodes, with the exception that graphene nanoplatelets were employed as the support material instead of carbon black. Prior to the catalyst ink deposition, a thin layer of carbon black was applied to the CFP as a SL. Efforts were made to disperse the graphene nanoplatelets with an IL, but these attempts were unsuccessful. As a result, Nafion was chosen as the binder. Cyclic voltammograms were obtained for 5 mM $NaNO_2$ under CO_2 in 0.1 M $NaHCO_3$, as illustrated in Figure 2.13A. Notably, The CFP electrodes modified with CoPc/G catalyst containing

SL exhibited significantly higher currents compared to those without a SL. Thus, the utilization of a supporting layer in this type of electrode proves to be advantageous.
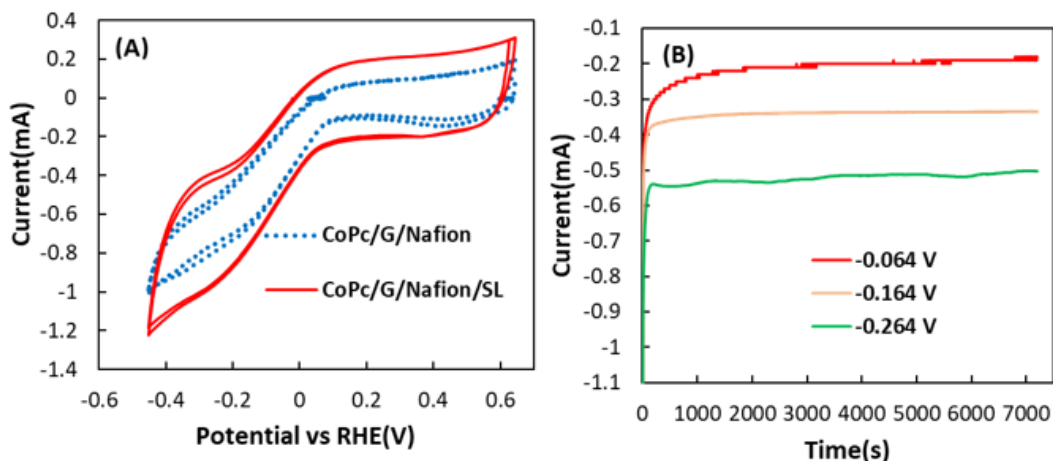
Figure 2.13 (A) CV of electrodes with Nafion as the binder and CoPc/G as the catalyst, with and without a SL. All other experimental parameters are the same described in Figure 2.12. (B) CA for electrolysis of the same solution at the electrode with a SL at potentials indicated inset.

Figure 2.13B illustrates current vs. time plots during the electrolysis of 5 mM $NaNO_2$ under CO_2 in 0.1 M $NaHCO_3$ at the aforementioned electrodes. As the potential was decreased, the current exhibited an increasing trend. Notably, at a potential of -0.264 V, the electrode demonstrated the highest average current among all the tested overpotentials (-0.52 mA). Furthermore, in the context of three distinct potentials, the electrode operating at -0.164 V demonstrated the most substantial urea concentration, reaching 5.8 μM (Table 2.5). Notably, at this specific potential, the faradaic efficiency also achieved its highest value of 3.3%, along with a notably elevated rate of urea formation at 0.03 μmol h^{-1}. Conversely, when subjected to the highest overpotential, the electrode exhibited a significantly reduced faradaic efficiency and rate (Figure 2.14).

Table 2.5 *Average currents and concentrations of urea formation achieved through the application of a CoPc/G catalyst with a SL. The experimental factors remain consistent with those detailed in Table 1.2.*

Potential vs. RHE (V)	Average current (mA)	Urea concentration (μM)
−0.064	−0.213	2.3
−0.164	−0.343	5.8
−0.264	−0.525	2.4
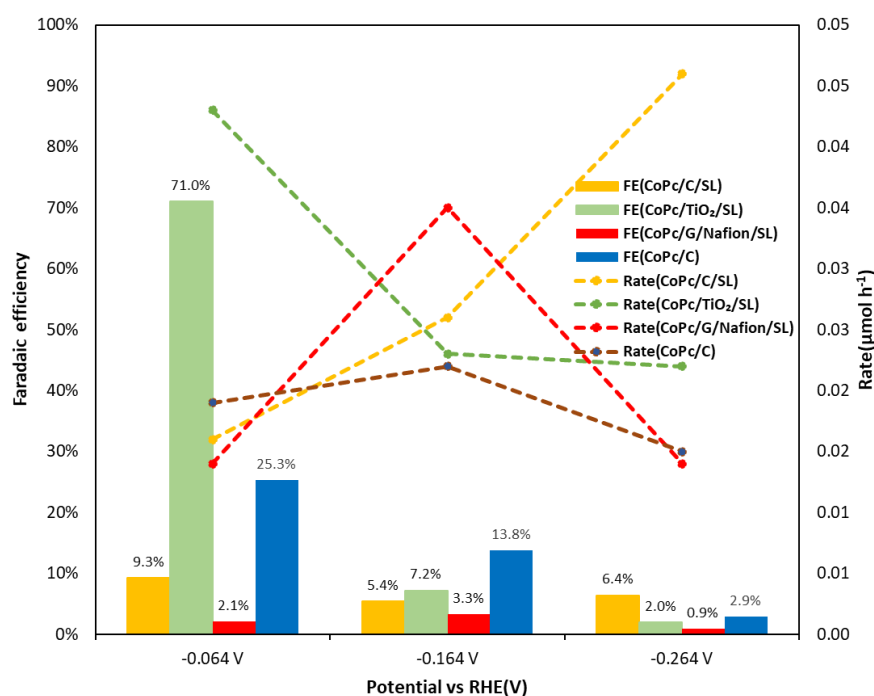
Figure 2.14 *FE and rate of urea formation for different catalysts including Nafion or mixed ILs as the binders.*

2.5.6 Changing the nitrite concentration

Another approach utilized to boost the rate of urea formation was the elevation of the nitrite concentration in the electrolysis solution. This method was applied to the CFP electrodes modified with the mixed IL (BuPyPF$_6$ + P$_{66614}$NTf$_2$) as a binder and CoPc/C as the catalyst. The cyclic voltammogram (Figure 2.15A) shows that by increasing the nitrite concentration from 5 mM to 10 mM, a significant increase in the current is observed at potentials below ca. −0.08 V (vs. RHE).

In addition, a cathodic peak emerged at −0.3 V due to the coreduction of CO_2 and nitrite. The current vs time study of this system in a 10 mM nitrite electrolyte at three different potentials (Figure 2.15B) proves that by moving to more negative potentials, the average current will also increase from −0.047 mA at −0.064 V to −0.254 mA at –0.264 V. Additionally, at all three potentials, the electrode immersed in the 10 mM nitrite concentration electrolyte solution exhibited higher current (solid lines) compared to those in the 5 mM $NaNO_2$ electrolyte solution (dash lines) (Figure 2.15B). On the other hand, the urea concentration and faradaic efficiency analyses show that the second applied potential (−0.164 V) gave the highest urea concentration (10.1 µM) while the lowest applied potential (−0.064 V) produced the highest faradaic yield (29.7%) in this kind of electrochemical systems (Table 2.6 and Figure 2.16). Moreover, the faradaic efficiency of urea formation for the electrode in the 10 mM $NaNO_2$ electrolyte solution was found to be higher than that of the electrode in the 5 mM $NaNO_2$ electrolyte solution, both at the lowest and highest potentials. However, the rate of urea formation was more than double at all three applied potentials, with a notable increase up to 0.06 µmol h^{-1} at –0.164 V for the electrode in the 10 mM $NaNO_2$ solution. In summary, this investigation indicated that elevating the nitrite concentration from 5 mM to 10 mM resulted in an increased availability of nitrite ions for the coreduction of CO_2 and nitrite reaction, leading to a substantial enhancement in the rate of urea formation.
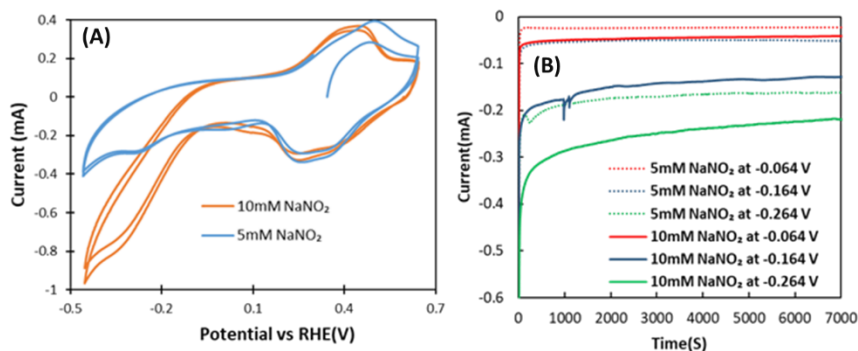
Figure 2.15 (A) Comparison of CVs for electrodes containing CoPc/C and mixed IL in 5 mM and 10 mM NaNO2, as well as 0.1 M NaHCO3 under CO2 (B) CAs performed for electrolysis of 10 mM NaNO2 under CO2 in 0.1 M NaHCO3 with the same electrode at the potentials indicated inset.

Table 2.6 *Specification of urea formation for electrolysis of 10 mM NaNO$_2$ under CO$_2$ in 0.1 M NaHCO$_3$ at electrodes modified with mixed IL and CoPc/C catalysts over 2 h.*

Potential vs. VS. RHE (V)	Average current (mA)	Urea concentration (μM)
−0.064	−0.047	7.3
−0.164	−0.149	10.1
−0.264	−0.254	5.5
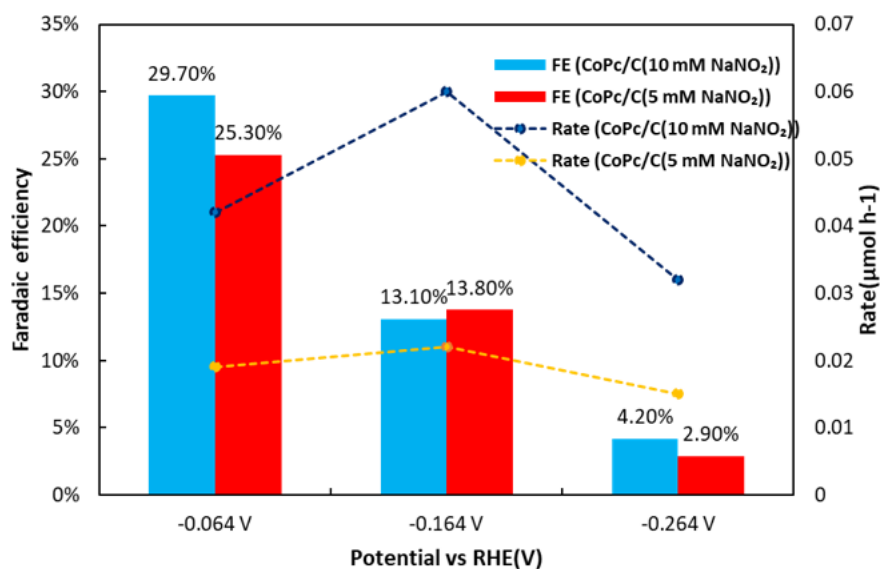
Figure 2.16 *Comparison of FEs and rates of urea formation for the electrodes described in Figure 2.15B.*

2.5.7 Changing the ratio of two ILs

In addition to the aforementioned strategies, another approach employed to enhance the rate of urea formation involved changing the IL ratio, i.e., BuPyPF$_6$:P$_{66614}$NTf$_2$, added to the CoPc/C containing CFP electrodes.

Three electrodes were created using different combinations of BuPyPF$_6$ and P$_{66614}$NTf$_2$ ILs in 1:1, 1:2, and 1:3 (by mass) ratios. The results of CV tests conducted on these electrodes, using 0.1 M NaHCO$_3$ and 5 mM NaNO$_2$ in the presence of CO$_2$, are illustrated in Figure 2.17.

From the graph (Figure 2.17), the electrode containing the 1:2 ratio of mixed ILs exhibited the highest reduction peak, indicating superior performance compared to the other ratios. Conversely, the 1:3 ratio yielded the lowest currents. These observations imply that the choice of ratio significantly influences the electrochemical behavior of the system, with the 1:2 and 1:1 ratio demonstrating better performance. However, two challenges were encountered during the experimentation process. Firstly, the CV results were inconsistent across repeated tests. Secondly, achieving a homogeneous ink solution was problematic. The mixture of $BuPyPF_6$ and $P_{66614}NTf_2$ resulted in ink that was not well-mixed, making it difficult to coat the electrode surface evenly. As a result, the electrode coatings were uneven, affecting the accuracy of subsequent measurements and analyses.

In summary, changing the $BuPyPF_6$:$P_{66614}NTf_2$ ratio had a significant impact on ink formulation, electrode preparation, and system stability. The observed variations in current intensity among different ratios indicate the importance of the ratio in determining electrochemical performance. However, the challenges of reproducibility and obtaining a homogeneous ink highlight the need for further optimization and careful consideration when adjusting the mixture ratios.
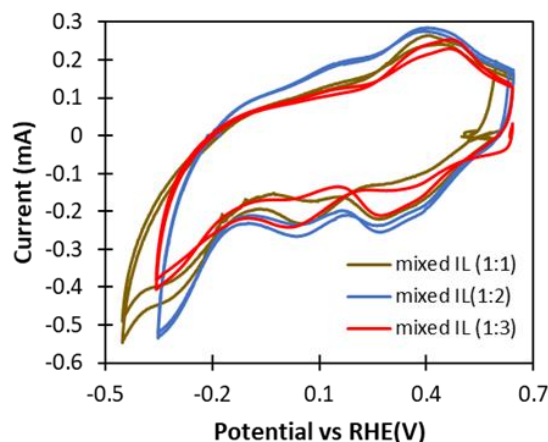
Figure 2.17 *Comparison of CVs for electrodes containing CoPc/C and different ratios of mixed IL in 5 mM and 10 mM NaNO₂, as well as 0.1 M NaHCO₃ under CO₂.*

2.6 Conclusions

Incorporation of ionic liquids into CoPc/C catalyst layers increases the rate and faradaic efficiency for urea formation from coreduction of NO_2^- and CO_2, relative to a Nafion binder.

Increasing the hydrophobicity of the IL increases efficiency but decreases the current and rates of both urea and ammonia formation, presumably by decreasing access of water and the reactants. The IL also appear to modulate the selectivity of the coreduction of NO_2^- and CO_2 through their influence on the electronic structure, arrangement (e.g., aggregation vs adsorption on the carbon support) and/or mobility (e.g., via solubilization) of the CoPc catalyst.

Adsorption of CoPc on a carbon supported Cu catalyst enhanced the current for coreduction of NO_2^- and CO_2 greatly and produced a strong synergistic increase in the rate of urea formation. This appears to arise from coupling of $–NH_x$ species on the Cu surface with PcCo-CO adsorbed onto, or close to, the Cu surface.

The incorporation of various metal nanoparticles as co-catalysts, including Pd/C, Ir/C, and Rh/C alongside CoPc/Pd/C, resulted in a significant increase in the rate of urea formation. This enhancement was attributed to the synergistic effects and the increased surface area, facilitating adsorption of reactive species.

Moreover, the utilization of supporting materials such as TiO_2 nanoparticles and graphene nanoplatelets, with a thin carbon black layer as a supporting layer (SL), proved effective in improving electrode stability and reactant accessibility. Consequently, this led to higher rates of urea production. Particularly, TiO_2 nanoparticles demonstrated remarkable potential as both a catalyst and supporting material, achieving an impressive 71% urea yield when combined with CoPc.

Furthermore, the elevation of nitrite concentration in the electrolysis solution also played a crucial role in enhancing the rate of urea formation. By providing more reactants for the coreduction of CO_2 and nitrite reactions, the increased nitrite concentration contributed to higher urea production rates.

2.7 References

(1)   Tang, C.; Zheng, Y.; Jaroniec, M.; Qiao, S. Electrocatalytic Refinery for Sustainable Production of Fuels and Chemicals. *Angew. Chem. Int. Ed*. **2021**, 60 (36), 19572–19590. https://doi.org/10.1002/anie.202101522.

(2)   Wei, X.; Yin, Z.; Lyu, K.; Li, Z.; Gong, J.; Wang, G.; Xiao, L.; Lu, J.; Zhuang, L. Highly Selective Reduction of CO_2 to C_{2+} Hydrocarbons at Copper/Polyaniline Interfaces. *ACS Catal*. **2020**, 10 (7), 4103–4111. https://doi.org/10.1021/acscatal.0c00049.

(3)   Mei, Z.; Zhou, Y.; Lv, W.; Tong, S.; Yang, X.; Chen, L.; Zhang, N. Recent Progress in Electrocatalytic Urea Synthesis under Ambient Conditions. *ACS Sustain. Chem. Eng*. **2022**, 10 (38), 12477–12496. https://doi.org/10.1021/acssuschemeng.2c03681.

(4)   Tao, Z.; Rooney, C. L.; Liang, Y.; Wang, H. Accessing Organonitrogen Compounds via C–N Coupling in Electrocatalytic CO_2 Reduction. *J. Am. Chem. Soc*. **2021**, 143 (47), 19630–19642. https://doi.org/10.1021/jacs.1c10714.

(5)   Shibata, M.; Yoshida, K.; Furuya, N. Electrochemical Synthesis of Urea on Reduction of Carbon Dioxide with Nitrate and Nitrite Ions Using Cu-Loaded Gas-Diffusion Electrode. *J. Electroanal. Chem*. **1995**, 387 (1–2), 143–145. https://doi.org/10.1016/0022-0728(95)03992-P.

(6)   Shibata, M.; Yoshida, K.; Furuya, N. Electrochemical Synthesis of Urea at Gas-Diffusion Electrodes. *J. Electroanal. Chem*. **1998**, 442 (1–2), 67–72. https://doi.org/10.1016/S0022-0728(97)00504-4.

(7)   Shibata, M.; Furuya, N. Electrochemical Synthesis of Urea at Gas-Diffusion Electrodes. *J. Electroanal. Chem*. **2001**, 507 (1–2), 177–184. https://doi.org/10.1016/S0022-0728(01)00363-1.

(8)   Siva, P.; Prabu, P.; Selvam, M.; Karthik, S.; Rajendran, V. Electrocatalytic Conversion of Carbon Dioxide to Urea on Nano-$FeTiO_3$ Surface. *Ionics* **2017**, 23 (7), 1871–1878. https://doi.org/10.1007/s11581-017-1985-1.

(9)   Cao, N.; Quan, Y.; Guan, A.; Yang, C.; Ji, Y.; Zhang, L.; Zheng, G. Oxygen Vacancies Enhanced Cooperative Electrocatalytic Reduction of Carbon Dioxide and Nitrite Ions to Urea. *J. Colloid Interface Sci*. **2020**, 577, 109–114. https://doi.org/10.1016/j.jcis.2020.05.014.

(10)   Feng, Y.; Yang, H.; Zhang, Y.; Huang, X.; Li, L.; Cheng, T.; Shao, Q. Te-Doped Pd Nanocrystal for Electrochemical Urea Production by Efficiently Coupling Carbon Dioxide Reduction with Nitrite Reduction. *Nano Lett*. **2020**, 20 (11), 8282–8289. https://doi.org/10.1021/acs.nanolett.0c03400.

(11)   Meng, N.; Huang, Y.; Liu, Y.; Yu, Y.; Zhang, B. Electrosynthesis of Urea from Nitrite and CO_2 over Oxygen Vacancy-Rich ZnO Porous Nanosheets. *Cell Rep. Phys. Sci*. **2021**, 2 (3), 100378. https://doi.org/10.1016/j.xcrp.2021.100378.

(12)   Shibata, M.; Yoshida, K.; Furuya, N. Electrochemical Synthesis of Urea at Gas-Diffusion Electrodes: III. Simultaneous Reduction of Carbon Dioxide and Nitrite Ions with Various Metal Catalysts. *J. Electrochem. Soc*. **1998**, 145 (2), 595–600. https://doi.org/10.1149/1.1838309.

(13)   Liu, S.; Yin, S.; Wang, Z.; Xu, Y.; Li, X.; Wang, L.; Wang, H. AuCu Nanofibers for Electrosynthesis of Urea from Carbon Dioxide and Nitrite. *Cell Rep. Phys. Sci.* **2022**, 3 (5), 100869. https://doi.org/10.1016/j.xcrp.2022.100869.

(14)   Zhang, G.-R.; Etzold, B. J. M. Ionic Liquids in Electrocatalysis. *J. Energy Chem*. **2016**, 25 (2), 199–207. https://doi.org/10.1016/j.jechem.2016.01.007.

(15)   Zhang, G.; Etzold, B. J. M. Emerging Applications of Solid Catalysts with Ionic Liquid Layer Concept in Electrocatalysis. *Adv. Funct. Mater*. **2021**, 31 (28), 2010977. https://doi.org/10.1002/adfm.202010977.

(16)   Zhang, G.; Straub, S.; Shen, L.; Hermans, Y.; Schmatz, P.; Reichert, A. M.; Hofmann, J. P.; Katsounaros, I.; Etzold, B. J. M. Probing CO_2 Reduction Pathways for Copper Catalysis Using an Ionic Liquid as a Chemical Trapping Agent. *Angew. Chem*. **2020**, 132 (41), 18251–18258. https://doi.org/10.1002/ange.202009498.

(17)   Suryanto, B. H. R.; Matuszek, K.; Choi, J.; Hodgetts, R. Y.; Du, H.-L.; Bakker, J. M.; Kang, C. S. M.; Cherepanov, P. V.; Simonov, A. N.; MacFarlane, D. R. Nitrogen Reduction to Ammonia at High Efficiency and Rates Based on a Phosphonium Proton Shuttle. *Science* **2021**, 372 (6547), 1187–1191. https://doi.org/10.1126/science.abg2371.

(18)   Zhou, F.; Azofra, L. M.; Ali, M.; Kar, M.; Simonov, A. N.; McDonnell-Worth, C.; Sun, C.; Zhang, X.; MacFarlane, D. R. Electro-Synthesis of Ammonia from Nitrogen at Ambient

Temperature and Pressure in Ionic Liquids. *Energy Environ. Sci*. **2017**, 10 (12), 2516–2520. https://doi.org/10.1039/C7EE02716H.

(19)   Su, W.-Y.; Cheng, S.-H. Functionalized Ionic Liquid and Sol-Gel Composite Film for the Electrochemical Reduction and Determination of Nitrite without Interference from Dissolved Oxygen. *Int. J. Electrochem. Sci*. **2012**, 7 (10), 9058–9073. https://doi.org/10.1016/S1452-3981(23)16180-3.

(20)   Li, Y.; Wang, H.; Liu, X.; Guo, L.; Ji, X.; Wang, L.; Tian, D.; Yang, X. Nonenzymatic Nitrite Sensor Based on a Titanium Dioxide Nanoparticles/Ionic Liquid Composite Electrode. *J. Electroanal. Chem*. **2014**, 719, 35–40. https://doi.org/10.1016/j.jelechem.2014.02.006.

(21)   Li, L.; Tang, C.; Xia, B.; Jin, H.; Zheng, Y.; Qiao, S.-Z. Two-Dimensional Mosaic Bismuth Nanosheets for Highly Selective Ambient Electrocatalytic Nitrogen Reduction. *ACS Catal*. **2019**, 9 (4), 2902–2908. https://doi.org/10.1021/acscatal.9b00366.

(22)   Chen, L.; Ma, J.; Huang, Y.; Dai, M.; Li, X. Optimization of a Colorimetric Method to Determine Trace Urea in Seawater: Trace Urea Analysis in Seawater. *Limnol. Oceanogr. Methods* **2015**, 13 (6), 303–311. https://doi.org/10.1002/lom3.10026.

(23)   Li, D.; Xu, N.; Zhao, Y.; Zhou, C.; Zhang, L.; Wu, L.; Zhang, T. A Reliable and Precise Protocol for Urea Quantification in Photo/Electrocatalysis. *Small Methods* **2022**, 6 (9), 2200561. https://doi.org/10.1002/smtd.202200561.

(24)   Akther, J.; Song, C.; Fatih, K.; Pickup, P. Electrochemical Production of Ammonia and Urea from Coreduction of Nitrite and Carbon Dioxide at Iron Phthalocyanine Electrodes and Comparison of Analytical Methods. *J. Electrochem. Soc*. **2023**. https://doi.org/10.1149/1945-7111/acbc9d.

(25)   Xia, J.; Yang, S.-Z.; Wang, B.; Wu, P.; Popovs, I.; Li, H.; Irle, S.; Dai, S.; Zhu, H. Boosting Electrosynthesis of Ammonia on Surface-Engineered MXene Ti_3C_2. *Nano Energy* **2020**, 72, 104681. https://doi.org/10.1016/j.nanoen.2020.104681.

(26)   Kozub, B. R.; Compton, R. G. Voltammetric Studies of the Redox Mediator, Cobalt Phthalocyanine, with Regard to Its Claimed Electrocatalytic Properties. *Sens. Actuators B Chem*. **2010**, 147 (1), 350–358. https://doi.org/10.1016/j.snb.2010.02.062.

(27)   Li, J.-Z.; Wu, X.-C.; Yuan, R.; Lin, H.-G.; Yu, R.-Q. Cobalt Phthalocyanine Derivatives as Neutral Carriers for Nitrite-Sensitive Poly(Vinyl Chloride) Membrane Electrodes. *Analyst* **1994**, 119 (6), 1363. https://doi.org/10.1039/an9941901363.

(28)   Yang, G.-L.; Hsieh, C.-T.; Ho, Y.-S.; Kuo, T.-C.; Kwon, Y.; Lu, Q.; Cheng, M.-J. Gaseous CO_2 Coupling with N-Containing Intermediates for Key C–N Bond Formation during Urea Production from Coelectrolysis over Cu. *ACS Catal*. **2022**, 12 (18), 11494–11504. https://doi.org/10.1021/acscatal.2c02346.

(29)   Fu, J.; Yang, Y.; Hu, J.-S. Dual-Sites Tandem Catalysts for C–N Bond Formation via Electrocatalytic Coupling of CO_2 and Nitrogenous Small Molecules. *ACS Mater. Lett*. **2021**, 3 (10), 1468–1476. https://doi.org/10.1021/acsmaterialslett.1c00375.

(30)   Huang, Y.; Wang, Y.; Liu, Y.; Ma, A.; Gui, J.; Zhang, C.; Yu, Y.; Zhang, B. Unveiling the Quantification Minefield in Electrocatalytic Urea Synthesis. *Chem. Eng. J*. **2023**, 453, 139836. https://doi.org/10.1016/j.cej.2022.139836.

(31)   Demir, E.; Göktug, Ö.; İnam, R.; Doyduk, D. Development and Characterization of Iron (III) Phthalocyanine Modified Carbon Nanotube Paste Electrodes and Application for Determination of Fluometuron Herbicide as an Electrochemical Sensor. *J. Electroanal. Chem.* **2021**, 895, 115389. https://doi.org/10.1016/j.jelechem.2021.115389.

(32)   Soucy, T. L.; Liu, Y.; Eisenberg, J. B.; McCrory, C. C. L. Enhancing the Electrochemical CO_2 Reduction Activity of Polymer-Encapsulated Cobalt Phthalocyanine Films by Modulating the Loading of Catalysts, Polymers, and Carbon Supports. *ACS Appl. Energy Mater*. **2022**, 5 (1), 159–169. https://doi.org/10.1021/acsaem.1c02689.

(33)   Ghani, F.; Kristen, J.; Riegler, H. Solubility Properties of Unsubstituted Metal Phthalocyanines in Different Types of Solvents. *J. Chem. Eng. Data* **2012**, 57 (2), 439–449. https://doi.org/10.1021/je2010215.

(34)   Mao, Z.; Gu, H.; Lin, X. Recent Advances of Pd/C-Catalyzed Reactions. *Catalysts* **2021**, 11 (9), 1078. https://doi.org/10.3390/catal11091078.

(35)   Zhang, Y.; Weidenkaff, A.; Reller, A. Mesoporous Structure and Phase Transition of Nanocrystalline TiO$_2$. *Mater. Lett*. **2002**, 54 (5–6), 375–381. https://doi.org/10.1016/S0167-577X(01)00597-3.

(36)   Li, H.; Wang, D.; Fan, H.; Wang, P.; Jiang, T.; Xie, T. Synthesis of Highly Efficient C-Doped TiO$_2$ Photocatalyst and Its Photo-Generated Charge-Transfer Properties. *J. Colloid Interface Sci.* **2011**, 354 (1), 175–180. https://doi.org/10.1016/j.jcis.2010.10.048

Chapter 3

The application of other catalysts: FePc and FeTsPc

3.1 Introduction

3.1.1 FePc

FePc, also known as iron (II) phthalocyanine, is a crystalline substance with a distinct blue color. Its unique structure consists of a macrocycle formed by four isoindole units, creating a two-dimensional conjugated π-electron system within the molecule. FePc exhibits thermal stability within a temperature range of 573-623 K.[1] Despite its remarkable electrochemical properties, FePc faces limitations due to its relatively low electrical conductivity (measured at $1.4{\sim}5.7{\times}10^{-7}$ S cm^{-1}).[2] To enhance its performance, FePc requires an electrically conductive support material.[3]
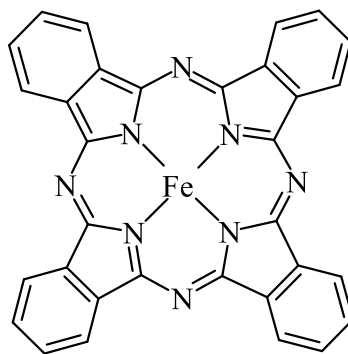
Figure 3.1 *Chemical structure of iron (II) phthalocyanine (FePc).*

Amongst the various nanocarbons, carbon black and carbon nanotubes (CNTs) are popular choices to be used as supporting materials in electrocatalysis due to their excellent electrical conductivity, extensive surface area, and affordability. Additionally, mesoporous carbon, characterized by a three-dimensional architecture and regular micropore and macropore structures, also holds promise as a support material for optimizing the catalytic performance of FePc.[3] FePc has gained considerable attention as an electrocatalyst with diverse applications.[4] One such application is the reduction of CO_2, where FePc effectively converts CO_2 molecules into valuable carbon-based compounds. For instance, recent research has focused on the development of FePc-graphene composites, combining single-atom iron catalysts and graphene, for electrochemically

reducing CO_2 to CO.[5] These composites have shown promising catalytic performance, with the most effective ones exhibiting an initial increase in voltage of 190 mV and a faradaic efficiency of over 90% when converting CO_2 to CO. Furthermore, computational analyses have highlighted the collaborative role of Fe(II)Pc, Fe(III)Pc, and graphene in the catalytic process.[5]

Additionally, FePc has demonstrated notable catalytic activity in the reduction of nitrite ions.[6] A significant early study in this field investigated the reduction of nitrite in an acidic solution using carbon composite ceramic electrodes (CCCEs) incorporating FePc.[6] These CCCEs exhibited highly desirable properties, including high porosity, excellent electrical conductivity, and hydrophobicity. Despite FePc showing weak redox peaks in voltammetry analysis, the CCCEs consistently exhibited a linear response in the reduction of nitrite within a concentration range of 0.05-3 mM. To enhance FePc electrocatalytic activity, FePc molecules were effectively integrated into a silica matrix through adsorption onto carbon with a large surface area. This integration resulted in the development of rough and porous CCCEs, facilitating efficient electrochemical reactions. Notably, the electrodes demonstrated impressive sensitivity, with a detection limit of at least 0.05 mM and maintained linearity across a wide concentration range. These findings highlight the potential of CCCEs as highly effective sensors, particularly in challenging environmental conditions.[6]

However, a significant obstacle in utilizing FePc as an electrocatalyst is its susceptibility to surface instability, which leads to diminished catalytic activity under harsh operating conditions.[7] This limitation hinders its long-term stability and effectiveness. To address this challenge, researchers, led by Jahnke et al,[7] have explored the application of high-temperature heat treatment as a strategy to enhance the stability of FePc. Heat treatment has proven successful in improving the thermal and mechanical stability of supported electrocatalysts, particularly those incorporating metal complexes with porphyrin or phthalocyanine ligands, as demonstrated in fuel cell applications.[7] Building upon previous work, the study conducted by the Kim group aimed to investigate the effects of heat treatment on supported FePc for electrochemical nitrite reduction.[8] The researchers employed advanced techniques such as X-ray absorption fine structure (XAFS) analysis to examine the structural modifications induced by heat treatment in FePc and establish their correlation with the observed catalytic activity. The objective of their investigation was to gain insights into the potential of FePc as a robust and effective electrode material for various electrochemical applications, with a specific emphasis on nitrite reduction.[8]

3.1.2 FeTsPc

FeTsPc (Iron (III) phthalocyanine-4,4',4",4'''-tetrasulfonic acid) is a specific derivative of FePc that has garnered significant interest as an electrode material due to its exceptional properties such as physical adhesion to the surface of the electrode caused by its nucleophilic effect and potential sensing applications.[9] The Demir group conducted a comprehensive research project focusing on harnessing the capabilities of FeTsPc by fabricating composite materials of FePc and with multi-walled carbon nanotube powders (MWCNTP) for electrode enhancement.[10] Through the drop-dry method, the FeTsPc/MWCNTP composite material was successfully immobilized onto glassy carbon electrodes (GCE) and multi-walled carbon nanotube paste electrodes (MWCNTPE). The modified electrodes exhibited superior electrochemical properties, exemplified by a remarkable six-fold increase in the anodic peak current for detecting the herbicide fluometuron compared to unmodified electrodes.[10]
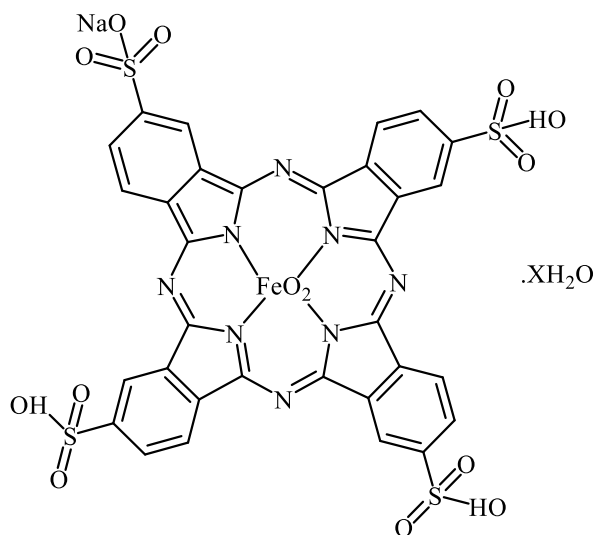
Figure 3.2 *Chemical structure of iron (III) phthalocyanine-4,4',4",4'''-tetrasulfonic acid (FeTsPc).*

In the realm of carbon dioxide detection, the Paul group conducted a study with a primary focus on enhancing the gas sensing capabilities of polypyrrole (PPy) by incorporating FeTsPc as a dopant.[11] The resulting FeTsPc−doped PPy material exhibited exceptional attributes for CO gas sensing, including rapid response times of less than 1 s when exposed to 300 mg of CO gas in 1 L of air (i.e. 300 ppm of CO gas). By acting as an efficient catalyst, FeTsPc facilitated enhanced sensitivity by converting pyrrole molecules into polypyrrole. This study showcases the potential of FeTsPc−doped PPy as a CO sensing material, making it highly suitable for real-time gas sensing

applications. Further optimization and fabrication of sensor devices based on this material hold substantial promise for critical CO detection in industrial and polluted environments.[11]

The feasibility of utilizing FeTsPc as an electrode for tetrabromobisphenol A (TBBPA) oxidation was examined in the presence of humic acid (HA).[12] The results revealed that FeTsPc, acting as a catalyst in combination with $KHSO_5$, effectively degraded TBBPA, achieving a degradation efficiency of approximately 100% and leading to debromination, resulting in the removal of approximately 18% of the bromine content at a pH value of 8, a pH similar to that found in landfill leachates. It is also reported that the debromination yielded to less toxic compounds with lower molecular weights including 4-(2-hydoroxyisopropyl)-2,6-dibromophenol and 4-(isopropylene)-2,6-dibromophenol. Additionally, during the oxidation process, nearly 48% of the bromine present in the degraded TBBPA was taken into HA, resulting in less toxic products than the parent molecule, i.e. TBBPA. This study highlights the superior catalytic capability of FeTsPc compared to other iron (III)-porphyrin catalysts for TBBPA degradation.[12]

Moreover, an investigation was carried out to assess the efficacy of FeTsPc as a catalyst for the degradation of phenols and bisphenol A (BPA) in water under optimized conditions.[13] The adsorption efficiency of the catalyst was found to be influenced by the pH of the solution so that a range of solution pH (from pH = 2 to 11) was investigated and proved that pH = 2 is the optimized condition for the catalyst adsorption. The results of the study demonstrated that the immobilized FeTsPc catalyst effectively decomposed the targeted organic compounds. The degradation process involved the generation of hydroxyl radicals, utilization of ultraviolet light, adsorption, and harnessing the photosensitizing properties of the metal phthalocyanine[13].

Discussing different applications of FePc and FeTsPc as active catalysts in electrochemical reactions, we are going to investigate the potential of modified CFP electrodes utilizing mixed ionic liquids ($BuPyPF_6$ + $P_{66614}NTf_2$) as the binder, and FeTsPc/C and FeTsPc/C as the catalysts for the simultaneous coreduction of CO_2 and nitrite under ambient temperature and pressure. Additionally, this chapter aims to assess the impact of various binders (Nafion and Sustainion) on the performance of IL-containing FePc/C or FeTsPc/C electrodes, ultimately aiming to optimize the electrocatalytic efficiency for the production of urea and ammonia.

3.2 Experimental

3.2.1 Catalyst preparation

Carbon black (100 mg; Vulcan XC-72; Cabot) was dispersed in tetrahydrofuran (5 mL; THF; 99.9%; Sigma Aldrich) by sonication for 1 h. Iron (II) phthalocyanine (10 mg; 90%; Sigma Aldrich) in THF (1 mL) was then added and the mixture was sonicated for 2 h. The solvent was allowed to evaporate at room temperature in a fume hood overnight, and then the catalyst was dried in an oven at 80 °C for 1 h. A FePc/Cu/C catalyst were prepared using the same method, with the only difference being the substitution of carbon black with commercial carbon-supported Cu catalysts (Cu/C; 40% Cu on Vulcan carbon; Fuel Cell Store).

3.2.2 Electrode preparation

FePc/C, FePc/Cu/C, or FeTsPc (10 mg) were combined with the IL (10 mg; $P_{66614}NTf_2$ (≥95.0%, Sigma Aldrich), and/or BuPyPF$_6$ (98.0+%, Fisher Scientific)) via dispersion in 0.3 mL of THF and 2-propanol (1:1 volume ratio), and subsequently the mixture was sonicated for 1 h to form a uniform catalyst ink. The ink was drop coated onto glassy carbon (GC; 0.071 cm^2; CH Instruments) or (CFP; 1 cm^2) electrodes to give a catalyst loading of 1.5 mg cm^{-2} and IL loading of 1.5 mg cm^{-2} prepared on CFP with a mixture of the two IL were heated in an oven for 30 min at 75 °C to improve stability.

Iron(III) phthalocyanine-4,4',4'',4'''-tetrasulfonic acid compound with oxygen monosodium hydrate ((FeTsPc) 0.3 mg, dye content 80% Sigma Aldrich), carbon black (10 mg; Vulcan XC-72; Cabot), and the IL (10 mg; $P_{66614}NTf_2$ (≥95.0%, Sigma Aldrich), and/or BuPyPF$_6$ (98.0+%, Fisher Scientific)) were dispersed in 0.3 mL of THF and 2-propanol (1:1 volume ratio) by sonication for 2 h to form a uniform catalyst ink. For Nafion-containing electrodes, 5.075 mg (112 µL) of 5% Nafion solution (75 µL; 5.14 mass% in a mixture of lower aliphatic alcohols and 51.9% water; Dupont) was added to the ink and sonicated for 10 minutes. For Sustainion – containing electrodes, 5.075 mg (6.41 µL) of Sustainion (XA-9 5% in ethanol, Dioxide Materials) was added to the ink and sonicated for 10 min. The ink was drop-coated onto (CFP; 1 cm^2; TGP-H-090 Toray Industries-total thickness of 280 µm) electrodes to achieve a catalyst loading of 1.5 mg cm^{-2} and an IL loading of 1.5 mg cm^{-2}. The electrodes prepared on CFP with a mixture of the two ILs were then heated in an oven for 30 min at 75 °C to enhance stability.

Regarding the electrodes coated with Sustainion, a primary Sustainion solution was prepared by obtaining 5.075 mg (6.41 µL) of the Sustainion solution, which was then diluted 15 times using ethanol (Analytical grade). Subsequently, 15 µL of the diluted Sustainion solution, containing 0.96 µL (i.e., 0.769 mg) of Sustainion, were applied to the surface of each electrode with a micro pipette. This ensured that the mass of Sustainion in the catalyst layer was equal to 25% of the total mass of the catalyst layer.

3.2.3 Electrochemistry

Electrochemical measurements were made at ambient temperature in a glass cell with a Pt counter electrode and a saturated calomel reference electrode (SCE; 0.241 V vs SHE). Potentials are reported relative to RHE, at -0.486 V vs SHE under N_2 (pH = 8.30) or -0.395 V vs SHE under CO_2 (pH = 6.75). CV is conducted with a scan rate of 10 mV s^{-1}. The working and counter electrode compartments were separated by a porous glass frit. All measurements were made in aqueous 0.1 M NaHCO$_3$ at an ambient temperature of ca. 20 °C. All the applied working electrodes conformed to a surface area of 1 cm^2 of CFP unless otherwise stated.

3.2.4 Product analysis

The determination of urea and ammonia concentrations followed the procedures discussed in section 2.3.4 of Chapter 2.

3.3 Result and discussion

3.3.1 FePc/C catalysts

3.3.1.1 BuPyPF$_6$ as a binder

The impact of a hydrophilic IL BuPyPF$_6$ on the GC electrode with FePc/C catalyst was investigated. The voltammograms of the electrodes in a 0.1 M NaHCO$_3$ solution, with and without the addition of 5 mM NaNO$_2$, under N_2 and CO_2 environments, were analyzed. Under N_2, in the absence of NaNO$_2$, two primary quasi-reversible redox waves were observed at formal potentials of +0.74 V and -0.03 V for the Fe(+3/+2) and Pc($-2/-3$) (or Fe(+2/+1)) couples of the FePc, respectively.[14] The voltammograms exhibited similar characteristics in the presence of NaNO$_2$ under N_2, but with enhanced cathodic currents below approximately +0.12 V due to the reduction

of NO_2^-. When CO_2 is present in the absence of nitrite, the replacement of N_2 gas with CO_2 leads to the conversion of CO_2 into H_2CO_3. This conversion causes a shift in pH from 8.3 to 6.8. As a consequence, the waves on the graph shift towards higher potentials. Notably, a noticeable rise in current is observed at potentials lower than approximately −0.23 V due to the reduction of CO_2. [15] When both NO_2^- and CO_2 were present, a substantial increase in current was observed at potentials below 0.00 V, accompanied by a cathodic peak at −0.14 V. These results suggest a considerable coreduction of both NO_2^- and CO_2, in addition to their individual reduction processes. Previous research has reported the formation of urea under similar experimental conditions, as well as the generation of CO and NH_3. [16]
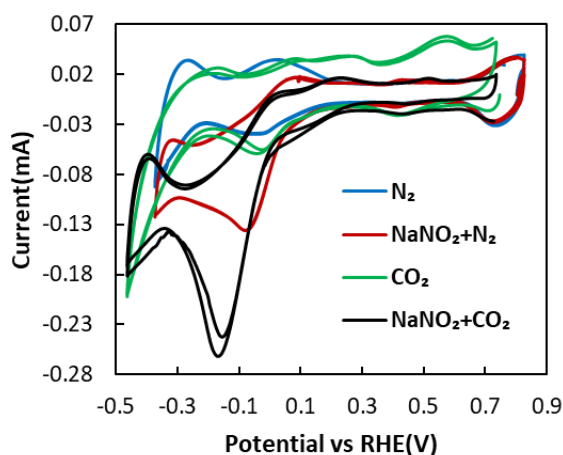
Figure 3.3 Cyclic voltammograms for GC electrodes modified with $BuPyPF_6$ as a binder and FePc/C as catalysts with and without 5 mM $NaNO_2$, under N_2 and CO_2.

3.3.1.2 $BuPyPF_6$ + $P_{66614}NTf_2$ as binders

When comparing the electrode incorporating a mixed IL system comprising with the aforementioned electrode in the presence of nitrite under a CO_2 environment, a notable decrease in the current magnitude was observed (Figure 3.2). The incorporation of hydrophobic $P_{66614}NTf_2$ could significantly impact the accessibility of reactants, especially water molecules, to the catalyst surface and the diffusion of ions during the redox processes. Additionally, the presence of hydrophobic $P_{66614}NTf_2$ may decrease the mobility of reactants, resulting in a suppression of the current.
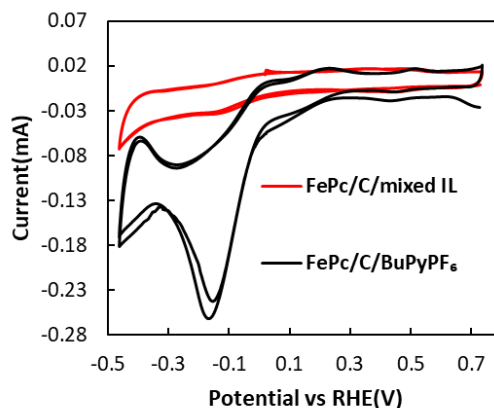
Figure 3.4 CVs for GC electrodes modified with BuPyPF$_6$ or mixed IL as a binder and FePc/C as catalysts in the presence of 0.1 M NaHCO$_3$ and 5 mM NaNO$_2$ under CO$_2$.

3.3.2 Cu/C as a co-catalyst

The presence of the Cu/C as a co-catalyst resulted in the highest current observed when nitrite was present under N_2, indicating its potential to enhance the reduction of nitrite ions. This enhancement can be attributed to the synergistic effect between FePc/C and Cu/C, which promotes the catalytic activity towards nitrite reduction.

However, under a nitrogen atmosphere without nitrite ions, the current remained nearly unchanged, suggesting that the presence of Cu/C as a co-catalyst alone did not significantly influence the overall electrochemical behavior of the electrode under these conditions.

Moreover, the decrease in current upon the introduction of CO_2 indicates that the electrode with Cu/C as a co-catalyst is not very effective at CO_2 reduction.

Furthermore, the addition of Cu/C as a co-catalyst did not lead to a significant improvement in the reduction of nitrite ions, nor did it result in the desired synergistic effect for simultaneous CO_2 and nitrite reduction to form urea.
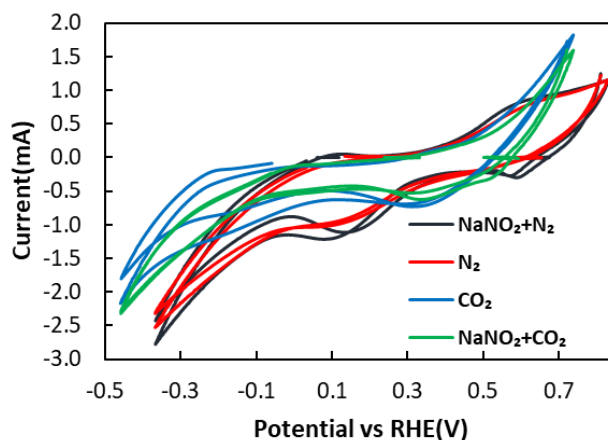
Figure 3.5 *CVs conducted for the electrodes changed with mixed IL as a binder and FePc/Cu/C as catalysts in 0.1 M NaHCO₃, with and without 5 mM NaNO₂, under N₂ and CO₂.*

3.3.3 FeTsPc/C catalyst

The CV for FeTsPc as a catalyst is shown in Figure 3.6. The experiments were conducted in a solution containing 0.1 M $NaHCO_3$ and 5mM $NaNO_2$ under CO_2. The electrode was modified with mixed IL ($P_{66614}NTf_2$ and $BuPyPF_6$). Voltammograms show a quasi-reversible redox wave at a formal potential of +0.29 V ($\Delta E_p = 0.05$ V) for the Fe (3+/2+) couple.[13] At a potential of approximately +0.04 V, there is an increase in the current, with a cathodic peak at −0.15 V indicating coreduction of CO_2 and NO_2^-.

After CV, a blue color was observed to be released from the electrode into the electrolyte, resulting in a noticeable light blue color change in the electrolyte. This is due to a partial loss of FeTsPc from the modified electrode surface into solution, preventing heterogeneous, electrochemically controlled catalysis. To inhibit catalyst loss two different binding materials were introduced to the catalyst ink mixture, Nafion or Sustainion, at different loadings. By utilizing Nafion and Sustainion separately, along with applying a thin layer of Sustainion as a surface coating on the catalyst, three different electrodes were prepared for further testing and analysis.
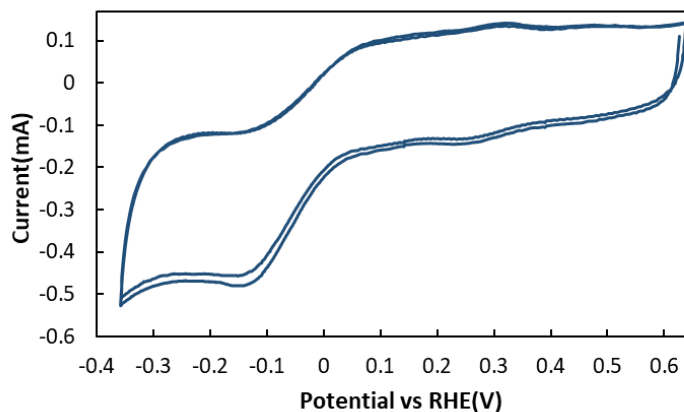
Figure 3.6 *Cyclic voltammograms for the electrode modified with mixed IL as a binder and FeTsPc/C as catalysts in the presence of 0.1 M NaHCO₃ and 5 mM NaNO₂ under CO₂.*

3.3.3.1 Binding effects

The analysis of the CVs revealed intriguing findings when Sustainion was employed as a binder in conjunction with the prepared catalyst. The CV response displayed a distinct cathodic peak indicative of CO_2 and nitrite reduction. However, the current obtained using Sustainion as a binder was not the highest among the binding materials investigated. Interestingly, when Sustainion was applied as a thin layer directly on the catalyst surface, the CVs measurements yielded the lowest current. Conversely, the utilization of Nafion as a binder resulted in the highest current, but it did not exhibit any discernible features associated with CO_2 and nitrite reduction (Figure 3.5A).

Further examination of the CVs of electrodes with and without binders shed light on the impact of binder incorporation on catalyst stability and electrochemical performance. The addition of binders improved the stability of the catalyst on the electrode surface, as evidenced by the reduced intensity of the blue color observed in the electrolyte solution during CV experiments. Moreover, the CVs conducted before and after chronoamperometry exhibited good stability (Figure 3.6). Notably, the electrode incorporating a mixed Sustainion binder demonstrated exceptional stability and reasonably high current, reaching approximately −0.35 mA. However, it is essential to consider that the electrode without Sustainion and Nafion displayed the highest current, implying that the use of a binder in conjunction with an ionic liquid does not necessarily lead to a favorable electrochemical system in all cases.
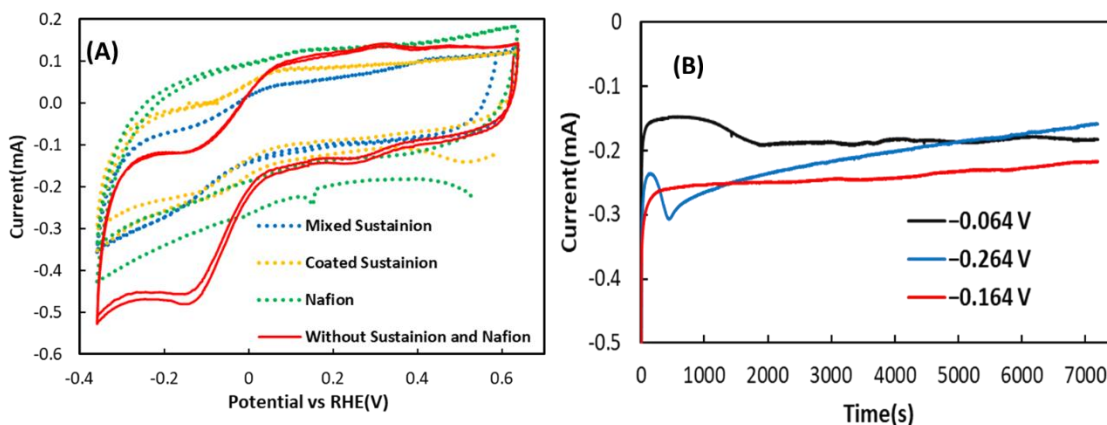
Figure 3.7 CVs performed for electrodes containing FeTsPc/C and mixed IL as well as other binders: Sustainion and Nafion in 0.1 M NaHCO₃ and 5 mM NaNO₂ under CO₂. (B) CA for the same electrolysis solution and electrode without Sustainion and Nafion.
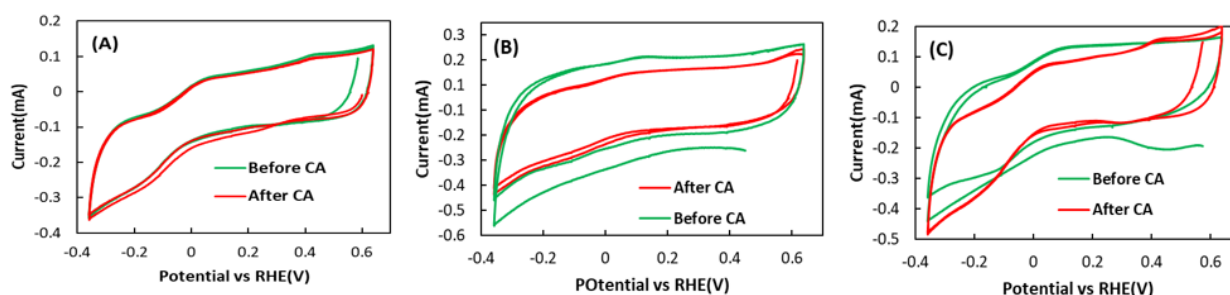
Figure 3.8 CVs curves measured after and before chronoamperometry for the electrodes containing mixed IL and FeTsPc/C with different binders: (A) Mixed Sustainion, (B)Nafion and (C) Coated Sustainion. All other experimental parameters were the same as described in Figure 3.5A.

Figure 3.5B presents the chronoamperometry results of electrodes without Sustainion and Nafion, operating in a solution of 0.1 M NaHCO₃ and 5 mM NaNO₂ under the presence of CO₂. The experiment involved applying various constant potentials, −0.064, −0.164, and −0.264 V (vs. RHE), for a duration of two hours. Throughout the electrolysis process, the obtained currents exhibited excellent stability.

It was observed that the lowest average current was recorded at a potential of −0.064 V. Conversely, the highest average current was associated with a potential of −0.164 V (Table 3.1). As the potential becomes more negative, the concentration, faradaic efficiency, and rate of ammonia production all increase. The highest recorded values for concentration, faradaic efficiency, and rate were 198 µM, 89.3%, and 1.18 µmol h⁻¹, respectively, during ammonia production at −0.264 V.

Regarding urea formation, it is worth mentioning that at an intermediate potential (-0.164 V), the concentration, faradaic efficiency, and rate reach their highest points, with values of 14.8 µM, 11.7%, and 0.08 µmol h^{-1}, respectively (Table 3.1) and (Figure 3.7). This observation highlights the excellent catalytic activity of the electrode at this specific potential for urea formation. Comparing the rate of urea formation with other catalysts, such as CoPc/C.

Table 3.1 Average currents and concentrations of urea and ammonia for electrolysis of 5 mM NaNO₂ in 0.1 M NaHCO₃ under CO₂ at CFP electrodes modified with mixed ILs and FeTsPc/C catalysts over 2h.

Potentials RHE (V)	Average current (mA)	Urea Con.(µM)	Ammonia Con.(µM)
−0.064 V	−0.180	7.8	41
−0.164V	−0.243	14.8	83
−0.264V	−0.214	4.5	198
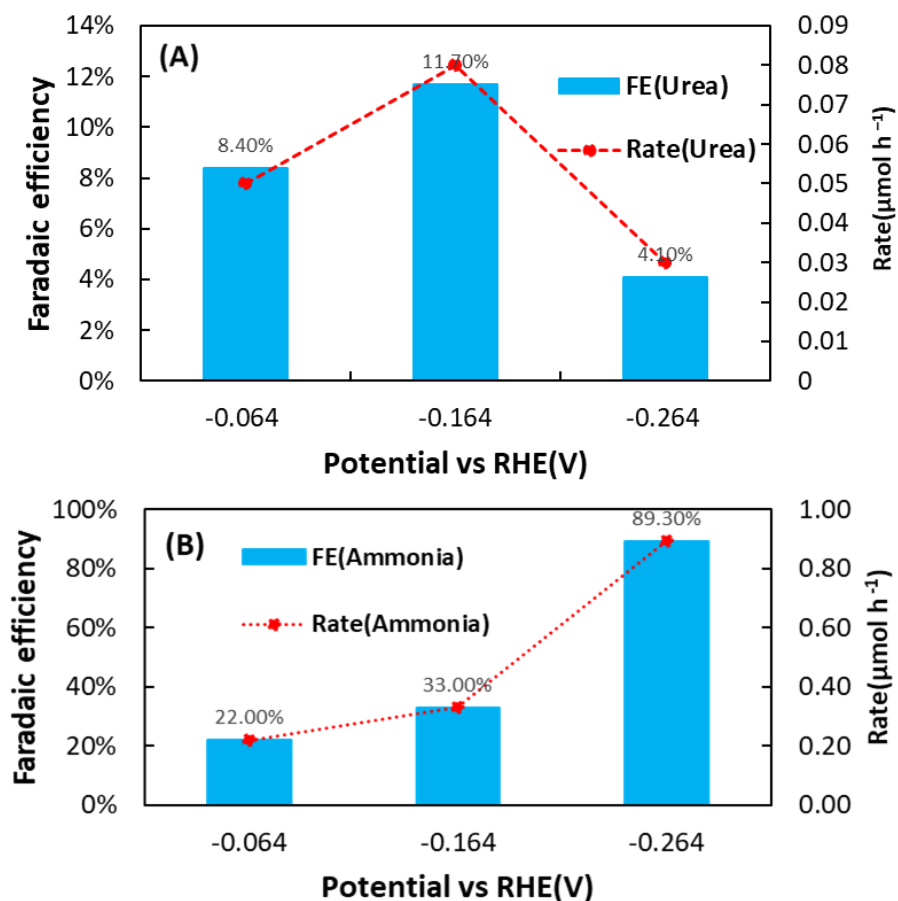
Figure 3.9 Faradaic yields of (A) urea and (B) ammonia, calculated from the data in Table 3.1.

3.4 Conclusions

In this chapter, the investigation revolved around modified CFP electrodes utilizing mixed ILs (BuPyPF$_6$ + P$_{66614}$NTf$_2$) as binder and FePc/C and FePc/Cu/C as catalysts for simultaneous coreduction of CO$_2$ and nitrite under ambient temperature and pressure. As the FePc/C and FePc/Cu/C catalysts exhibited limited effectiveness for this purpose, the focus shifted to the application of FeTsPc/C as the catalyst.

Interestingly, the addition to various binders like Nafion or Sustainion to IL containing FeTsPc/C electrodes resulted in a substantial decrease in the current within the voltammogram.

Consequently, the choice was made to proceed without any binder. Therefore, this modified electrode showcased a remarkable performance in the electrocatalysis of the coreduction of CO_2 and nitrite. It demonstrated an 11.7% faradaic efficiency in producing urea and exhibited an impressive rate of 0.08 µmol h^{-1} at −0.164 V vs RHE. Moreover, this electrode effectively facilitated ammonia production, resulting an 89.3% faradaic efficiency and a rate of 1.18 µmol h^{-1} at −0.264 V vs RHE.

3.5 References

(1)   Kanemitsu, Y.; Yamamoto, A.; Funada, H.; Masumoto, Y. Photocarrier Generation in Metal-Free Phthalocyanines: Effect of the Stacking Habit of Molecules on the Photogeneration Efficiency. *J. Appl. Phys*. **1991**, 69 (10), 7333–7335. https://doi.org/10.1063/1.347587.

(2)   Khrishnakumar, K. P.; Menon, C. S. Determination of the Thermal Activation Energy and Grain Size of Iron Phthalocyanine Thin Films. *Mater. Lett*. **2001**, 48 (2), 64–73. https://doi.org/10.1016/S0167-577X(00)00281-0.

(3)   Bhowmick, G. D.; Kibena-Põldsepp, E.; Matisen, L.; Merisalu, M.; Kook, M.; Käärik, M.; Leis, J.; Sammelselg, V.; Ghangrekar, M. M.; Tammeveski, K. Multi-Walled Carbon Nanotube and Carbide-Derived Carbon Supported Metal Phthalocyanines as Cathode Catalysts for Microbial Fuel Cell Applications. *Sustain. Energy Fuels* **2019**, *3* (12), 3525–3537. https://doi.org/10.1039/C9SE00574A.

(4)   Li, B.; Sun, L.; Bian, J.; Sun, N.; Sun, J.; Chen, L.; Li, Z.; Jing, L. Controlled Synthesis of Novel Z-Scheme Iron Phthalocyanine/Porous WO_3 Nanocomposites as Efficient Photocatalysts for CO_2 Reduction. *Appl. Catal. B Environ*. **2020**, 270, 118849. https://doi.org/10.1016/j.apcatb.2020.118849.

(5)   Li, X.; Chai, G.; Xu, X.; Liu, J.; Zhong, Z.; Cao, A.; Tao, Z.; You, W.; Kang, L. Electrocatalytic Reduction of CO_2 to CO over Iron Phthalocyanine-Modified Graphene Nanocomposites. *Carbon* **2020**, 167, 658–667. https://doi.org/10.1016/j.carbon.2020.06.036.

(6)   Ha, S. Y.; Kim, S. Preparation and Characterization of Sol–Gel Derived Carbon Composite Ceramic Electrodes: Electrochemical and XANES Study of Nitrite Reduction. *J. Electroanal. Chem.* **1999**, 468 (2), 131–138. https://doi.org/10.1016/S0022-0728(99)00152-7.

(7)   Jahnke, H.; Schönborn, M.; Zimmermann, G. Organic Dyestuffs as Catalysts for Fuel Cells. *In Physical and Chemical Applications of Dyestuffs*; Schäfer, F. P., Gerischer, H., Willig, F., Meier, H., Jahnke, H., Schönborn, M., Zimmermann, G., Eds.; *Top. Curr. Chem*. Springer-Verlag: Berlin/Heidelberg, **1976**; Vol. 61, pp 133–181. https://doi.org/10.1007/BFb0046059.

(8)   Kim, S.; Kwag, G. Increased Catalytic Activity of Iron Phthalocyanine on the Electrochemical Nitrite Reduction upon Heat-Treatment Probed by X-Ray Absorption Fine Structure. *Bull. Korean Chem. Soc*. **2002**, 23 (1), 25–26. https://doi.org/10.5012/BKCS.2002.23.1.025.

(9)   Demir, E.; Silah, H.; Uslu, B. Phthalocyanine Modified Electrodes in Electrochemical Analysis. *Rev. Anal. Chem*. **2022**, 52 (2), 425–461. https://doi.org/10.1080/10408347.2020.1806702.

(10)   Demir, E.; Göktug, Ö.; İnam, R.; Doyduk, D. Development and Characterization of Iron (III) Phthalocyanine Modified Carbon Nanotube Paste Electrodes and Application for Determination of Fluometuron Herbicide as an Electrochemical Sensor. *J. Electroanal. Chem*. **2021**, 895, 115389. https://doi.org/10.1016/j.jelechem.2021.115389.

(11)   Paul, S.; Radhakrishnan, S. Iron (III) Phthalocyanine (FePcTsA) Doped Polypyrrole for Fast Detection of Carbon Dioxide. *In International Conference on Materials for the Future - Innovative Materials, Processes, Products and Applications – ICMF*; **2013**.

(12)   Maeno, S.; Mizutani, Y.; Zhu, Q.; Miyamoto, T.; Fukushima, M.; Kuramitz, H. The Oxidation of Tetrabromobisphenol A by Potassium Monopersulfate with an Iron(III)-Phthalocyanine-Tetrasulfonic Acid Catalyst in the Presence of Humic Acid. *J. Environ. Sci. Health A* **2014**, 49 (9), 981–987. https://doi.org/10.1080/10934529.2014.894810.

(13)   Norman, M.; Żółtowska-Aksamitowska, S.; Zgoła-Grześkowiak, A.; Ehrlich, H.; Jesionowski, T. Iron(III) Phthalocyanine Supported on a Spongin Scaffold as an Advanced Photocatalyst in a Highly Efficient Removal Process of Halophenols and Bisphenol A. *J. Hazard. Mater.* **2018**, 347, 78–88. https://doi.org/10.1016/j.jhazmat.2017.12.055.

(14) Zagal, J. H.; Griveau, S.; Silva, J. F.; Nyokong, T.; Bedioui, F. Metallophthalocyanine-Based Molecular Materials as Catalysts for Electrochemical Reactions. *Coord. Chem. Rev.* **2010**, 254 (23–24), 2755–2791. https://doi.org/10.1016/j.ccr.2010.05.001.

(15) Manbeck, G. F.; Fujita, E. A Review of Iron and Cobalt Porphyrins, Phthalocyanines and Related Complexes for Electrochemical and Photochemical Reduction of Carbon Dioxide. *J. Porphyr. Phthalocyanines* **2015**, 19 (01–03), 45–64. https://doi.org/10.1142/S1088424615300013.

(16) Shibata, M.; Furuya, N. Electrochemical Synthesis of Urea at Gas-Diffusion Electrodes. *J. Electroanal. Chem.* **2001**, 507 (1–2), 177–184. https://doi.org/10.1016/S0022-0728(01)00363-1.

Chapter 4

The application of other catalysts: MoS$_2$

4.1 Introduction

Molybdenum disulfide (MoS$_2$) nanoparticles have gained significant attention in the field of materials science due to their distinct characteristics and versatile applications in catalysis. As a member of the transition-metal dichalcogenide family,[1] MoS$_2$ possesses a layered structure primarily held together by Van der Waals forces, with layers positioned at a nanoscale distance from one another.[2] Each MoS$_2$ layer consists of a central molybdenum atom sandwiched between two sulfur atoms. The arrangement of Mo and S atoms determines the structural variations of MoS$_2$, such as 1TMoS$_2$, 2H-MoS$_2$, and 3R-MoS$_2$. The 1T-MoS$_2$ structure features one S-Mo-S layer per unit cell, with exposed molybdenum atoms on the surface. In contrast, 2H-MoS$_2$ and metastable 3R-MoS$_2$ exhibit a trigonal prismatic structure, with two and three S-Mo-S units per layer, respectively. The stacking order differs between 2H-MoS$_2$ and metastable 3R-MoS$_2$, and the latter readily transforms into the 2H phase.[3] These structural differences significantly influence the physicochemical properties of MoS$_2$. The 1T-MoS$_2$ structure demonstrates metallic characteristics, displaying excellent conductivity and superior electron transfer capabilities. In contrast, the 2H-MoS$_2$ structure exhibits semiconductor properties and exceptional stability. Consequently, 2H-MoS$_2$ has garnered attention for its semiconducting behavior, while 1T-MoS$_2$ has shown promise for applications requiring metallic properties.[4] In addition to the well-known crystalline forms of MoS$_2$ (1-T, 2-H, and 3-R), material scientists have shown growing interest in amorphous MoS$_2$. Amorphous MoS$_2$ nanoparticles are characterized by a disordered arrangement of structural units. Furthermore, compared to crystalline MoS$_2$, the amorphous form exhibits a higher concentration of unsaturated and deficient atoms on its surface. These distinctive features of amorphous MoS$_2$ contribute to its versatility in catalytic applications, including electrochemical and photochemical hydrogen generation, nitrogen reduction to valuable products,[5–9] reduction of nitroarenes,[10] degradation of organic contaminants, as well as energy storage and biological applications.[11] The unique properties of amorphous MoS$_2$ make it an attractive material for a wide range of catalytic applications. One area where MoS$_2$ has shown remarkable potential is in the electrocatalytic reduction of carbon dioxide, particularly in the production of carbon monoxide. Extensive research

has been dedicated to understanding the distinctive properties of MoS_2 edges, which serve as a rich source of active sites for catalysis.[12–14]

The edges of MoS_2 possess remarkable tunability due to the inherent instability of sulfur edges and their susceptibility to doping.[15,16] Theoretical studies have elucidated the selective binding capacity of MoS_2 edges, where bridging sulfur atoms exhibit an affinity for binding COOH* and CHO* species, while CO* binds preferentially to the metal atoms.[17] Experimental techniques such as scanning transmission electron microscopy (STEM) analysis and first principal density functional theory (DFT) modeling have confirmed this selectivity. Furthermore, it has been established that the exceptional catalytic performance of MoS_2 is primarily ascribed to the metallic character and high d-electron density of the molybdenum-terminated edges.[12]

The research implemented by Nørskov group focused on examining the application of active edge sites in MoS_2 considered as the catalyst to reduce CO_2.[15] They investigated the CO_2 reduction activity of layered MoS_2 by examining the binding energies of CO_2 reduction intermediates and discovered that the bridging sulfur atoms located at the edges of MoS_2 possess a unique capability to selectively bind COOH* and CHO* intermediates while excluding CO*. This deviation from the expected behavior based on transition-metal scaling relations indicates that MoS_2 exhibits significantly improved activity compared to conventional transition-metal catalysts. Furthermore, the study demonstrated that the bridging S atoms at the edges of MoS_2 selectively enhance the stability of CHO* and COOH* intermediates, surpassing the stability provided by traditional transition-metal catalysts. This suggests a substantial improvement in the catalytic activity when using MoS_2 as a catalyst.[15] Additionally, the study suggests that all edges examined in the research have the potential to be active in the process of CO_2 reduction to CO. They offer valuable insights into the significance of maximizing edge sites in nanostructured MoS_2 to achieve improved catalytic performance. The study proposes that stabilizing specific edges in undoped MoS_2 can increase the selectivity for CO_2 reduction over competing reactions. Overall, the results highlight the importance of active edge sites in MoS_2 for complex electrochemical processes and present opportunities for their broader application in various catalytic systems.[15]

MoS_2 also has shown remarkable potential as a catalyst in various nitrogen reduction reactions (NRR) for several compelling reasons. Firstly, the presence of molybdenum, an essential component of Mo-based nitrogenase, enables the fixation of nitrogen gas under normal

71

environmental conditions.[18,19] Additionally, sulfur plays a vital role in nitrogenase by forming S-Mo-S units. MoS_2 exists in different stacking configurations and phases, contributing to its diverse chemical and physical properties. This unique characteristic enhances its electrocatalytic capabilities.[20–22] Secondly, the two-dimensional structure of MoS_2 provides active sites along its edges, thanks to its high aspect ratio. This structure allows for the introduction of sulfur vacancies and plane defects, creating more active centers on the surface of MoS_2. Consequently, MoS_2 exhibits improved ability to adsorb and break apart N_2 molecules.[23,24] Furthermore, the electronic structure of MoS_2 can be effectively tuned by introducing heteroatoms. This adjustment optimizes its energy band gap and enhances its efficiency in NRR.[25,26]

Zhang and colleagues have explored the potential of MoS_2 as a catalyst for NRR through theoretical predictions and electrochemical tests.[27] Their findings demonstrate that MoS_2 exhibits impressive performance, achieving faradaic efficiency (1.17%) and NH_3 yield (8.08×10^{-11} mol s^{-1} cm^{-1}) at −0.5 V vs. RHE in 0.1 M Na_2SO_4, even under acidic conditions. These results establish MoS_2 as an active electrocatalyst for NRR, highlighting its potential for efficient N_2 reduction under ambient conditions.[27]

The Nakamura group has also focused on MoS_2 as a catalyst for the electrochemical reduction of nitrate/nitrite to ammonia across a wide pH range.[28] Their investigations revealed that MoS_2 displays superior catalytic activity by enabling concerted proton-electron transfer (CPET), similar to natural denitrification processes. Experimental analysis further unveiled that MoS_2 facilitates the conversion of nitrite to ammonia through intermediate steps. These findings position molybdenum sulfide as a bioinspired catalyst for denitrification and suggest its role in prebiotic ammonia synthesis through geoelectrical current supply. Additionally, the Nakamura group demonstrated that a bioinspired molybdenum sulfide compound effectively catalyzes denitrification under prebiotic oceanic conditions. By coupling nitrite reduction with hydrogen sulfide oxidation, ammonia formation is facilitated, supporting the notion that geoelectrical currents in deep-sea hydrothermal vents contributed to prebiotic ammonia synthesis. Unlike noble metal-based catalysts, molybdenum sulfide exhibits significant activity across a wide pH range, highlighting the importance of CPET-induced redox transitions in nitrate/nitrite reduction. Protonated reductive Mo-S species likely facilitate nitrate/nitrite activation through hydrogen bonding with substrates. Consequently, molybdenum sulfide serves as an ideal model for understanding the specificity of nitrate reductase and designing analogous catalysts.[28]

Discussing different applications of MoS_2 as active catalysts in electrochemical reactions, we are going to investigate the potential of modified CFP electrodes utilizing mixed ionic liquids ($BuPyPF_6$ + $P_{66614}NTf_2$) and Nafion as the binder, for the simultaneous coreduction of CO_2 and nitrite under ambient temperature and pressure to optimize the electrocatalytic efficiency to produce urea and ammonia.

4.2 Experimental

4.2.1 Catalyst preparation. Carbon black (10 mg; Vulcan XC-72; Cabot), molybdenum(IV) sulfide nanopowder, (2 mg; 90 nm diameter, 99%; Sigma Aldrich) and 50 µL of 5% Nafion solution (5.14 mass% in a mixture of lower aliphatic alcohols and 51.9% water; Dupont) were dispersed in 2-propanol (50 µL) and H_2O (200 µL) and sonicated for 3 h.

For catalysts containing mixed ILs ,Carbon black (10 mg; Vulcan XC-72; Cabot), molybdenum(IV) sulfide nanopowder, (2 mg; 90 nm diameter, 99%; Sigma Aldrich) and 10 mg; $P_{66614}NTf_2$ (≥95.0%, Sigma Aldrich) and/or $BuPyPF_6$ (98.0+%, Fisher Scientific)were dispersed in a mixture of THF and 2-propanol (1:1 volume ratio, 0.3 mL) by sonication for 1 hour to form a homogeneous catalyst ink.

4.2.2 Electrode preparation. The ink was drop casted onto (CFP; 1 cm^2; TGP-H-090 Toray industries-total thickness of 280 µm) electrodes to give a catalyst loading of 1.5 mg cm^{-2} and IL loading of 1.5 mg cm^{-2} prepared on CFP with a mixture of the two IL were heated in an oven for 30 min at 75 °C to improve stability. Note that all the cyclic voltammograms in this chapter were carried out using 10 mV s^{-1} scan rate. The applied electrode was CFP modified with mixed IL ($BuPyPF_6$ + $P_{66614}NTf_2$) as a binder and MoS_2/C as the catalyst.

4.2.3 Electrochemistry. Electrochemical measurements were made at ambient temperature in a glass cell with a Pt counter electrode and a saturated calomel reference electrode (SCE; 0.241 V vs SHE). Potentials are reported relative to RHE (reversible hydrogen electrode), at −0.486 V vs SHE under N_2 (pH = 8.30) or −0.395 V vs SHE under CO_2 (pH = 6.75). CV is conducted at a scan rate of 10 mV s^{-1}. The working and counter electrode compartments were separated by a porous

glass frit. All measurements were made in aqueous 0.1 M $NaHCO_3$ at an ambient temperature of ca. 20 °C. All the applied working electrodes are 1 cm^2 of carbon fiber paper (CFP).

4.2.4 Product analysis. The determination of urea and ammonia concentrations followed the procedures discussed in section 2.3.4 of chapter 2.

4.3 Result and discussion

4.3.1 Electrodes modified with mixed ILs as a binder and the MoS_2/C catalyst

To explore CO_2 and N_2 reduction on the MoS_2 catalyst surface in a 0.1 M $NaHCO_3$ solution, the CV conducted on CFP electrodes modified using a mixed IL as a binder. These tests were executed by altering the purging gas from N_2 to CO_2. Significantly, the results revealed a consistent cathodic current across the different purging gas conditions. This uniform current response suggests limited reactivity of the MoS_2/C catalyst toward CO_2 reduction. Furthermore, the introduction of a gas mixture containing both CO_2 and N_2 failed to result in any observable coreduction of N_2 and CO_2. (Figure 4.1).
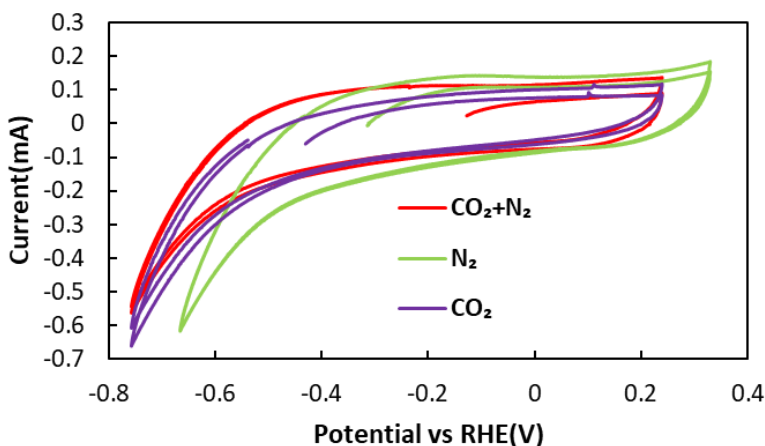
Figure 4.1 CVs recorded for MoS_2/C catalyst with mixed ILs as the binder in 0.1 M $NaHCO_3$ under N_2, CO_2 and N_2+CO_2.

Figure 4.2A demonstrates that the addition of 5 mM NaNO$_2$ to the electrolyte solution and the transition from N$_2$ to CO$_2$ as the purging gas resulted in minimal variations in the cathodic current.
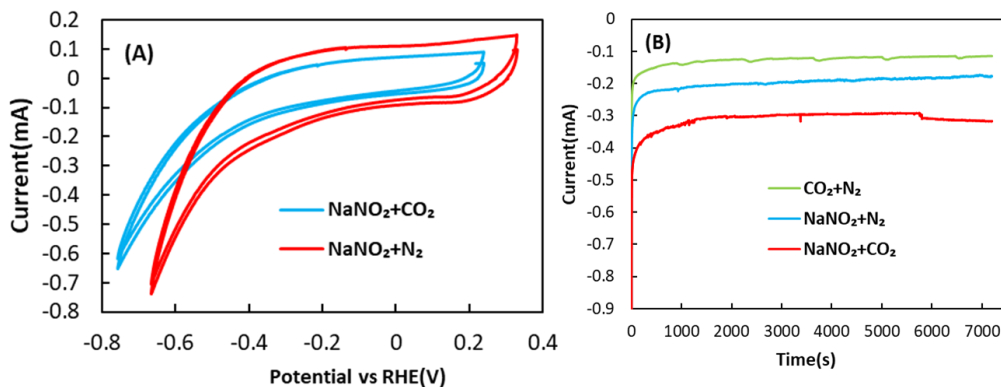
Figure 4.2 (A) Cyclic voltammograms performed for the electrodes containing MoS$_2$/C and mixed ILs in 0.1 M NaHCO$_3$ and 5 mM NaNO$_2$ under N$_2$ and CO$_2$. (B) CA for the same electrode and the same solution under CO$_2$, N$_2$, and N$_2$+CO$_2$ at −0.664 V.

To investigate the potential production of urea through the coreduction of (NO$_2^-$ and CO$_2$), (NO$_2^-$ and N$_2$), and (CO$_2$ and N$_2$ without NO$_2^-$) at the MoS$_2$/C catalyst, electrolysis was performed at a potential of −0.664 V vs. RHE for a duration of 2 h. As depicted in Figure 4.2B, a reasonably stable current was maintained during the electrolysis process. While no changes in the cathodic current were observed in CV, a notable disparity in current was evident upon switching the gas from N$_2$ to CO$_2$ in chronoamperometry. The highest current was achieved when the electrode was exposed to nitrite under CO$_2$, whereas the lowest current was recorded in the absence of nitrite under both CO$_2$ and N$_2$; however, a substantial current was still observed.

The average currents and urea concentration recorded in Table 4.1 correspond to the currents observed during chronoamperometry experiments. The experimental setup involving nitrite and N$_2$ demonstrated the lowest concentration of urea (2.2 μM), the lowest faradaic efficiency, and lowest rate. In contrast, when nitrogen gas was replaced with CO$_2$, the concentration of urea increased to 4.5 μM and the highest rate of urea formation (0.03 μmol h^{-1}). Surprisingly, the system without nitrite exhibited the highest faradaic efficiency for urea formation, achieving 5.46%. As a result, nitrite was found to have a negative impact on the faradaic efficiency, suggesting that the system with nitrite is not suitable for efficient urea formation using this catalyst

system. Therefore, these particular experimental setups do not appear to be viable for the production of urea from nitrite. However, they may still hold potential for the synthesis of urea directly from N_2 and CO_2 (Figure 4.5 A).

4.3.2 Electrodes modified with Nafion as a binder and the MoS$_2$/C catalyst

The experimental use of Nafion as a binder, instead of an IL, in a CV study with a 0.1 M NaHCO$_3$ electrolyte solution has yielded intriguing results. By switching the gas in the system from N_2 to CO_2, a significant increase in current was observed. Furthermore, when both CO_2 and N_2 gases were simultaneously present, the system exhibited an intermediate current (Figure 4.3).
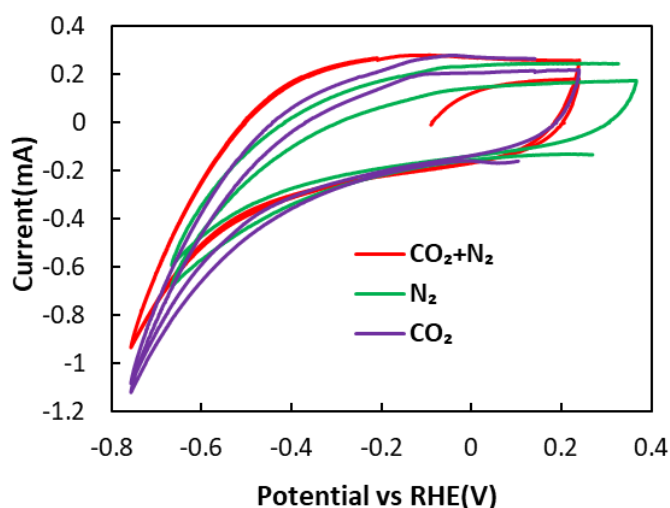
Figure 4.3 *CVs obtained for MoS$_2$/C catalyst with Nafion as the binder. All other experimental details were the same as Figure 4.1.*

The system consisting of 0.1 M NaHCO$_3$ with the addition of 5 mM NaNO$_2$ underwent CV, revealing a significant disparity in the current upon switching the gas from N_2 to CO_2. (Figure 4.4A). This change resulted in a notable increase in the current, indicating that CO_2 plays a crucial role in enhancing the electrochemical reactions within the system compared to N_2.
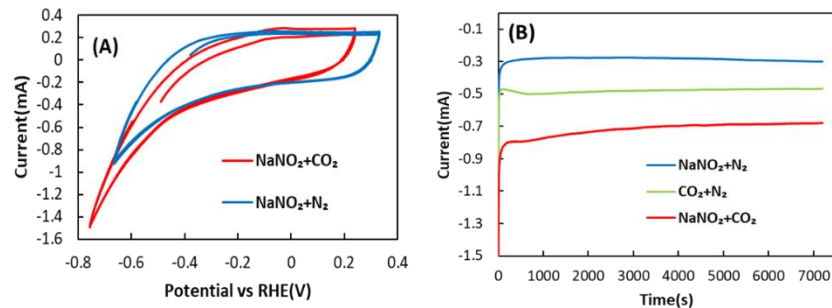
Figure 4.4 (A) CVs performed using the electrodes modified with MoS₂/C catalyst and Nafion as the binder. All other experimental parameters were the same as described in Figure 4.2(B) Chronoamperometry for electrolysis of the same solution and aforementioned electrode under CO_2, N_2 and N_2+CO_2 at −0.664 V.

To further investigate the behavior of the system, chronoamperometry experiments were conducted (Figure 4.4B), focusing on the electrolyte containing nitrite under different gas atmospheres. These experiments provided interesting insights. Under CO_2, the system demonstrated the highest current, suggesting a synergistic interaction between CO_2 and nitrite ions, leading to an amplified electrochemical response. In contrast, under N_2, the system exhibited the lowest current, indicating that N_2 has a limited impact on the electrochemical behavior of the nitrite-containing electrolyte. In the system containing only $NaHCO_3$ (without nitrite), an interesting observation was made when both CO_2 and N_2 gases were present. An intermediate current was observed under these conditions. These results demonstrate the significant importance of CO_2 in the occurrence of the electrochemical reaction, resulting in higher relative currents.

In terms of urea formation, the highest urea concentration was observed in the system with nitrite and CO_2, which coincided with the highest current. However, the system exhibited a low faradaic efficiency (1.54%). On the other hand, in the absence of nitrite, the urea concentration was significantly lower (1.3 µM). Interestingly, when comparing the use of an IL as a binder in the electrode, the most beneficial system in terms of faradaic efficiency (5.4%) was the one without nitrite. The reason for the improved performance of the ILs-based system in urea formation might be attributed to the hydrophobic nature of the ILs, which can suppress the hydrogen evolution reaction. As a result, the ILs-based system may yield higher amounts of urea compared to using Nafion as a binder in the electrode.

Regarding the rate of urea formation, the system without nitrite demonstrates the lowest rate of urea production (0.01 µmol h^{-1}). Conversely, with the introduction of nitrite into the system, the rate of urea formation increases to 0.03 µmol h^{-1} (Figure 4.5B). This enhanced rate is observed under both CO_2 and N_2 conditions. The system with both an IL and Nafion shows a similar rate of urea production under nitrite and CO_2 conditions.

Table 4.1 Specification of urea achieved through the application of MoS₂ with mixed IL or Nafion as the binder for electrolysis of 0.1 M NaHCO₃ over 2 h at −0.664 V.

Electrolysis conditions	Mixed IL as the binder		Nafion as the binder	
	Average current (mA)	Urea concentration (µM)	Average current (mA)	Urea concentration (µM)
Nitrite under CO_2	−0.311	4.5	−0.720	5.7
Nitrite under N_2	−0.198	2.2	−0.286	4.3
No nitrite under CO_2 +N_2	−0.127	3.6	−0.480	1.3
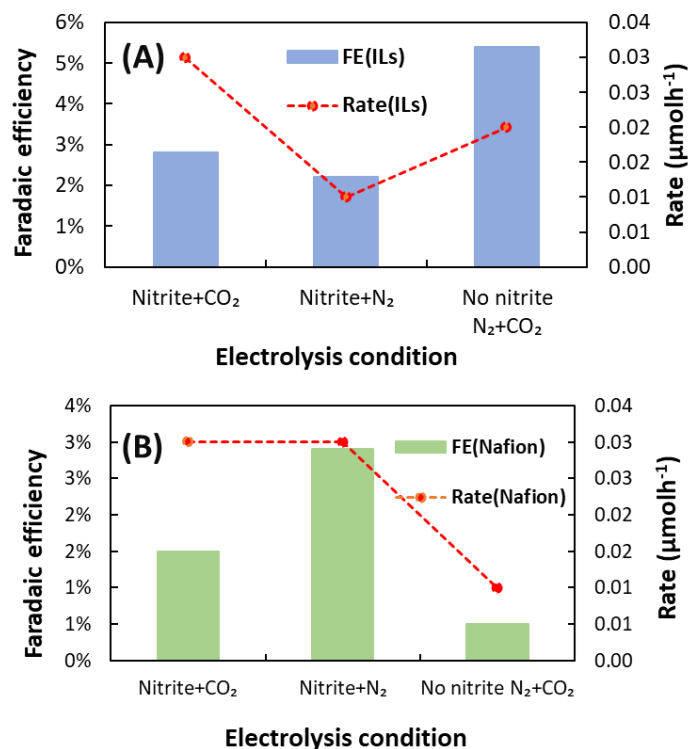
Figure 4.5 *FE and rate of urea formation calculated from Table 4.1.*

4.4 Conclusions

In this chapter, the preliminary results on the utilization of MoS_2 nanoparticles as catalysts, coupled with two distinct binders including Nafion and mixed ILs was explored for the synthesis of urea at ambient temperature and pressure. The investigation encompassed various conditions involving different electrolytic solutions: 0.1 M $NaHCO_3$ under both N_2 and CO_2 gases, as well as 0.1 M $NaHCO_3$ and 5 mM $NaNO_2$ under either CO_2 or N_2, all at a potential of -0.664 V vs RHE.

Within the electrolyte solution containing nitrite under N_2 gas, the electrode with Nafion as the binder exhibited superior faradaic efficiency and a higher rate of urea formation compared to the electrode with IL binder. However, when transitioning the gas from N_2 to CO_2, the electrode modified with ILs showed greater faradaic efficiency than the electrode with Nafion as the binder.

Notably, the rate of urea formation remained constant under these conditions, reaching its peak at 0.03 µmol h^{-1}.

When nitrite was absent in the electrolysis solution, the electrode modified with ILs performed better than the one with Nafion. This electrode achieved the highest efficiency in terms of urea production, reaching 5.4%. Moreover, it also had a higher rate of producing urea compared to the electrode with Nafion.

According to our results, once the mixed ILs is applied as the binder, the urea formation is not dependant on the presence of nitrite in the system. Indeed, the IL containing system uses N_2 as the source of nitrogen in order to generate urea. In case of Nafion as the binder, however, the best results were achieved in the presence of both nitrite and N_2 as the nitrogen source.

4.5 References

(1)   Lupan, O.; Cretu, V.; Deng, M.; Gedamu, D.; Paulowicz, I.; Kaps, S.; Mishra, Y. K.; Polonskyi, O.; Zamponi, C.; Kienle, L.; Trofim, V.; Tiginyanu, I.; Adelung, R. Versatile Growth of Freestanding Orthorhombic α-Molybdenum Trioxide Nano- and Microstructures by Rapid Thermal Processing for Gas Nanosensors. *J. Phys. Chem. C* **2014**, 118 (27), 15068–15078. https://doi.org/10.1021/jp5038415.

(2)   Li, X. L.; Li, T. C.; Huang, S.; Zhang, J.; Pam, M. E.; Yang, H. Y. Controllable Synthesis of Two-Dimensional Molybdenum Disulfide (MoS_2) for Energy-Storage Applications. *ChemSusChem* **2020**, 13 (6), 1379–1391. https://doi.org/10.1002/cssc.201902706.

(3)   Jiao, Y.; Hafez, A. M.; Cao, D.; Mukhopadhyay, A.; Ma, Y.; Zhu, H. Metallic MoS_2 for High Performance Energy Storage and Energy Conversion. *Small* **2018**, 14 (36), 1800640. https://doi.org/10.1002/smll.201800640.

(4)   Zhang, X.; Lai, Z.; Tan, C.; Zhang, H. Solution-Processed Two-Dimensional MoS_2 Nanosheets: Preparation, Hybridization, and Applications. *Angew. Chem. Int. Ed*. **2016**, 55 (31), 8816–8838. https://doi.org/10.1002/anie.201509933.

(5)   Zhao, Y.; Zhang, X.; Wang, T.; Song, T.; Yang, P. Fabrication of RGO/CdS@2H, 1T, Amorphous MoS_2 Heterostructure for Enhanced Photocatalytic and Electrocatalytic Activity. *Int. J. Hydrog. Energy* **2020**, 45 (41), 21409–21421. https://doi.org/10.1016/j.ijhydene.2020.05.217.

(6)   Wang, J.; Fan, Y.; Pan, R.; Hao, Q.; Wu, Y.; Van Ree, T.; Holze, R. Regulating Graphitic Carbon Nitride/Co-catalyst by an Amorphous MoS_2 Conformal Multifunctional Intermediate Layer for Photocatalytic Hydrogen Evolution. *ACS Appl. Energy Mater.* **2021**, 4 (11), 13288–13296. https://doi.org/10.1021/acsaem.1c02872.

(7)   Chang, K.; Pang, H.; Hai, X.; Zhao, G.; Zhang, H.; Shi, L.; Ichihara, F.; Ye, J. Ultra-Small Freestanding Amorphous Molybdenum Sulfide Colloidal Nanodots for Highly Efficient Photocatalytic Hydrogen Evolution Reaction. *Appl. Catal. B Environ*. **2018**, 232, 446–453. https://doi.org/10.1016/j.apcatb.2018.03.087.

(8)   Yu, H.; Xiao, P.; Wang, P.; Yu, J. Amorphous Molybdenum Sulfide as Highly Efficient Electron-Cocatalyst for Enhanced Photocatalytic H_2 Evolution. *Appl. Catal. B Environ.* **2016**, 193, 217–225. https://doi.org/10.1016/j.apcatb.2016.04.028.

(9)   Wei, L.; Chen, Y.; Lin, Y.; Wu, H.; Yuan, R.; Li, Z. MoS_2 as Non-Noble-Metal Co-Catalyst for Photocatalytic Hydrogen Evolution over Hexagonal $ZnIn_2S_4$ under Visible Light Irradiations. *Appl. Catal. B Environ.* **2014**, 144, 521–527. https://doi.org/10.1016/j.apcatb.2013.07.064.

(10)   Lu, Z.; Saji, S. E.; Langley, J.; Lin, Y.; Xie, Z.; Yang, K.; Bao, L.; Sun, Y.; Zhang, S.; Ng, Y. H.; Song, L.; Cox, N.; Yin, Z. Selective N_2/H_2O Adsorption onto 2D Amphiphilic Amorphous Photocatalysts for Ambient Gas-Phase Nitrogen Fixation. *Appl. Catal. B Environ.* **2021**, 294, 120240. https://doi.org/10.1016/j.apcatb.2021.120240.

(11)   Saha, N.; Sarkar, A.; Ghosh, A. B.; Dutta, A. K.; Bhadu, G. R.; Paul, P.; Adhikary, B. Highly Active Spherical Amorphous MoS_2: Facile Synthesis and Application in Photocatalytic Degradation of Rose Bengal Dye and Hydrogenation of Nitroarenes. *RSC Adv.* **2015**, 5 (108), 88848–88856. https://doi.org/10.1039/C5RA19442C.

(12)   Lu, Q.; Rosen, J.; Zhou, Y.; Hutchings, G. S.; Kimmel, Y. C.; Chen, J. G.; Jiao, F. A Selective and Efficient Electrocatalyst for Carbon Dioxide Reduction. *Nat. Commun.* **2014**, 5 (1), 3242. https://doi.org/10.1038/ncomms4242.

(13)   Hong, X.; Chan, K.; Tsai, C.; Nørskov, J. K. How Doped MoS_2 Breaks Transition-Metal Scaling Relations for CO_2 Electrochemical Reduction. *ACS Catal.* **2016**, 6 (7), 4428–4437. https://doi.org/10.1021/acscatal.6b00619.

(14)   Asadi, M.; Kumar, B.; Behranginia, A.; Rosen, B. A.; Baskin, A.; Repnin, N.; Pisasale, D.; Phillips, P.; Zhu, W.; Haasch, R.; Klie, R. F.; Král, P.; Abiade, J.; Salehi-Khojin, A. Robust Carbon Dioxide Reduction on Molybdenum Disulphide Edges. *Nat. Commun.* **2014**, 5 (1), 4470. https://doi.org/10.1038/ncomms5470.

(15)   Chan, K.; Tsai, C.; Hansen, H. A.; Nørskov, J. K. Molybdenum Sulfides and Selenides as Possible Electrocatalysts for CO_2 Reduction. *ChemCatChem* **2014**, 6 (7), 1899–1905. https://doi.org/10.1002/cctc.201402128.

(16)   Mao, X.; Wang, L.; Xu, Y.; Li, Y. Modulating the MoS_2 Edge Structures by Doping Transition Metals for Electrocatalytic CO_2 Reduction. *J. Phys. Chem. C* **2020**, 124 (19), 10523–10529. https://doi.org/10.1021/acs.jpcc.0c01070.

(17)   Kibsgaard, J.; Lauritsen, J. V.; Lægsgaard, E.; Clausen, B. S.; Topsøe, H.; Besenbacher, F. Cluster−Support Interactions and Morphology of MoS_2 Nanoclusters in a Graphite-Supported Hydrotreating Model Catalyst. *J. Am. Chem. Soc*. **2006**, 128 (42), 13950–13958. https://doi.org/10.1021/ja0651106.

(18)   Foster, S. L.; Bakovic, S. I. P.; Duda, R. D.; Maheshwari, S.; Milton, R. D.; Minteer, S. D.; Janik, M. J.; Renner, J. N.; Greenlee, L. F. Catalysts for Nitrogen Reduction to Ammonia. *Nat. Catal*. **2018**, 1 (7), 490–500. https://doi.org/10.1038/s41929-018-0092-7.

(19)   Danyal, K.; Dean, D. R.; Hoffman, B. M.; Seefeldt, L. C. Electron Transfer within Nitrogenase: Evidence for a Deficit-Spending Mechanism. *Biochemistry* **2011**, 50 (43), 9255–9263. https://doi.org/10.1021/bi201003a.

(20)   Kappera, R.; Voiry, D.; Yalcin, S. E.; Branch, B.; Gupta, G.; Mohite, A. D.; Chhowalla, M. Phase-Engineered Low-Resistance Contacts for Ultrathin MoS_2 Transistors. *Nat. Mater*. **2014**, 13 (12), 1128–1134. https://doi.org/10.1038/nmat4080.

(21)   Wang, Y.; Wang, M.; Lu, Z.; Ma, D.; Jia, Y. Enabling Multifunctional Electrocatalysts by Modifying the Basal Plane of Unifunctional 1T′-MoS_2 with Anchored Transition Metal Single Atoms. *Nanoscale* **2021**, 13 (31), 13390–13400. https://doi.org/10.1039/D1NR02251B.

(22)   Liu, Z.; Wang, K.; Li, Y.; Yuan, S.; Huang, G.; Li, X.; Li, N. Activation Engineering on Metallic 1T-MoS_2 by Constructing In-Plane Heterostructure for Efficient Hydrogen Generation. *Appl. Catal. B Environ*. **2022**, 300, 120696. https://doi.org/10.1016/j.apcatb.2021.120696.

(23)   Dang, Q.; Tang, S.; Liu, T.; Li, X.; Wang, X.; Zhong, W.; Luo, Y.; Jiang, J. Regulating Electronic Spin Moments of Single-Atom Catalyst Sites via Single-Atom Promoter Tuning on S-Vacancy MoS_2 for Efficient Nitrogen Fixation. *J. Phys. Chem. Lett.* **2021**, 12 (34), 8355–8362. https://doi.org/10.1021/acs.jpclett.1c02432.

(24)   Zhao, J.; Zhao, J.; Cai, Q. Single Transition Metal Atom Embedded into a MoS_2 Nanosheet as a Promising Catalyst for Electrochemical Ammonia Synthesis. *Phys. Chem. Chem. Phys*. **2018**, 20 (14), 9248–9255. https://doi.org/10.1039/C7CP08626A.

(25)   Li, F.; Tang, Q. A Di-Boron Pair Doped MoS$_2$ (B2@MoS$_2$) Single-Layer Shows Superior Catalytic Performance for Electrochemical Nitrogen Activation and Reduction. *Nanoscale* **2019**, 11 (40), 18769–18778. https://doi.org/10.1039/C9NR06469A.

(26)   Jain, A.; Bar Sadan, M.; Ramasubramaniam, A. Identifying a New Pathway for Nitrogen Reduction Reaction on Fe-Doped MoS$_2$ by the Coadsorption of Hydrogen and N$_2$. *J. Phys. Chem. C* **2021**, 125 (36), 19980–19990. https://doi.org/10.1021/acs.jpcc.1c04499.

(27)   Zhang, L.; Ji, X.; Ren, X.; Ma, Y.; Shi, X.; Tian, Z.; Asiri, A. M.; Chen, L.; Tang, B.; Sun, X. Electrochemical Ammonia Synthesis via Nitrogen Reduction Reaction on a MoS$_2$ Catalyst: Theoretical and Experimental Studies. *Adv. Mater.* **2018**, 30 (28), 1800191. https://doi.org/10.1002/adma.201800191.

(28)   Li, Y.; Yamaguchi, A.; Yamamoto, M.; Takai, K.; Nakamura, R. Molybdenum Sulfide: A Bioinspired Electrocatalyst for Dissimilatory Ammonia Synthesis with Geoelectrical Current. *J. Phys. Chem. C* **2017**, 121 (4), 2154–2164. https://doi.org/10.1021/acs.jpcc.6b08343.

Chapter 5

Conclusions and future works

The focus of this research was to examine the coreduction of CO_2 and nitrite for the electrosynthesis of urea and ammonia under ambient temperature and pressure conditions. To achieve this, a diverse set of electrocatalysts was employed mainly supported on carbon black. The catalyst was utilized in conjunction with mixed ILs, including one with hydrophobic properties and another with hydrophilic characteristics. The selection of these ILs played a pivotal role in regulating the catalyst's selectivity and activity. The optimal ratio of the IL mixture was also determined by assessing the ink formulation, electrode preparation and stability in terms of diverse IL ratios.

The electrochemical behavior was analyzed through CV before and after chronoamperometry experiments. These investigations were conducted in a solution comprising 0.1 M $NaHCO_3$ and 5 mM $NaNO_2$ under CO_2. Subsequent analysis of the solution was carried out to quantify the concentrations of urea and ammonia produced during 2 hours of electrolysis.

The catalyst suite encompassed four variations: CoPc, FePc, FeTsPc, and MoS_2, all supported on carbon black. In the case of CoPc, alternative supporting materials, including Cu, Pd, Ir, Rh nanoparticles supported on carbon, TiO_2 nanoparticles, and graphene nanoplatelets, were explored to determine their impacts on production yields and rates of formation. To enhance the electrode stability in some of the electrocatalysts, a supplementary carbon black support layer was introduced before the deposition of the catalyst ink on the surface of the CFP electrode. Additionally, the effectiveness of FePc catalyst supported either on Cu/C or C was examined via CV, revealing their limited catalytic applicability for CO_2 and nitrite coreduction.

The utilization of the other electrocatalysts exhibited varying effects on the faradaic efficiency and production rates of urea across different applied potentials are shown in Figure 5.1.
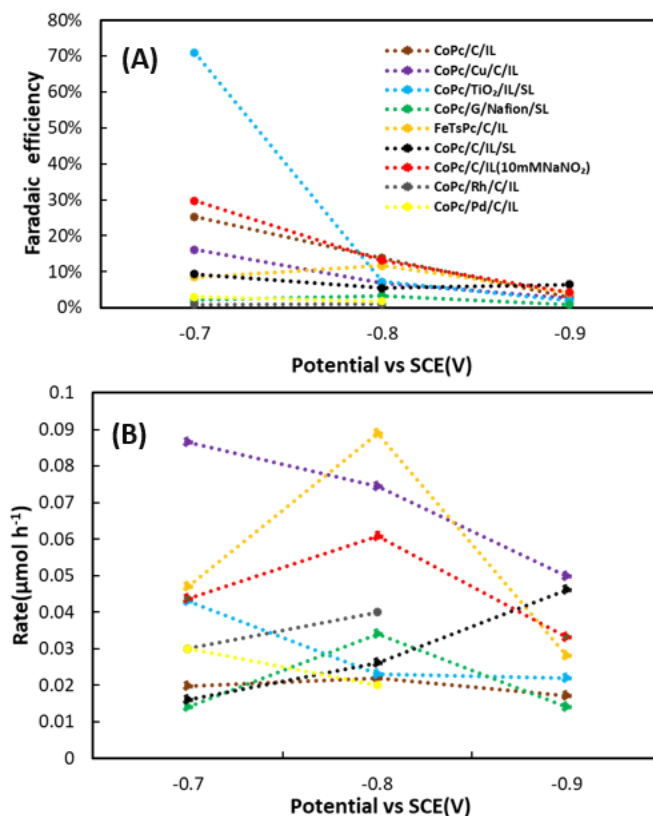
Figure 5.1 *(A) FE and (B) rate of urea formation at CFP electrodes modified with various electrocatalysts.*

As shown in Figure 5.1A, the faradaic efficiencies of all the electrocatalysts decrease as we move to more negative potentials. Notably, the highest faradaic efficiencies are seen at the lowest potentials, highlighting the energy efficiency of the catalyst. At −0.164 V, the faradaic efficiency goes below 14% for all catalysts, and at −0.264 V, it drops below 10%. This makes −0.064 V the most effective potential for the coreduction process. At this potential, the CoPc/TiO$_2$ catalyst achieves an impressive 71% faradaic efficiency (blue dotted line). Following that, the CoPc/C catalyst in 10 mM NaNO$_2$ shows the second-highest efficiency at 29.7% (red dotted line). Both the CoPc/C and CoPc/Cu/C catalysts also do well in terms of their faradaic efficiencies, ranking third and fourth, respectively.

Looking at urea formation rates, on the other hand, the highest rates generally appear at −0.164 V. However, since faradaic efficiencies remain below 14% at this potential, its importance diminishes. Therefore, our focus shifts to −0.064 V, where the faradaic efficiency is notably higher with no significant loss at the urea formation rates.

At −0.064 V, an interesting change occurs with the CoPc/Cu/C catalyst (purple dotted line, see Figure 5.2). Ranked the fourth one in terms of faradaic efficiency, it leads in reaction rate among all catalysts. The FeTsPc catalyst shows the second-highest rate, even though its faradaic efficiency is low (below 10%, orange dotted line). The third-highest rate belongs to the CoPc/C catalyst with 10 mM $NaNO_2$, which has good faradaic efficiency (red dotted line). Meanwhile, the CoPc/TiO_2 catalyst, which showed the highest faradaic efficiency, now ranks fourth in the urea formation rate (blue dotted line).

It is important to note that although the CoPc/C catalyst showed a high faradaic efficiency, its very low urea formation rate might make it an unsuitable catalyst (brown dotted line). Similarly, despite its high rate, the FeTsPc catalyst's low faradaic efficiency makes it inefficient for this electrolysis. The best catalysts in terms of both faradaic efficiency and urea formation rate are the CoPc/TiO_2, CoPc/C with 10 mM $NaNO_2$, and CoPc/Cu/C catalysts. These modified electrodes showed great potential for the efficient and fast catalysts for the coreduction of CO_2 and nitrite in order to produce urea.

In the context of the MoS_2 catalyst, a potential of −0.664 V, based on its CV results, was applied while employing IL and Nafion as the binding agents. Under these controlled conditions, the attained faradaic efficiencies stood at 2.8% and 1.54%, respectively, marking their position on the lower end among the assortment of investigated catalysts. Simultaneously, the rate was quantified at 0.03 $\mu mol\ h^{-1}$ for both scenarios, placing it within the range of moderate rates observed among the various catalysts studied, reflecting its measured effectiveness in the context of urea production.

A summary of the effects of the application of the electrocatalysts on the faradaic efficiency and formation rate of ammonia in different applied potentials are shown in Figure 5.2.
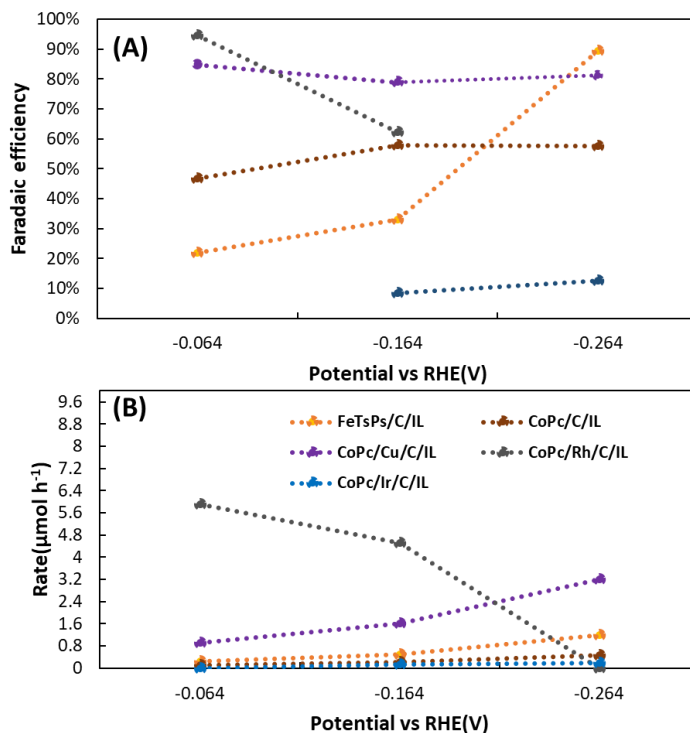
Figure 5.2 *(A) Faradaic efficiency and (B) rate of ammonia formation at CFP electrodes modified with various electrocatalysts.*

In the realm of the applied potentials, the various electrocatalysts have demonstrated noteworthy variations in faradaic efficiency for ammonia production. In the case of the FeTsPc/C catalyst (orange dotted line, Figure 5.2A, there was a discernible increasing trend, whereas the CoPc/Rh/C catalyst (gray dotted line, Figure 5.2A) exhibited a diminishing trend as potentials increase. Remarkably, the CoPc/Ir (blue dotted line) catalyst exhibited notably lower faradaic efficiency for ammonia generation.

Turning attention to the rate of ammonia production, a general uptrend was observed as potentials are elevated, except in the instance of the CoPc/Rh/C catalyst. Despite the CoPc/C catalyst boasting a commendable faradaic efficiency, its viability as a suitable catalyst for ammonia production was questioned by its relatively low formation rate.

Within the potential range of −0.064 V to −0.164 V, both the CoPc/Rh/C and CoPc/Cu/C catalysts (gray and purple dotted lines respectively) stood out with the highest faradaic efficiencies and formation rates. Hence, these catalysts emerged as the prime candidates for facilitating ammonia synthesis via the coreduction of CO_2 and nitrite.

Overall, two industrially important chemicals, urea and ammonia, have been synthesized electrochemically via the coreduction of environmentally detrimental chemicals, namely CO_2 and nitrite. In some of our electrocatalytic systems, high values of faradaic efficiency and rates of formation for both urea and ammonia have been achieved. These results demonstrate the promise of the applied method, making it a valuable addition to the available toolbox for the production of these compounds in order to be utilized across diverse industries. One remaining challenge with this method is that the products are being synthesized in aqueous systems, requiring additional separation processes for their extraction.

Appendix A

Supporting information for chapter 2
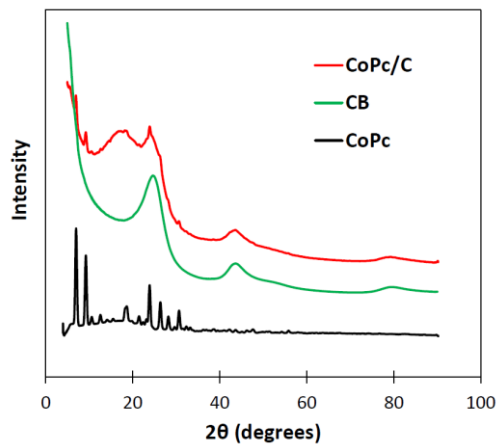
Figure A.1 X-ray diffraction patterns for CoPc, Vulcan carbon black, and the CoPc/C catalyst obtained with a Rigaku XtaLAB Synergy-S X-ray diffractometer.
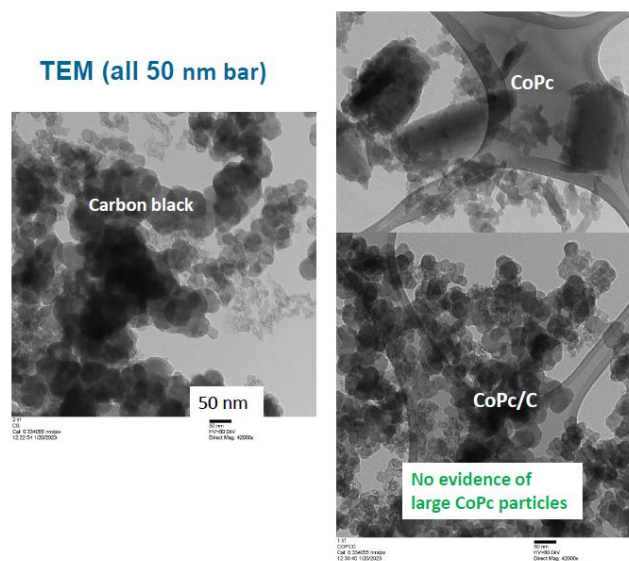
Figure A.2 Transmission electron microscopy images of Vulcan carbon black, CoPc, the CoPc/C catalyst, obtained with a Tecnai TM Spirit transmission electron microscope (Faculty of Medicine at Memorial University).
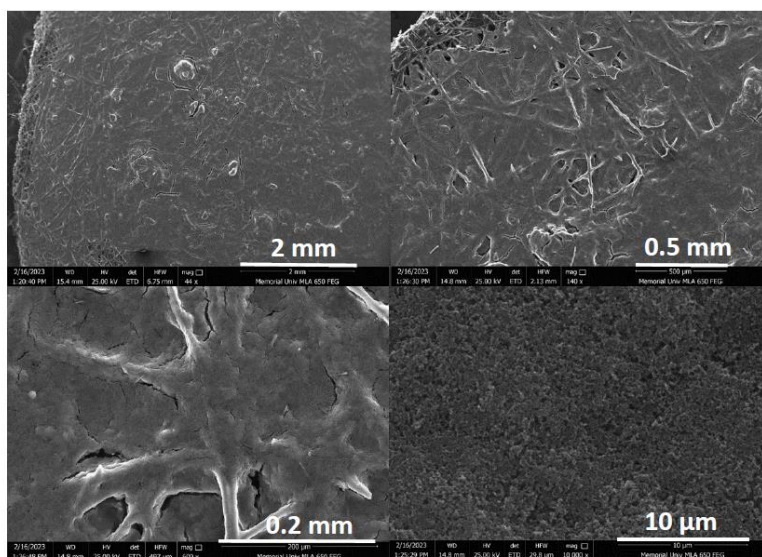
Figure A.3 Scanning electron microscopy images of a (CoPc/C+BuPyPF$_6$+P$_{66614}$NTf$_2$)/CFP electrode obtained with an FEI Quanta 400 scanning electron microscope.
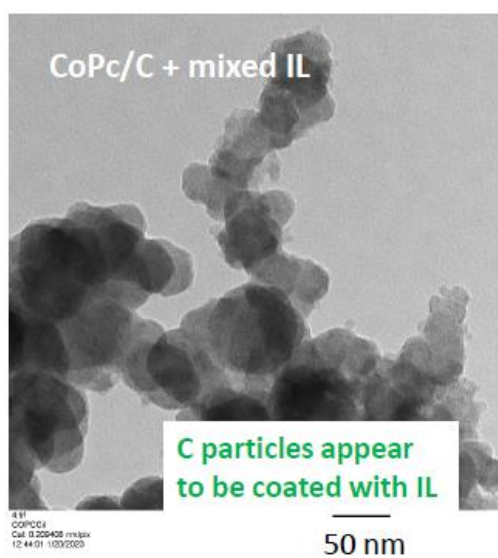
Figure A.4 Transmission electron microscopy image of CoPc/C+BuPyPF$_6$+P$_{66614}$NTf$_2$ prepared from the catalyst ink used to prepare CoPc/C+BuPyPF$_6$+P$_{66614}$NTf$_2$ electrodes.

91

Table A.1 Average currents, electrolyte volume, and concentrations of urea and ammonia from electrolysis of 5 mM NaNO₂ in 0.1 M NaHCO₃ under CO₂ at CoPc/C/CFP electrodes over 2 h.

Binder	Potential vs RHE (V)	Average current (mA)	Electrolyte volume (mL)	Urea concentration (μM)	Ammonia concentration (μM)
Nafion	−0.064	−0.117	15	1.3	43
Nafion	−0.164	−0.325	15	2.6	69
Nafion	−0.264	−0.770	15	3.6	380
BuPyPF₆	−0.064	−0.340	12	6.6	140
BuPyPF₆	−0.164	−0.605	12	3.9	202
BuPyPF₆	−0.264	−0.704	12	6.0	342
Mixed IL	−0.064	−0.025/−0.037[a]	12	3.3	18
Mixed IL	−0.164	−0.053/−0.073[a]	12	3.8	35
Mixed IL	−0.264	−0.175/0.172[a]	12	2.6	77

a. Urea and ammonia were measured with different electrodes.

Table A.2 *Specifications of urea and ammonia using Cu/C and CoPc/Cu/C catalyst. All the experimental details were the same as Table A.1*

Catalyst	Potential vs RHE (V)	Average current (mA)	Urea concentration (μM)	Ammonia concentration (μM)
Cu/C	−0.064	−0.192	3.7	143
Cu/C	−0.164	−0.320	2.6	219
Cu/C	−0.264	−0.514	8.6	414
CoPc/Cu/C	−0.064	−0.173	14.4	152
CoPc/Cu/C	−0.164	−0.347	12.4	284
CoPc/Cu/C	−0.264	−0.634	8.3	534